THE UNIVERSITY OF
WARWICK

AUTHOR: **Ian Hughes** DEGREE: **Ph.D.**

TITLE: **A First-Principles Approach to Modelling Magnetism in Strongly-Correlated Electron Systems**

DATE OF DEPOSIT: .....

I agree that this thesis shall be available in accordance with the regulations governing the University of Warwick theses.

I agree that the summary of this thesis may be submitted for publication.

I **agree** that the thesis may be photocopied (single copies for study purposes only).

Theses with no restriction on photocopying will also be made available to the British Library for microfilming. The British Library may supply copies to individuals or libraries. subject to a statement from them that the copy is supplied for non-publishing purposes. All copies supplied by the British Library will carry the following statement:

> "Attention is drawn to the fact that the copyright of this thesis rests with its author. This copy of the thesis has been supplied on the condition that anyone who consults it is understood to recognise that its copyright rests with its author and that no quotation from the thesis and no information derived from it may be published without the author's written consent."

AUTHOR'S SIGNATURE: .....

USER'S DECLARATION

1. I undertake not to quote or make use of any information from this thesis without making acknowledgement to the author.
2. I further undertake to allow no-one else to use this thesis while it is in my care.

DATE SIGNATURE ADDRESS

.....

.....

.....

.....

.....

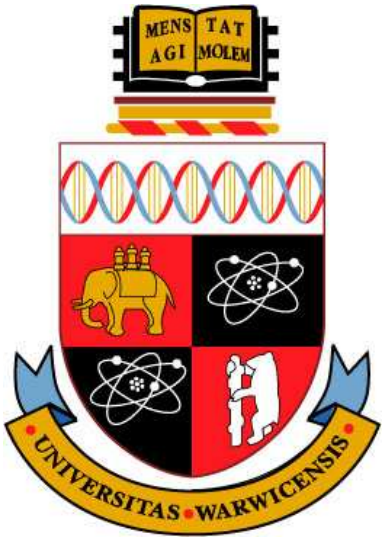

A First-Principles Approach to Modelling Magnetism in Strongly-Correlated Electron Systems

by

Ian Hughes

Thesis

Submitted to the University of Warwick

for the degree of

Doctor of Philosophy

Department of Physics

October 2007

THE UNIVERSITY OF WARWICK

Contents

List of Tables

List of Figures

Acknowledgments

I would like to pay special thanks to Prof. Julie Staunton for her excellent supervision throughout my PhD studies. I would also like to thank the EPSRC and the CCLRC's Centre for Materials Physics and Chemistry for funding me, and the Centre for Scientific Computing at the University of Warwick for providing computing resources.

Much of the work presented in this thesis was inspired by, and grew out of collaborations with research colleagues based at Daresbury Laboratory and the University of Halle, and also the Max Planck Institute in Halle. In particular, I would like to thank Prof. Walter Temmerman, Dr. Dzidka Szotek, Dr. Martin Lüders, Mr. Markus Däne, Prof. Dr. Wolfram Hergert and Dr. Arthur Ernst for all their suggestions and advice. Dr. Axel Svane and Prof. Dr. Julian Poulter are also thanked for many useful discussions.

I would also like to mention my officemates Mark and Amitesh, who have been excellent company over the last few years. Above all, however, I thank my parents for all their support, and Rebecca for her understanding and encouragement.

Declarations

This thesis is submitted to the University of Warwick as my application towards the degree of Doctor of Philosophy, and presents details of research carried out in the Theoretical group of the Department of Physics between October 2003 and July 2007. The content of this thesis is my own work, unless stated otherwise, carried out under the supervision of Prof. J. B. Staunton. No part of this thesis has previously been submitted for a research degree at any other institution.

Parts of this work have been published in, or will be submitted for publication in, the following papers:

- I. D. Hughes, M. Däne, A. Ernst, W. Hergert, M. Lüders, J. Poulter, J. B. Staunton, A. Svane, Z. Szotek and W. M. Temmerman "Lanthanide contraction and magnetism in the heavy rare earth elements", *Nature* **446**, 650 (2007).

- S. Ostanin, A. Ernst, L. M. Sandratskii, P. Bruno, M. Däne, I. D. Hughes, J. B. Staunton, W. Hergert, I. Mertig and J. Kudrnovský, "Mn-Stabilized Zirconia: From Imitation Diamonds to a New Potential High-T_C Ferromagnetic Spintronics Material", *Phys. Rev. Lett.* **98**, 016101 (2007).

- I. D. Hughes *et al*, "Onset of Magnetic Order in Strongly-Correlated Systems

from *ab initio* Electronic Structure Calculations: Application to Transition Metal Oxides", in preparation for *New. J. Phys.*

Abstract

We present an *ab initio* theoretical formalism for investigating the onset of magnetic order in strongly-correlated electron systems. The formalism is based on spin density functional theory, with a self-interaction corrected local density approximation (SIC-LDA). The self-interaction correction is implemented locally, within the KKR multiple-scattering method. Thermally induced magnetic fluctuations are treated using a mean-field 'disordered local moment' (DLM) approach and we use a linear response technique to generate the paramagnetic spin susceptibility.

We apply the formalism to the heavy rare earth metals, where the magnetic ordering tendencies are analysed in terms of the underlying electronic structure. The formation of incommensurate magnetic structures is shown to be promoted through a Fermi surface nesting mechanism. Our calculations yield an accurate, parameter free, estimate of the magnetic ordering temperature of gadolinium. Using this element as a magnetic prototype, we propose a 'unified phase diagram', from which the magnetic ordering tendencies of any heavy rare earth system can be found. This diagram is used to predict critical alloy concentrations, at which new magnetic phases appears. We also examine magnetic ordering in transition metal oxides and outline how our first principles linear response approach can be adapted to study compositional correlations, which we illustrate by investigating the presence of atomic short range order in gadolinium-yttrium alloys.

Chapter 1

Introduction

When atoms are brought together to form a solid, the behaviour of the valence electrons is most easily understood in terms of one of two opposite limits. The first, which emphasises the particle-like nature of an electron, corresponds to when the electrons remain bound to a particular nuclei, occupying atomic orbitals as in the Heitler-London [1] picture. The second, which emphasises the wave character of an electron, corresponds to delocalised electrons propagating through a lattice, influenced only by the potential due to the periodic arrangement of nuclei. For such Bloch states, a momentum space, band type picture emerges. This thesis is concerned with a class of systems that fall between these two well understood limits, namely those termed 'Strongly-Correlated'. Such systems contain electron states which can not be described using a real space atomic picture, nor can the electrons be viewed as moving through a static mean field lattice potential. In particular, with regards to the latter point, the influence of electrons on each other is such that they cannot be treated as independent and their motions can be said to be correlated.

Many technologically important materials, such as the high temperature

cuprate superconductors [2], fall into the Strongly-Correlated category. Other examples include dilute magnetic semiconductors [3] and the colossal magnetoresistive manganites [4], which have promising future applications as spintronic materials. There has hence been much theoretical effort directed towards trying to understanding these systems. (For a recent review of theoretical models for correlated electron systems see reference [5].) However, one aspect of this problem which has so far received little attention has been a description of finite temperature magnetism in these systems. It is this aspect that we address in this thesis.

To develop a fully quantum mechanical description of a many electron system one can adopt either of two approaches. The first is the so-called model Hamiltonian approach, where the Hamiltonian is simplified to take into account only a few relevant degrees of freedom. This involves specifying parameters, which have to be adjusted for each system of interest, so as to give some desired physical behaviour or agreement with experimental data. The second, perhaps more appealing, approach is to start with the many electron Hamiltonian and employ some parameter-free approximation to try and find the eigenfunctions and eigenvalues. As well as offering greater insight into the underlying electronic mechanisms that govern the properties of a material, such 'first-principles' approaches also have much predictive power. The most successful first-principles approach is the density functional theory (DFT) [6], where the many electron Hamiltonian is mapped onto an effective one electron Hamiltonian. This involves specifying a one-electron exchange-correlation potential, which in the so-called local density approximation (LDA) is approximated by that of a homogeneous electron gas. Although this approach has proved to be remarkably successful for describing the ground state properties of many systems, it often fails for systems where the electron-electron

interaction is strong enough to change the nature of the ground state, e.g. by causing states to spatially localise.

Describing finite temperature magnetism in metals, even in non strongly correlated systems, is highly non-trivial. In particular a Heisenberg type model, of the sort applicable to magnetic insulators, can not be used to treat metals since this relies on there being a well defined spin at each atomic site. A band-like Stoner picture, on the other hand, fails to reproduce magnetic ordering temperatures, due its neglect of thermally excited spin fluctuations. The so-called disordered local moment (DLM) theory [7] combines the best aspects of both these two approaches. In particular, it offers an itinerant description of electrons, whilst still allowing well-defined moments to be associated with each site. These moments are established through the collective motion of the electrons and as such the DLM theory can be considered as a model of spin correlations. Charge correlations, on the other hand, have so far only been treated on the level of a homogeneous electron gas during first principles implementations of the DLM, since the LDA has always been employed in these. One consequence of this is that all valence electrons are described as band like, which gives qualitatively wrong physics for rare earth or transition metal oxide systems, where localised electron states set up atomic like magnetic moments. In this thesis we present a new implementation of the DLM model, able to describe strongly-correlated systems, which treats both localised and delocalised electrons on an equal footing.

We begin, in chapter 2, by outlining the density functional theory and describe how the resulting one electron equations can be solved using a multiple-scattering (KKR) method [8]. This choice of method is crucial, since it can easily be generalised, via the so-called coherent-potential approximation (CPA), to deal with disorder. This aspect will be important when treating thermally activated spin

fluctuations. After outlining how the conventional (LDA) implementation of DFT fails to describe systems characterised by strong electron-electron correlations, we review in chapter 3 various attempts to go beyond the LDA in order to treat correlation effects. We focus particularly on one approach, the self-interaction correction (SIC) [9], which is the method that we employ in this thesis. Central to our being able to incorporate the SIC into a first-principles DLM scheme, is a recently proposed multiple-scattering implementation of this method, known as the local-SIC (LSIC). This is outlined in chapter 4, where we illustrate the method using the famous $\alpha \rightarrow \gamma$ in cerium [10].

The DLM approach to magnetism is outlined in chapter 5, where we begin by describing how paramagnetic disorder, arising from thermally activated spin fluctuations, can be treated using a first principles KKR-CPA method. After detailing how the paramagnetic spin susceptibility can be evaluated through a linear response approach, we go onto present some new extensions to the DLM formalism. In particular, in section 5.4 we outline how the DLM approach can be generalised to systems with more than one atom per unit cell, enabling complex lattice structures to be investigated. This formalism is illustrated with calculations for manganese stabilised cubic zirconia, the results of have been published in reference [11]. In section 5.5 we present the main achievement of this thesis, the LSIC implementation of the DLM method, which constitutes the first fully *ab initio* theory of finite temperature magnetism in strongly-correlated electron systems. After illustrating the formalism with a test calculation for γ-Ce, we apply it in chapter 6 where a major investigation of heavy rare earth magnetism is undertaken, the salient points of which have been published in reference [12]. We show how the underlying electronic structure of the paramagnetic state, and more particularly the Fermi surface shape, influences the magnetic ordering tendencies of these systems.

With reference to the RKKY model of magnetism [13], we argue that gadolinium can be used as a magnetic prototype for the whole heavy rare earth series. From this we propose a 'unified phase diagram' of heavy rare earth magnetism, from which the magnetic ordering tendencies of any heavy rare earth systems can be obtained, provided that the lattice parameters are known. On the basis of this phase diagram we can make predictions about the heavy rare earths which can be tested experimentally, such as the value of critical alloy concentrations at which new magnetic phases appear.

In chapter 7 we outline some further applications of our first principles formalism. In section 7.1 we describe how the linear response approach used to evaluate the paramagnetic spin susceptibility can be adapted to study atomic short range order (ASRO) in alloys. We illustrate this by investigating the presence of compositional correlations in gadolinium-yttrium alloys. In section 7.2 we present additional results obtained from our DLM-SIC scheme for magnetism, this time for some d-electron systems, namely the transition metal oxides. Finally, in section 7.3, we outline a possible 2D implementation of the DLM scheme, which could be used to investigate magnetic surfaces.

We end in chapter 8 with conclusions concerning the main developments and findings of this thesis, along with a discussion of possible future work arising from these.

Chapter 2

'First-Principles' Theory of Electronic Structure

2.1 Density Functional Theory

The fundamental Hamiltonian for a system of interacting electrons can be written as (atomic units used)

$$\hat{H} = -\frac{1}{2}\sum_i \bigtriangledown_i^2 + \sum_i V_{ext}(\mathbf{r}_i) + \frac{1}{2}\sum_i \sum_{j\neq i} \frac{1}{|\mathbf{r}_i - \mathbf{r}_j|}, \tag{2.1}$$

where V_{ext} is some external potential which may incorporate the effect of fixed nuclei. Over the last forty years Density Functional Theory (DFT) has become the primary tool for calculating the electronic structure of systems described by such a Hamiltonian. The foundations of DFT were laid by Hohenberg and Kohn, who proved a theorem that the electronic groundstate energy is a unique functional of the electron charge density, $n(\mathbf{r})$, and that this functional is minimised when evaluated for the true groundstate density, $n_0(\mathbf{r})$ [14]. The widespread utilisation of DFT can be attributed to an *ansatz* made by Kohn and Sham, who postulated that the ground state density can be represented by the ground state density of an

auxiliary system of non-interacting particles [15]. This provides a means to reduce the complicated interacting many-problem body to a simpler independent particle problem. In the Kohn-Sham approach the electron density is given by

$$n(\mathbf{r}) = \sum_{\sigma} n_{\sigma}(\mathbf{r}) = \sum_{\sigma} \sum_{i=\mathrm{occ}} \left|\psi_i^{\sigma}(\mathbf{r})\right|^2, \tag{2.2}$$

where $\psi_i^{\sigma}(\mathbf{r})$ are single electron wavefunctions of some auxiliary independent particle system and the summation is over all occupied states, $i = \mathrm{occ}$, and spins, σ. The groundstate energy functional of the full interacting many-body system can then be expressed as

$$\begin{aligned} E = \frac{1}{2} \sum_{\sigma} \sum_{i} |\bigtriangledown \psi_i^{\sigma}(\mathbf{r})|^2 + \sum_{\sigma} \int \mathbf{dr} V_{ext}^{\sigma}(\mathbf{r}) n(\mathbf{r}) \\ + \frac{1}{2} \int \mathbf{dr} \int \mathbf{dr'} \frac{n(\mathbf{r}) n(\mathbf{r'})}{|\mathbf{r} - \mathbf{r'}|} + E_{xc}[n_{\uparrow}, n_{\downarrow}], \end{aligned} \tag{2.3}$$

where the first term is the independent-particle kinetic energy, the second term is the interaction energy with some external potential, V_{ext}^{σ}, and the third term is the classical Hartree energy. The fourth term, E_{xc}, contains all the many-body effects of exchange and correlation. Minimising Eq. 2.3 with respect to the density, n, leads to one-electron equations of the form

$$\left(-\frac{1}{2} \bigtriangledown^2 + v_{eff}^{\sigma}(\mathbf{r}) \right) \psi_{\alpha\sigma}(\mathbf{r}) = \varepsilon_{\alpha\sigma} \psi_{\alpha\sigma}(\mathbf{r}), \tag{2.4}$$

where v_{eff}^{σ} is an effective one-body potential given by

$$v_{eff}^{\sigma}(\mathbf{r}) = V_{ext}^{\sigma}(\mathbf{r}) + V_H[n](\mathbf{r}) + V_{xc,\sigma}[n_{\uparrow}, n_{\downarrow}], \tag{2.5}$$

where the Hartree potential, V_H, and exchange-correlation potential, V_{xc}, are defined by

$$V_H[n](\mathbf{r}) = \int \mathbf{dr'} \frac{n(\mathbf{r'})}{|\mathbf{r} - \mathbf{r'}|}, \tag{2.6}$$

$$V_{xc,\sigma}[n_\uparrow, n_\downarrow] = \frac{\delta E_{xc}[n_\uparrow, n_\downarrow]}{\delta n_\sigma(\mathbf{r})}. \tag{2.7}$$

Equations 2.4 and 2.5 constitute the Kohn-Sham (KS) equations of DFT. In principle the KS equations, together with the expression for the charge density, Eq. 2.2, form a set of closed equations which can be solved self-consistently. However, apart from the most simple systems the form of $E_{xc}[n_\uparrow, n_\downarrow]$ is unknown. Hence to make the scheme numerically tractable approximations must be made. The most common approximation, valid when $n(\mathbf{r})$ is slowly varying, is the Local Density Approximation (LDA). Here the exchange-correlation energy density at each point in space is assumed to be the same as in a homogeneous electron gas which has the same charge density as at the given point:

$$E_{xc}[n_\uparrow, n_\downarrow] = \int \mathbf{dr}\ n(\mathbf{r}) \epsilon_{xc}^{hom}(n_\uparrow(\mathbf{r}), n_\downarrow(\mathbf{r})). \tag{2.8}$$

The parametrisation we use in this thesis for ϵ_{xc}^{hom} is that proposed by Perdew and Wang [16]. The groundstate properties of a wide variety of real materials can be described remarkably well with the LDA. This success can be partially attributed to the fact that the approximation obeys the sum rule for the exchange-correlation hole in the charge density [17]. For a detailed review of DFT calculations, including applications of the LDA to real systems, see references [18, 6].

2.2 Multiple Scattering Theory Approach

In the previous section it was shown how the many body problem can be reduced to an independent particle problem, resulting in one electron equations of the form 2.4. In this section a multiple scattering theory approach to solving such equations is outlined. The first use of a multiple scattering method to calculate stationary electronic states was by Korringa [19], who proposed a scheme based on the theory

of lattice interferences [20]. An equivalent scheme was later formulated by Kohn and Rostoker [21], using a variational technique. Hence the multiple scattering approach for the calculation of electronic structure is generally referred to as the KKR method. An important feature of this method is that it separates the single site scattering problem, presented by a single potential in free space, from the multiple scattering problem arising when an infinite array of such potentials are brought together in a lattice. A useful consequence of this is that the formalism shows a clear separation between potential and structural properties, with some quantities depending only on the geometry of the lattice.

The single site potentials of relevance to this thesis are those that have been generated self-consistently using Eq. 2.5. In the following discussion it will be assumed that these potentials have a muffin-tin form, i.e. they are spherically symmetric and are equal to some constant, V_{MTZ}, outside a certain radius, R_{MT}. To simplify the algebra the energy zero will be shifted to coincide with V_{MTZ}, hence the potential will be zero for all radii greater than R_{MT}. In so-called *f*ull potential treatments the potentials can be of arbitrary shape. Such treatments are important in systems in reduced symmetry, such as at surfaces. For details see reference [22].

The spherical symmetry means that the solution of the Schrödinger equation (in units where $\hbar^2/2m_e = 1$),

$$\left(-\bigtriangledown^2 + v\left(\mathbf{r}\right)\right)\psi\left(\mathbf{r}\right) = E\psi\left(\mathbf{r}\right), \tag{2.9}$$

can be written in the form

$$\psi\left(\mathbf{r}\right) = \sum_L a_L(E) R_l(E,r) Y_L(\hat{r}), \tag{2.10}$$

where $R_l(E,r)$ is the solution of the radial Schrödinger equation

$$[-\frac{1}{r}\frac{d^2}{dr^2}r + \frac{l(l+1)}{r^2} + v(r)]R_l(E,r) = ER_l(E,r) \tag{2.11}$$

and $Y_L(\hat{r})$ is a spherical harmonic where L stands for the pair of angular momentum indices l,m. The asymptotic form of $R_l(E,r)$ as $r \to \infty$ is

$$R_l(E,r) = \frac{1}{\sqrt{E}r}\sin[\sqrt{E}r - \frac{l\pi}{2} + \delta_l(E)], \tag{2.12}$$

which differs from the free electron solution only by a shift of phase, $\delta_l(E)$. Hence $\delta_l(E)$ is usually referred to as the phase shift.

In scattering theory the aim is to find solutions $\psi_{\mathbf{k}}(\mathbf{r})$ of 2.9, such that $E = \mathbf{k}^2$ and the asymptotic form of the wavefunction can be written as

$$\psi_{\mathbf{k}}(\mathbf{r}) = e^{i\mathbf{k}\cdot\mathbf{r}} + f_k(\theta)\frac{e^{ikr}}{r}, \tag{2.13}$$

where θ is the angle between the vectors $\mathbf{k}$ and $\mathbf{r}$ and $f_k(\theta)$ is the so-called scattering amplitude. For such *scattering state* solutions, written in the form of Eq. 2.10, it turns out that [23]

$$a_L(k^2) = 4\pi i^l e^{i\delta_l} Y_L^*(\hat{k}), \tag{2.14}$$

and, furthermore,

$$f_k(\theta) = \sum_l \frac{(2l+1)}{k} f_l P_l(cos\theta), \tag{2.15}$$

where P_l is a Legendre polynomial and

$$f_l = \sin\delta_l e^{i\delta_l}. \tag{2.16}$$

It is evident from Eqs. 2.13, 2.15 & 2.16 that the asymptotic form of the scattering state is completely determined by the phase shift, $\delta_l(E)$. Hence phase shifts offer a very efficient description of the single site scattering problem. It turns out

that phase shifts also play an important role in describing the multiple scattering problem, where an array of scattering centres (atomic potentials) are brought together to form a solid. In particular, the phase shifts describe the degree of localisation of states in the solid. For example, localised electronic states are characterised by phase shifts that have very sharp resonances, whereas band-like states have more slowly varying phase shifts. The time spent by an electron at each scattering centre, known as the *Wigner delay time*, is proportional to the energy derivative of the phase shift. Hence if a phase shift is resonant an electron will spend a long time at each site as it travels through the solid. This long Wigner delay time reflects the strong degree of localisation at a resonance and the fact that an electron can become trapped in a metastable bound state.

Before proceeding with a mathematical treatment of the multiple scattering problem, the single site problem will now be reformulated using a Green's function method, whereby the differential Eq. 2.9 is replaced by an equivalent integral equation. This Green's function formalism is particularly useful when it comes to treating disordered systems, as detailed in the next section of this thesis. In addition, many useful observables can be calculated from the Green's function. Formally the Green's function corresponding to a Hamiltonian, H, is defined by

$$G(E) = \lim_{\epsilon \to 0} (E + i\epsilon - H)^{-1}. \tag{2.17}$$

The Green's function can be represented in real space by writing it in terms of a complete set of orthonormal wavefunctions, $\psi_i(\mathbf{r})$, that are eigenfunctions of H with corresponding eigenvalue ϵ_i [24]:

$$G(\mathbf{r}, \mathbf{r}', E) = \sum_i \frac{\psi_i(\mathbf{r})\psi_i^*(\mathbf{r}')}{E - \epsilon_i}. \tag{2.18}$$

From Eqs. 2.9 & 2.18 it follows that the Green's function corresponding to the

Hamiltonian $H = -\bigtriangledown^2 + v(\mathbf{r})$ is given by the Dyson integral equation

$$G(\mathbf{r}, \mathbf{r}', E) = G_0(\mathbf{r}, \mathbf{r}', E) + \int d\mathbf{r}''\ G_0(\mathbf{r}, \mathbf{r}'', E) v(\mathbf{r}'') G(\mathbf{r}'', \mathbf{r}', E), \tag{2.19}$$

where $G_0(\mathbf{r}, \mathbf{r}', E)$ is the free particle Green's function, corresponding to the Hamiltonian $H_0 = -\bigtriangledown^2$. A useful way of solving Eq. 2.19 is to introduce the so-called t-matrix, defined by the relation

$$G(\mathbf{r}, \mathbf{r}', E) = G_0(\mathbf{r}, \mathbf{r}', E) + \int d\mathbf{r}'' \int d\mathbf{r}'''\ G_0(\mathbf{r}, \mathbf{r}'', E) t(\mathbf{r}'', \mathbf{r}''', E) G_0(\mathbf{r}''', \mathbf{r}', E). \tag{2.20}$$

From Eq. 2.19 it follows that t must satisfy

$$t(\mathbf{r}, \mathbf{r}', E) = v(\mathbf{r})\delta(\mathbf{r} - \mathbf{r}') + \int d\mathbf{r}''\ v(\mathbf{r}) G_0(\mathbf{r}, \mathbf{r}'', E) t(\mathbf{r}'', \mathbf{r}', E). \tag{2.21}$$

Recall from earlier that the muffin tin potential, $v(\mathbf{r})$, is zero outside a radius R_{MT}. This means that electrons move freely when $r > R_{MT}$ and so their energy is given by the square of their momentum. A useful consequence of this is that for the scattering problem considered here only the 'on the energy shell' components of the t-matrix need to be evaluated. To define these 'on the energy shell' components it is convenient to first express the t-matrix in a plane wave representation:

$$t(\mathbf{k}, \mathbf{k}', E) = \int d\mathbf{r} \int d\mathbf{r}' e^{-i\mathbf{k}\cdot\mathbf{r}} t(\mathbf{r}, \mathbf{r}', E) e^{i\mathbf{k}'\cdot\mathbf{r}'}. \tag{2.22}$$

In this representation, being 'on the energy shell' simply means that the wavevectors $\mathbf{k}, \mathbf{k}'$ satisfy $k^2 = k'^2 = E$. When this condition is met, it follows that

$$t(\mathbf{k}, \mathbf{k}', E) = \sum_{L,L'} i^{-l+l'} (4\pi)^2 Y_L(\hat{\mathbf{k}}) t_{L,L'}(E) Y^*_{L'}, (\hat{\mathbf{k}}') \tag{2.23}$$

where the angular momentum components of the 'on the energy shell' t-matrix $t_{L,L'}$ are defined as

$$t_{L,L'} = \int d\mathbf{r} \int d\mathbf{r}'\ j_l(\sqrt{E}r) Y^*_L(\hat{\mathbf{r}}') t(\mathbf{r}, \mathbf{r}', E) Y_{L'}(\hat{\mathbf{r}}') j_{l'}(\sqrt{E}r) \tag{2.24}$$

and the expansion

$$e^{i\mathbf{k}\cdot r} = 4\pi \sum_{L} i^l j_l(kr) Y_L^*(\hat{\mathbf{k}}) Y_L(\hat{\mathbf{r}}) \tag{2.25}$$

has been used [25], where j_l is a spherical bessel function. For a spherical symmetric potential, e.g. a muffin tin potential, the t-matrix is diagonal and takes the form $t_{LL'}(E) = t_L(E)\delta_{LL'}$. These t-matrix components, t_L, are related to the scattering amplitudes, f_l, which, by Eq. 2.16, are related in turn to the phase shifts [26]:

$$t_L(E) = -\frac{1}{\sqrt{E}} f_l(E) = -\frac{1}{\sqrt{E}} \sin\delta_l e^{i\delta_l}. \tag{2.26}$$

From the earlier discussion about phaseshifts, it follows that the 'on the energy shell' t-matrix provides a complete description of the single-site scattering problem. The t-matrix also plays a central role in the multiple scattering problem, which will be outlined now.

In the multiple scattering problem the single-site potential, $v(\mathbf{r})$, is replaced by a potential $V(\mathbf{r}) = \sum_i v_i(\mathbf{r} - \mathbf{R_i})$, where $v_i(\mathbf{r} - \mathbf{R_i})$ is a muffin-tin potential centred at $\mathbf{R_i}$. The muffin-tin potentials are assumed to be non-overlapping, hence one scattering event is completely over before the next begins. This means that only 'on the energy shell' scattering needs to be dealt with. The first step in the mathematical treatment of the multiple-scattering problem is to define a scattering matrix, T, for the potential $V(\mathbf{r})$, which, by analogy with Eq. 2.20, satisfies

$$G(\mathbf{r}, \mathbf{r}', E) = G_0(\mathbf{r}, \mathbf{r}', E) + \int d\mathbf{r}'' \int d\mathbf{r}''' \; G_0(\mathbf{r}, \mathbf{r}'', E) T(\mathbf{r}'', \mathbf{r}''', E) G_0(\mathbf{r}''', \mathbf{r}', E), \tag{2.27}$$

where G is the Green's function for the Hamiltonian $H = -\bigtriangledown^2 + V(\mathbf{r})$. G_0 is the free-particle Green's function, which describes the propagation of electrons in free space from one scattering site to another. For $\mathbf{r}$ in the muffin-tin sphere surrounding $\mathbf{R}_i$ and $\mathbf{r}'$ in the muffin-tin sphere surrounding $\mathbf{R}_j$ with $i \neq j$ it is

given by [26]

$$G_0(\mathbf{r},\mathbf{r}',E) = \sum_{LL'} i^l j_l(\sqrt{E} \mid \mathbf{r}-\mathbf{R}_i \mid) Y_L(\widehat{\mathbf{r}-\mathbf{R}_i}) G_{0,LL'}(\mathbf{R}_i-\mathbf{R}_j,E)\times \\ Y^*_{L'}(\widehat{\mathbf{r}'-\mathbf{R}_j}) j_{l'}(\sqrt{E} \mid \mathbf{r}'-\mathbf{R}_j \mid)(-i)^{l'}, \tag{2.28}$$

where $G_{0,LL'}$ are so-called *structure constants*, which depend only on the spatial arrangements of the scatterers and are given by

$$G_{0,LL'}(\mathbf{R}_i-\mathbf{R}_j,E) = -4\pi i\sqrt{E}\sum_{L''} i^{l''} C^{L''}_{LL'}\; h^+_{l''}(\sqrt{E} \mid \mathbf{R}_i-\mathbf{R}_j \mid) Y_{L''}(\widehat{\mathbf{R}_i-\mathbf{R}_j}), \tag{2.29}$$

where $h^+_{l''}$ is a Hankel function and $C^{L''}_{LL'}$ is a Gaunt number defined by

$$C^{L''}_{LL'} = \int d\Omega\; Y^*_L(\Omega) Y_{L'}(\Omega) Y_{L''}(\Omega). \tag{2.30}$$

From Eq. 2.27 it follows that the scattering matrix, T, satisfies the operator equation

$$T = V + VG_0T. \tag{2.31}$$

A useful way of solving Eq. 2.31 is to introduce the *scattering path operator*, τ^{ij}, defined by [27]

$$\tau^{ij}(E) = v_i\delta_{ij} + \sum_k v_i G_0(E)\tau^{kj}(E). \tag{2.32}$$

The scattering path operator τ^{ij}, if operated on an incoming wave at the jth site, gives the outgoing wave from the i site. Identifying $\sum_{ij}\tau^{ij}$ with T and summing over all i and j in Eq. 2.32 gives Eq. 2.27. Hence Eq. 2.32 is an equivalent way of stating the multiple scattering problem. Rearranging Eq. 2.32 gives

$$\tau^{ij} = t_i\delta_{ij} + \sum_{k\neq i} t_i G_0 \tau^{kj}, \tag{2.33}$$

where

$$t_i = (1 - v_i G_0)^{-1} v_i. \tag{2.34}$$

Equation 2.34 is clearly just an operator version of the equation for the single-site t-matrix (Eq. 2.21). Hence, t_i is identified as being the t-matrix for the single-site potential v_i. The 'on the energy shell' components of $\tau^{ij}(\mathbf{r},\mathbf{r}',E) \equiv (< \mathbf{r} \mid \tau^{ij}(E) \mid \mathbf{r}' >$ can be defined in an analogous way to Eq. 2.23:

$$\tau^{ij}_{L,L'}(E) = \int d\mathbf{r}_i \int d\mathbf{r}'_j \; j_l(\sqrt{E}r_i) Y^*_L(\hat{\mathbf{r}}_i) \tau^{ij}(\mathbf{r}_i,\mathbf{r}'_j,E) Y_{L'}(\hat{\mathbf{r}}'_j) j_{l'}(\sqrt{E}r'_j), \quad (2.35)$$

where L and L' are the angular momenta about sites i and j respectively and $\mathbf{r}_i = \mathbf{r} - \mathbf{R}_i$ and $\mathbf{r}'_j = \mathbf{r}' - \mathbf{R}_j$. From Eq. 2.33 it follows that [25]

$$\tau^{ij}_{L,L'}(E) = t_{i,L}(E)\delta_{ij}\delta_{LL'} + \sum_{k\neq i}\sum_{L''} \; t_{i,L}(E) G_{0,LL'}(\mathbf{R}_i - \mathbf{R}_k, E) \tau^{kj}_{L'',L'}(E), \quad (2.36)$$

where use has been made of Eq. 2.28.

Consider now the case where the single-site scatterers are effective ions on a regular Bravais lattice. For a pure metal $t_L(E)$ will be the same on every site and hence, from Eq. 2.36, $\tau^{ij}_{L,L'}(E)$ will depend on i and j only through the vector distance $\mathbf{R}_i - \mathbf{R}_j$. This means that the lattice Fourier transform of $\tau_{L,L'}$ can be taken, defined by

$$\tau_{L,L'}(\mathbf{k},E) = \frac{1}{N}\sum_{ij} e^{i\mathbf{k}\cdot(\mathbf{R}_i - \mathbf{R}_j)} \tau^{ij}_{L,L'}(E), \quad (2.37)$$

where N is the total number of lattice sites and the vector $\mathbf{k}$ is restricted to the first Brillouin zone. $\tau_{L,L'}(\mathbf{k},E)$ is periodic in reciprocal space, i.e. $\tau_{L,L'}(\mathbf{k}+\mathbf{G},E) = \tau_{L,L'}(\mathbf{k},E)$ for all reciprocal lattice vectors, $\mathbf{G}$. The transformation of $\tau_{L,L'}(\mathbf{k},E)$ back to real space is given by

$$\tau^{ij}_{L,L'}(E) = \frac{1}{\Omega_{BZ}} \int_{BZ} \mathbf{dk} e^{-i\mathbf{k}\cdot(\mathbf{R}_i - \mathbf{R}_j)} \tau_{L,L'}(\mathbf{k},E), \quad (2.38)$$

where Ω_{BZ} is the volume of the Brillouin zone. Taking the lattice Fourier transform of the structure constants,

$$G_{0,LL'}(\mathbf{k},E) = \frac{1}{N}\sum_{ij} e^{-i\mathbf{k}\cdot(\mathbf{R}_i - \mathbf{R}_j)} G_{0,LL'}(\mathbf{R}_i - \mathbf{R}_k, E), \quad (2.39)$$

it follows from Eq. 2.36 that

$$\tau_{L,L'}(\mathbf{k},E) = [\underline{t}^{-1}(E) - \underline{G_0}(\mathbf{k},E)]^{-1}, \tag{2.40}$$

where $\underline{t}^{-1}(E)$ is a diagonal matrix with elements $t_L^{-1}(E)$ and $\underline{G_0}(\mathbf{k},E)$ stands for the matrix $G_{0,LL'}(\mathbf{k},E)$. Since the action of τ is to generate scattered waves from incident waves, a divergence will signify that there is a scattered wave even in the absence of an incident wave, i.e. a stationary state of the system. From Eq. 2.40 a divergence will occur when

$$\parallel t_L^{-1}(E)\delta_{LL'} - G_{0,LL'}(\mathbf{k},E) \parallel = 0. \tag{2.41}$$

This is the KKR secular equation, from which the band structure of a periodic crystal can be determined. In particular, the eigenenergies of a system at a given $\mathbf{k}$ correspond to those energies for which the determinant is zero when evaluated for that $\mathbf{k}$.

To conclude this section a quick outline will be given now on how the KKR method is used to solve the self-consistent problem posed by the Kohn-Sham equations, 2.4 and 2.5. It can be shown [28] that the electron charge density, $n(\mathbf{r})$, is related to the Green's function, $G(\mathbf{r},\mathbf{r}',E)$, by

$$n(\mathbf{r}) = -\frac{1}{\pi}\int_{-\infty}^{E_F} dE\ \mathrm{Im}G(\mathbf{r},\mathbf{r},E), \tag{2.42}$$

where E_F is the Fermi energy. Hence once the Green's function for the Kohn-Sham Hamiltonian, $H^{\mathrm{KS}} = -\frac{1}{2}\bigtriangledown^2 + v_{eff}^{\sigma}(\mathbf{r})$, has been evaluated the charge density can be determined by Eq. 2.42, from which a new effective potential can be obtained via Eq. 2.5. This effective potential can be used to construct a new Kohn-Sham Hamiltonian, $H^{\text{KS-new}}$. The whole cycle can then be repeated, i.e a new charge density can be evaluated using the Green's function for the Hamiltonian $H^{\text{KS-new}}$,

from which a new effective potential can be generated *et cetera*. This process can be continued until self-consistency is achieved. In practice, however, the effective potential obtained from Eq. 2.5 is usually mixed with the effective potentials from previous iterations before being used to construct the new Kohn-Sham Hamiltonian. This makes the self-consistency scheme more stable and usually leads to quicker convergence [29].

The evaluation of the Green's function, $G(\mathbf{r}, \mathbf{r}, E)$, is by far the most demanding part of the self-consistency scheme described above . A useful expression for the Green's function when $\mathbf{r}$ is in the neighbourhood of the ith scatterer and $\mathbf{r}'$ is in the neighbourhood of the jth scatterer is [30]

$$G(\mathbf{r}, \mathbf{r}', E) = \sum_{LL'} Z_L^i(\mathbf{r}_i, E)\tau_{L,L'}^{ij}(E)Z_{L'}^j(\mathbf{r}'_j, E) - \delta_{ij}\sum_L Z_L^i(\mathbf{r}_<, E)J_L^i(\mathbf{r}_>, E), \tag{2.43}$$

where Z_L^n and J_L^n are respectively the regular and irregular solutions to the Schrödinger equation 2.9 for the potential $v_n(\mathbf{r}_n)$ and $\mathbf{r}_<(\mathbf{r}_>)$ is the vector smaller (larger) in magnitude from the pair $(\mathbf{r}, \mathbf{r}')$. With the Green's function written in this form it is clear that solving the multiple-scattering equation (2.36) is an essential part of the self-consistency scheme. More specifically, Eqs. 2.42 and 2.43 show that in order to obtain the charge-density, $n(\mathbf{r})$, it is necessary to evaluate the site-diagonal scattering path operator, $\tau_{L,L'}^{ii}$. For the special case of a pure metal $\tau_{L,L'}^{ii}(E)$ is given by the Brillouin zone integral of Eq. 2.40:

$$\tau_{L,L'}^{ii}(E) = \frac{1}{\Omega_{BZ}}\int d\mathbf{k}\ \tau_{L,L'}(\mathbf{k}, E) = \frac{1}{\Omega_{BZ}}\int d\mathbf{k}\ [\underline{t}^{-1}(E) - \underline{G_0}(\mathbf{k}, E)]^{-1}_{L,L'} \tag{2.44}$$

In the next section the site-diagonal scattering path operator will be derived for another special case, namely that of substitutionally disordered alloy.

2.3 Substitutionally Disordered Alloys

In a substitutional alloy the scattering centres (atomic sites) occupy a regular Bravais lattice. However, unlike a pure metal, there is more than one type of scattering potential and, moreover, these different types of scattering potential are distributed randomly amongst the lattice sites. Substitutional alloys are therefore examples of *disordered* systems. In this thesis many different types of disorder will be encountered. The simplest case is that of two metals mixing together to form a random binary alloy, such as gadolinium and yttrium which will be investigated in chapter 7. Magnetic disorder, arising from thermally randomised magnetic moments, will be encountered throughout this thesis and will be discussed in detail in chapter 5. Finally valency disorder, where all lattice sites are occupied by the same element but the number of valence electrons varies between sites, will be discussed during the analysis of cerium in chapter 4. It turns out that all these types of disorder can be dealt with using methods underpinned by the substitutional alloy formalism which will be presented now. In order to prevent the algebra becoming too cumbersome, the following discussions will focus on the case where each scattering site is occupied either by a potential $v^A(\mathbf{r}-\mathbf{R_i})$, with probability c, or a potential $v^B(\mathbf{r}-\mathbf{R_i})$, with probability 1-c. The arguments which will be presented, however, are all valid in the more general substitutional alloy problem, where there are more than two types of scattering potential.

Probably the simplest way of solving the substitutional alloy problem is to use the *rigid band model* [31]. In this model the difference between the two potentials, v^A and v^B, is neglected. This means that when two metals, A and B, are alloyed together it is assumed that the states of the pure metal A are the same as those of the pure metal B or any A-B alloy. The only difference between

the systems is the number of electrons per atom. Although this is quite a drastic approximation, the original application of the rigid band model to CuNi alloys was remarkably successful in describing the magnetic properties of these systems. It has since been recognised, however, that the rigid band model generally gives a poor description of the physics of alloy systems [32] and should only be used in the *rigid band limit*, where the potentials of the alloy constituents are nearly identical. A more sophisticated approach to the problem is the *Virtual Crystal approximation (VCA)*. Here, an average potential, $\overline{v}(\mathbf{r}) = cv^A(\mathbf{r}) + (1-c)v^B(\mathbf{r})$, is associated with every scattering site. Unlike the rigid band model, the VCA gives exact results in the case of $c = 0$ or 1. However, it still misses out a lot of the physics associated with alloy systems. In particular within the VCA electron states, averaged over all configurations, have an infinite lifetime, whereas in real alloy systems electron states are expected to decay due to the random distribution of the scattering potentials. The infinite lifetime of states in the VCA model corresponds to the fact that the effective scatterers are elastic [33]. If, rather than averaging the potentials, the scattering amplitudes are averaged on each site, the effective scatterers obtained are inelastic and hence electron states have a finite lifetime. This is the *averaged t-matrix approximation (ATA)* [34], where an effective scattering amplitude $\overline{f}_l(E) = cf_l^A(E) + (1-c)f_l^B(E)$ is associated with every site. The ATA provides a much better description of averaged electronic structure than the VCA, e.g. yielding split band behaviour between A and B subbands, something which the VCA is unable to do [24]. It thus serves as a useful first approximation for studying alloy systems. However, the Herglotz analytic property [35] of the Green's function is not maintained by the ATA [36], which means that negative densities of states can occur. Such physically meaningless results do not arise in a more sophisticated theory of disorder, which

will now be outlined.

Both the VCA and the ATA involve replacing the disordered alloy system by an effective medium, consisting of an ordered array of effective scatterers which mimic the effect of the true alloy system on the average. In these approximations the medium is specified in terms of some average over a physical quantity, i.e. either the scattering potential or the scattering amplitude. A more abstract way of obtaining an effective medium is to determine it self-consistently. Such an approach was taken by Soven [37], who defined an effective medium by the requirement that averages over the occupation of a site embedded in the effective medium should yield quantities which are identical to that associated with a site of a medium itself. This has since become known as the *Coherent Potential Approximation (CPA)* and, when used in a multiple-scattering theory context, the resulting formalism is called the KKR-CPA [38, 39, 40]. Since the averages performed in the CPA involve only the occupation of a single site the CPA is a *single-site approximation*.

Formally, the KKR-CPA begins by associating some coherent potential, $v^c(\mathbf{r}-\mathbf{R_i})$, to every lattice site. Then, on one of the lattice sites, the coherent potential is replaced by $v^\alpha(\mathbf{r}-\mathbf{R_i})$, where $\alpha = A$ or B. An *impurity problem* is hence set up, where there is a single A or B impurity in an otherwise pure coherent potential lattice. Since the coherent potential lattice is translationally invariant the problem does not depend on the choice of impurity site. So, without loss of generality, it is assumed that the impurity is at the 0th site. Let $\widetilde{t}$ be the single-site matrix which describes scattering due to impurities in the pure coherent potential lattice. At the 0th site $\widetilde{t}$ is given by:

$$\widetilde{t}^{\alpha,0} = (v_0^\alpha - v_0^c) + (v_0^\alpha - v_0^c) G^c \widetilde{t}^{\alpha,0}, \tag{2.45}$$

where G^c is the Green's function of the pure coherent potential lattice. By definition, $\widetilde{t}$ will be zero for sites embedded in the effective medium. Hence the CPA condition says that the average of $\widetilde{t}^{\alpha,0}$ with respect to the occupation, α, must also be zero, i.e.:

$$c\widetilde{t}^{A,0} + (1-c)\widetilde{t}^{B,0} = 0. \tag{2.46}$$

The Green's function for the impurity problem described above, G^α, can be written in terms of the Green's function for the coherent potential lattice, G^c:

$$G^\alpha = G^c + G^c\widetilde{t}^{\alpha,0}G^c. \tag{2.47}$$

Using Eq. 2.46 it follows that

$$G^c = cG^A + (1-c)G^B. \tag{2.48}$$

Alternatively, G^α can be expressed in terms of the free-space Green's function G_0:

$$G^\alpha = G_0 + G_0T^\alpha G_0, \tag{2.49}$$

where T^α is the total T-matrix for the system, describing scattering by both the coherent potentials, v^c and the impurity potential v^α. Substituting Eq. 2.49 into Eq. 2.48 it follows that

$$T^c = cT^A + (1-c)T^B, \tag{2.50}$$

where T^c is the total scattering matrix for the pure coherent potential lattice and satisfies:

$$G^c = G_0 + G_0T^cG_0. \tag{2.51}$$

Equation 2.50 is often used to define the KKR-CPA, e.g. in references [41] and [28] . Physically Eq. 2.50 says that, on the average, an impurity potential causes no extra scattering when embedded into the effective medium.

Consider now the multiple-scattering equation (2.36) for the pure coherent potential lattice. Since the scattering potential, v^c, is the same on every site the solution of the multiple-scattering equation corresponds to that of a pure metal, i.e.:

$$\tau^{c,00}_{L,L'}(E) = \frac{1}{\Omega_{BZ}} \int d\mathbf{k} \; [(\underline{t^c})^{-1}(E) - \underline{G_0}(\mathbf{k}, E)]^{-1}_{L,L'} \; , \tag{2.52}$$

where $(\underline{t^c})^{-1}$ is a diagonal matrix with elements, $(t^c_L)^{-1}$, where t^c is the single site t-matrix for the coherent potential v^c. In the impurity problem the scattering potentials are site dependent and the t-matrices are given by $t_{i,L} = t^c_L + (t^\alpha_L - t^c_L)\delta_{i0}$. This means that the impurity site-diagonal scattering path operator, $\tau^{\alpha,00}_{L,L'}(E)$, cannot be expressed in a simple form like Eq. 2.52. However, by considering the full matrix form of the scattering path operators $\tau^{\alpha,ij}_{L,L'}(E)$ and $\tau^{c,ij}_{L,L'}(E)$ and applying some simple algebra [42] it is possible to express $\tau^{\alpha,00}_{L,L'}(E)$ in terms of $\tau^{c,00}_{L,L'}(E)$:

$$\tau^{\alpha,00}_{L,L'}(E) = \left(\tau^{c,00}[1 + [(t^\alpha)^{-1} - (t^c)^{-1}]\tau^{c,00}]^{-1}\right)_{LL'} \tag{2.53}$$

Equations 2.52 and 2.53 both involve the, as-yet, undetermined quantity t^c. In order to form a closed set of equations the CPA condition, Eq. 2.50, needs to be used. To use this condition recall that $T = \sum_{ij} \tau^{ij}$. It follows immediately then that

$$\tau^{c,00}_{L,L'}(E) = c\tau^{A,00}_{L,L'}(E) + (1-c)\tau^{B,00}_{L,L'}(E). \tag{2.54}$$

Equation 2.54 is a self-consistency criterion for the multiple-scattering substitutional alloy problem. It can be used in conjunction with the usual Kohn-Sham potential self-consistency procedure to generate a fully self-consistent scheme for calculating the electronic structure of substitutionally disordered systems. The central quantities of such a *self-consistent field* KKR-CPA (SCF-KKR-CPA) scheme are the partially averaged charge densities, $\overline{n}^A(\mathbf{r})$ and $\overline{n}^B(\mathbf{r})$. The partially aver-

aged charge density $\overline{n}^{\alpha}(\mathbf{r})$ is defined formally by evaluating the charge density at a site and then averaging over all possible alloy configurations, with the restriction that, at that particular site, the potential is always v^{α} . $\overline{n}^{A}(\mathbf{r})$ and $\overline{n}^{B}(\mathbf{r})$ can be thought of as being the charge density at an "average" A or B site, i.e. at an A or B site embedded in the effective CPA medium. They can be calculated via Eqs. 2.42 and 2.43, with the Green's function appropriately averaged over possible alloy configurations. For details about the implementation of a SCF-KKR-CPA scheme see reference [41].

In summary, we have shown in this section how the first-principles DFT scheme can be used to treat substitutionally disordered alloys. At this stage, however, we are still extremely limited as to which systems and phenomena we can actually describe using the DFT. For example, since DFT is a groundstate, $T = 0$, theory we are not able to describe systems in an excited, $T > 0$, state. In particular, the DFT theory does not take into account the effects of thermally activated spin fluctuations. We address this shortcoming in chapter 5. Aside from this, the LDA implementation of DFT has often been found to be inappropriate for describing the groundstate of systems with partially filled d or f shells. For example, application to the insulating transition metal oxides gives too small or zero band gaps [43]. The equilibrium volume, bulk moduli and cohesive energies of the lanthanide elements are also found to be in poor agreement with experiment [44]. The LDA also underestimates the stability of the antiferromagnetic phase of the high temperature oxide superconductors [45]. These issues will be addressed in the next chapter, where we outline attempts to go beyond the LDA implementation of DFT.

Chapter 3

Theoretical Treatments of Strongly-Correlated Systems

The previous chapter was concluded with a list of failings of the LDA, amongst which was its inability to describe the insulating groundstate of the transition metal oxides (TMOs). In order to explain this failure, as well as some of the other failings of the LDA, we must first understand what drives the insulating behaviour of these materials. In the theory of noninteracting or weakly interacting electron systems, where the band structure is determined only by the periodic lattice arrangement of the atoms, it is the filling of electron bands that determines whether or a system is metallic or insulating. For metals the highest occupied band is partially filled, meaning that there are states at the Fermi level, whereas for insulators the highest occupied band is completely filled and the Fermi level lies in a gap. Since TMOs have a partially filled d shell they are hence predicted to be metallic within this simple picture. The fact that they are observed to be insulating thus suggests that whatever effect it is that is driving this behaviour must be missing from the weakly interacting theory. It was Peierls [46] who first

pointed out the importance of electron-electron correlations and who suggested that strong Coulomb repulsions between electrons could be responsible for the insulating behaviour of these materials. Such correlation effects are most easily understood in terms of the Hubbard model [47], where we consider only a single orbital with room for two electrons. The Hamiltonian, in second-quantised form, for this model is

$$H = -\sum_{ij,\sigma} t_{ij} c^{\dagger}_{i\sigma} c_{j\sigma} + U \sum_{i} n_{i\uparrow} n_{i\downarrow}, \tag{3.1}$$

where t_{ij} describes electron hopping between sites i and j and U is the Coulomb repulsion between two electrons occupying the same site. $c^{\dagger}_{i\sigma}$ and $c_{i\sigma}$ are respectively the creation and annihilation operators for an electron of spin σ at site i and the number operator $n_{i\sigma} \equiv c^{\dagger}_{i\sigma} c_{i\sigma}$. For $t \gg U$ this model reduces to the noninteracting band theory. For $U \gg t$ hopping is completely suppressed and the model corresponds to an atomic like picture, with electrons bound to one particular atom. In the intermediate regime electrons are able to hop between sites, but their motions are significantly affected by the U Coulomb repulsion. In particular, there will be an energy cost U associated with double occupancy of the orbital. This will hinder the movement of the electrons and they can be said to move in a *correlated* way. A correlation energy gap, of the order of U, will open up between singly and doubly occupied orbitals (the so-called lower and upper Hubbard bands). Mott [48] suggested that such a gap would occur in the d-band of NiO, an archetypal TMO, to which the insulating behaviour of the system could be ascribed. Such systems have since been termed *Mott-Hubbard insulators*. However, more recent work [49] has discussed the importance of an oxygen ligand p band which appears between the lower and upper Hubbard bands in several of the TMOs and these systems have been reclassed as *charge transfer-insulators*. The term *Mott insulator*

is used now in a broad sense to describe any system whose insulating behaviour is driven by correlation effects.

Having established the origin of the band gaps in the TMOs, it becomes clear as to why the LDA fails to describe such systems. Specifically the LDA exchange-correlation functional, which depends only on the local electron density, is not able to take into account the correlated motion of the electrons. Generally speaking, *Strongly-Correlated* systems contain electrons that are neither fully itinerant, i.e. propagate as Bloch waves and for which the LDA is a good approximation, nor fully localised, for which a core-treatment is appropriate. In this chapter we describe several attempts to extend the LDA to this so-called middle ground, between the **k**-space band like and real-space atomic like pictures. In section 3.2 we focus on one particular approach, the self-interaction correction (SIC), which is the method that we employ in this thesis. For recent, more extensive reviews of the strongly-correlated electron problem, see references [5, 50].

3.1 Beyond the LDA

Perhaps the simplest approach to improving the LDA functional is to incorporate *gradient corrections*, i.e. derivatives of the electron density. Such corrections take into account local inhomogeneities in the electron gas, which may be substantial in systems containing highly localised states, where electrons densities are strongly peaked. The first attempt at expanding the exchange-correlation energy functional in terms of derivatives of the electron density was made by Hohenberg and Kohn [51]. Their *gradient expansion approximation* (GEA) was found not to offer much improvement over the LDA, often making the errors even worse. Progress in understanding the failure of the GEA was made by performing a wavevector

decomposition [52] of the energy difference $\delta E \equiv E_{xc} - E_{xc}^{LDA}$ between the true exchange correlation energy E_{xc} and the LDA result E_{xc}^{LDA}:

$$\delta E = \int d\mathbf{k}\ \delta E(\mathbf{k}). \tag{3.2}$$

For small enough values of k, the corresponding wavelength $\lambda = 2\pi/k$ will be larger than some characteristic length scale over which the electron density varies and so the LDA will be a good approximation. Thus, for $k \sim 0$, $\delta E(k) \approx 0$ and the gradient corrections should go to zero. The GEA, however, was actually found to give large contributions for k values in this range. Langreth and Mehl (LM) [53] corrected for this by introducing a cutoff wavevector, below which the gradient corrections were put to zero. A somewhat different approach was taken by Perdew and Wang [54], who proposed an exchange energy functional based not on a gradient expansion of the energy itself, but of the exchange-hole density. In their generalised gradient approximation (GGA), a real-space cutoff is used to enforce all conditions satisfied by the exact exchange-hole. In particular, the exchange-hole sum rule and a non-positive exchange hole density, both of which are obeyed by the LDA but which fail in the GEA, are satisfied in the GGA. The LM and GGA approaches both give significant improvements over the LDA, e.g. reducing by on average a half the errors in the calculated ground-state properties of the third-row elements [55], with the GGA being the slightly more accurate of the two approximations.

Although the GGA has proved to be extremely successful at computing ground-state properties, e.g. lattice parameters and bulk-moduli, it has failed to show much improvement over the LDA for quasiparticle energies [56], i.e. the excitation energies measured in photoemission experiments. Within DFT these energies are associated with the Kohn-Sham eigenvalues, however, since DFT is

a groundstate theory, there is no theoretical justification for this. Indeed, in order to properly calculate excitation energies a many-body Green's function approach should be used. Here, the quasiparticle energies E_i are obtained from the equation

$$[\frac{1}{2} \bigtriangledown^2 + V_H(\mathbf{r}) + V_{ext}(\mathbf{r})]\Psi_i(\mathbf{r}) + \int \mathbf{dr}'\Sigma(\mathbf{r}, \mathbf{r}'; E_i)\Psi_i(\mathbf{r}') = E_i\Psi_i(\mathbf{r}), \quad (3.3)$$

where V_H is the Hartree potential and V_{ext} is some one-body external potential. The self-energy operator Σ connects the full many body Greens function, G, to that where only one-body interactions are included, G_0, through the Dyson equation

$$G = G_0 + G_0\Sigma G. \quad (3.4)$$

Comparing equation 3.3 to the Kohn-Sham equation, Eq. 2.4, it is clear that the exact DFT exchange-correlation potential, V_{xc}, can be viewed as a local and energy-independent approximation to the self-energy operator. The inclusion of nonlocality and energy-dependent, dynamic correlations in the self-energy operator is important in describing quasiparticles. Hedin [57] proposed an approximation scheme for calculating the self-energy, based upon its expansion in the screened Coulomb potential, W. In the GW-approximation (GWA) only the first term of this expansion is used and the self-energy is given by

$$\Sigma(\mathbf{r}, \mathbf{r}'; \omega) = \frac{i}{2\pi} \int d\omega' \; G(\mathbf{r}, \mathbf{r}'; \omega + \omega')W(\mathbf{r}, \mathbf{r}'; \omega')e^{i\delta\omega'}. \quad (3.5)$$

In practical applications of the GWA it is useful to take the Green's function G_0 to be that corresponding to the LDA hamiltonian. The Dyson equation, Eq. 3.4, becomes then

$$G = G_0 + G_0\Delta\Sigma G, \quad (3.6)$$

where

$$\Delta\Sigma = \Sigma - V_{xc}. \quad (3.7)$$

The screened Coulomb potential W takes the form [58]

$$W(\mathbf{r}, \mathbf{r}'; \omega) = \int d\mathbf{r}'' \; \epsilon^{-1}(\mathbf{r}, \mathbf{r}''; \omega)\nu(|\mathbf{r}'' - \mathbf{r}'|), \tag{3.8}$$

where ν is the bare Coulomb potential and ϵ is the dielectric function. A zeroth evaluation of the screened potential, W_0, can be performed by using in Eq. 3.8 the dielectric function obtained from the Green's function G_0. Feeding G_0 and W_0 into Eq. 3.5 gives an initial estimate of the self-energy, $\Delta\Sigma_0 = iG_0W_0$. In principle the full Green's function G should then be calculated from Eq. 3.6, from which a new screened potential W and a new estimate of the self-energy, $\Delta\Sigma = iGW$, can be obtained. The scheme should then be continued until self-consistency is achieved, i.e. until the Green's function used to evaluate the self-energy agrees with the Green's function outputted from Eq. 3.6. However, since this self-consistency scheme is computationally very demanding, usually only the zeroth evaluation of the self-energy operator, $\Delta\Sigma_0$, is performed. Nonetheless, the GWA has proved to be very successful at reproducing excitation spectra. For example the band-gaps in semiconductors [59] and transition metal oxides [60], which are underestimated in the LDA, are found to be in good agreement with experiment.

A simpler approach for introducing non-locality into the self-energy operator, albeit without any frequency dependence, is to make the Kohn-Sham potentials orbital dependent. In the LDA+U approach [61] certain sets of orbitals, say the 3d or 4f, or identified as having largely atomic like characteristics and are treated in a non-LDA manner. In particular they are treated using a mean field Hartree-Fock type approximation, where the Coulomb interaction is taken into account by a term of the form $\frac{1}{2}U\sum_{i\neq j} n_i n_j$, where U is the Hubbard interaction parameter and n_i are orbital occupancies. A key assumption of the LDA+U approach is that the Coulomb energy as a function of the total number of electrons

$N = \sum n_i$ given by the LDA is a good approximation, such that this energy is given by $UN(N-1)/2$. Subtracting this away from the total LDA energy and replacing it with the Hubbard interaction term gives [62]

$$E = E^{LDA} - UN(N-1)/2 + \frac{1}{2}U\sum_{i\neq j} n_i n_j. \tag{3.9}$$

Taking the derivative of this energy functional with respect to the charge density, $n_i(\mathbf{r})$, of some particular orbital i leads to the following effective potential:

$$V_i(\mathbf{r}) = V^{LDA}(\mathbf{r}) + U(\frac{1}{2} - n_i). \tag{3.10}$$

The dependence of V_i on n_i means that the potential is orbital dependent, which opens up the possibility of broken symmetry, i.e. orbital polarised solutions. From Eq. 3.10 it is clear that the LDA+U potential is shifted with respect to its LDA value by $-U/2$ for occupied orbitals ($n_i = 1$) and $+U/2$ for unoccupied orbitals ($n_i = 0$). This will lead to the formation of lower and upper Hubbard bands, separated by U, thus reproducing the physics of Mott-Hubbard insulators. Such splitting between occupied and unoccupied orbitals is also obtained in the self-interaction correction method, which we outline in the next section. An advantage of this approach is that it does not require the on-site Coulomb parameter U to be inputted. Indeed, since this parameter is often obtained using experimental data, the LDA+U method can not be considered a true *ab initio* method.

Before going on to introduce the self-interaction correction, we describe one further method for incorporating strong electron correlations, the discussion of which will raise many ideas pertinent to this thesis. The CPA technique, which we described in section 2.3, is based around reducing a complicated lattice problem, namely that of compositional disorder, to an effective single-site problem. In the limit of infinite dimensions, such a single-site, mean-field approach becomes

exact. With this motivation in mind, we might hope to use a mean-field approach to reduce a lattice problem with many fermionic, as opposed to compositional, degrees of freedom to a single-site effective problem with less degrees of freedom. However, in fermionic systems with metallic spin and charge excitations, dynamic quantum fluctuations are important no matter what the dimension of the system is, so even in the limit of infinite dimensions these need to be taken into account [5]. The so-called *Dynamical mean field theory* (DMFT) approach [63] provides a means for doing this. Here, spatial degrees of freedom are mapped onto a single-site problem, with dynamical fluctuations taken fully into account. The method is most easily illustrated using the Hubbard model, as defined by the Hamiltonian in Eq. 3.1 and indeed was introduced in this context [63]. Within DMFT, a single-site effective dynamics for some site 0 is associated with this Hamiltonian, and is described in terms of an effective action, $S_{\rm eff}$, for the fermionic degrees of freedom $(c^{\dagger}_{0\sigma}, c_{0\sigma})$ at that site [64]:

$$S_{\rm eff} = -\int_0^\beta d\tau \int_0^\beta d\tau' \sum_\sigma c^{\dagger}_{0\sigma}(\tau)\mathcal{G}_0^{-1}(\tau-\tau')c_{0\sigma}(\tau') + U\int_0^\beta d\tau\ n_{0\uparrow}(\tau)n_{0\downarrow}(\tau). \tag{3.11}$$

Here, $\mathcal{G}_0(\tau-\tau')$ is an effective amplitude for a fermion to be created on the site 0 at time τ and to be destroyed at time τ'. It describes the interactions of the fermionic degrees of freedom at site 0 with the external 'bath' created by all other degrees of freedom on other sites. It can be thought of as being analogous to the Weiss molecular field in magnetism, which represents the magnetic field acting on a particular site arising from the spins at all the other sites. An important difference, however, is that in the classical magnetic case the Weiss field is just a number, whereas here the 'Weiss field' $\mathcal{G}_0(\tau-\tau')$ is a function of time. This reflects the existence of many energy scales in the fermionic system, which cannot

be described with a single number.

The effective action, given in Eq. 3.11, can be used to evaluate the time-dependent Green's function, $G(\tau)$, via

$$G(\tau - \tau') \equiv - < Tc(\tau)c^{\dagger}(\tau') >_{\mathrm{S_{eff}}}, \tag{3.12}$$

where T stands for time ordered product. The energy-dependent, wavevector decomposed, Green's function can also be evaluated according to

$$G(\mathbf{k}, i\omega_n) = \frac{1}{i\omega_n + \nu - \epsilon_{\mathbf{k}} - \Sigma(i\omega_n)}, \tag{3.13}$$

where ν is the chemical potential and

$$\epsilon_{\mathbf{k}} \equiv \sum_{ij} t_{ij} e^{i\mathbf{k}\cdot(\mathbf{R}_i - \mathbf{R}_j)}, \tag{3.14}$$

i.e. the band kinetic energy for wavevector $\mathbf{k}$. The self energy, $\Sigma(i\omega_n)$, is defined by

$$\Sigma(i\omega_n) = \mathcal{G}_0^{-1}(i\omega_n) - G^{-1}(i\omega_n). \tag{3.15}$$

By summing Eq. 3.13 over all $\mathbf{k}$ values and transforming it from time representation to energy representation, it can be equated with the Green's function in Eq. 3.12. This constitutes a self consistency condition for the Green's function, which can be solved to give both G and $\mathcal{G}_0$.

A DMFT scheme for more realistic systems can be constructed by replacing the model Hamiltonian parameters $\epsilon_{\mathbf{k}}$ in Eq. 3.13 with those from some *ab initio* electronic structure Hamiltonian. In particular, an LDA Hamiltonian can be used. In such an LDA+DMFT approach [65] certain orbitals, identified as giving rise to strong correlation effects, are separated out like in the LDA+U method, and the interactions of electrons in these orbitals are treated in a non-LDA manner. In particular, the interactions are described using the self-energy operator $\Sigma(i\omega_n)$. In

a more recent development [66], the self-consistent DMFT approach was combined with a GW treatment of the self-energy.

Since DMFT takes full account of local temporal fluctuations, it offers a very sophisticated description of local spin and charge fluctuations. It turns out that, when dealing with such fluctuations within the Hubbard model, the static, i.e. non time dependent, limit of the DMFT is equivalent to a much simpler CPA scheme [67]. When introducing the CPA method in the previous chapter, we noted that it would be used in this thesis to treat high temperature magnetic fluctuations. The treatment of magnetic (spin) fluctuations that we provide can hence be considered as the static, high temperature limit of some, as yet undeveloped, DMFT. We return to discussing point in chapter 8.

3.2 The Self-Interaction Correction

In chapter 2 the many-body system energy functional, Eq. 2.3, contained a classical Hartree term, E_H, corresponding to the direct Coulomb energy of the interacting electrons:

$$E_H[n] = \frac{1}{2} \int \mathbf{dr} \int \mathbf{dr}' \, \frac{n(\mathbf{r})n(\mathbf{r}')}{|\mathbf{r} - \mathbf{r}'|}, \tag{3.16}$$

where n is the electron charge density. $E_H[n]$ evidently contains a nonphysical contribution arising from electrons interacting with themselves, corresponding to when $\mathbf{r} = \mathbf{r}'$. In an exact electronic structure theory this *self-Coulomb* energy should be cancelled by an equal but opposite *self-exchange* and *self-correlation* energy term. However in the LDA approximation, where the exchange-correlation energy is evaluated using Eq. 2.8, this cancellation is imperfect. For hydrogen, which has only one electron, all of the Coulomb energy should be cancelled. For this system this energy $\approx$ 8.5ev, but within the LDA the magnitude of the exchange-

correlation energy is only 8.1ev [68], giving an unphysical net electron-electron interaction energy.

Perdew and Zunger [9] suggested a self-interaction corrected (SIC) version of the LDA, where the spurious self-interaction energy of each occupied electron state $\varphi_{\alpha\sigma}$ is subtracted explicitly from the LDA energy functional:

$$E^{SIC-LDA}[n_\uparrow, n_\downarrow] = E^{LDA}[n_\uparrow, n_\downarrow] - \sum_{\alpha\sigma}^{\text{occ}} \delta_{\alpha\sigma}^{SIC}, \tag{3.17}$$

where $E^{LDA}[n_\uparrow, n_\downarrow]$ is the usual LDA total energy functional, defined in Eq. 2.3, and the self-interaction correction for the state $\alpha\sigma$, $\delta_{\alpha\sigma}^{SIC}$, is given by:

$$\begin{aligned} \delta_{\alpha\sigma}^{SIC} &= E_H[n_{\alpha\sigma}] + E_{xc}^{LDA}[n_{\alpha\sigma}] \\ &= \frac{1}{2}\int \mathbf{dr} \int \mathbf{dr'}\ \frac{n_{\alpha\sigma}(\mathbf{r}) n_{\alpha\sigma}(\mathbf{r'})}{|\mathbf{r}-\mathbf{r'}|} + \int \mathbf{dr}\ n_{\alpha\sigma}(\mathbf{r}) \epsilon_{xc}^{hom}(n_{\alpha\sigma}(\mathbf{r}), 0), \end{aligned} \tag{3.18}$$

where $n_{\alpha\sigma}$ is the charge density of the orbital $\varphi_{\alpha\sigma}$. The self-interaction correction energy $\delta_{\alpha\sigma}^{SIC}$ evidently depends on the choice of orbitals, $\varphi_{\alpha\sigma}$. Therefore to find the absolute energy minimum of $E^{SIC-LDA}$ it is important to properly define the sets of orbitals for which to compute the self-interaction correction. In particular when implementing the SIC for extended systems, the Kohn-Sham orbitals defined by Eq. 2.2 should not be used to evaluate the self-interaction energy since in periodic solids these can be taken as Bloch waves, which give a completely delocalised electron density for which δ^{SIC} is identically zero [69]. For spatially localised states δ^{SIC} is finite. Indeed, δ^{SIC} is sometimes taken as a quantitative measure of the degree of localisation of orbitals [70]. An appropriate representation of orbitals in which to calculate self-interaction energy is offered by *Wannier* functions. These are defined in terms of the Fourier transforms of Bloch states and are spatially localised at lattice sites [71].

Minimising the energy functional, Eq. 3.17, with respect to the orbitals $\varphi_{\alpha\sigma}$

leads to the following set of self-consistent wave equations:

$$H^{tot}_{\alpha\sigma}\varphi_{\alpha\sigma}(\mathbf{r}) = \sum_{\alpha'} \epsilon_{\alpha\alpha'}\varphi_{\alpha'\sigma}(\mathbf{r}), \tag{3.19}$$

where the Lagrange multipliers $\epsilon_{\alpha\alpha'}$ ensure the orthogonality of the orbitals $\varphi_{\alpha\sigma}$ and the effective one-body, state-dependent Hamiltonian $H^{tot}_{\alpha\sigma}$ is given by

$$H^{tot}_{\alpha\sigma} = H^{LSDA} - \delta V^{SIC}_{\alpha\sigma}(\mathbf{r}), \tag{3.20}$$

where H^{LSDA} is the usual LDA Hamiltonian, defined in Eq. 2.4, and the SIC potential, $\delta V^{SIC}_{\alpha\sigma}$, is given by

$$\delta V^{SIC}_{\alpha\sigma}(\mathbf{r}) = V_H[n_{\alpha\sigma}](\mathbf{r}) - V^{LDA}_{xc}[n_{\alpha\sigma}, 0](\mathbf{r}), \tag{3.21}$$

where the Hartree potential, V_H, and exchange-correlation potential, V^{LDA}_{xc}, are defined in equations 2.6 and 2.7 respectively. The state dependence of δV^{SIC} is important since it permits broken-symmetry solutions, in particular those where orbitals are spatially localised [72]. Equation 3.19 can be converted into a standard eigenvalue problem using the unified Hamiltonian concept [73]. When applying the LDA-SIC scheme to a crystal solid the translational symmetry of the system can be exploited and the eigenvalue problem can be solved using a $\mathbf{k}$-space band structure method, the usual one employed being the linear-muffin-tin-orbitals (LMTO) method in the atomic sphere approximation (ASA) approximation [74]. This SIC-LMTO-ASA implementation involves repeated transformations back and forth between real-space, in which the Wannier orbitals $\varphi_{\alpha\sigma}$ are represented, and $\mathbf{k}$-space, in which the eigenvalue problem is solved. When performing self-consistent calculations various atomic configurations can be assumed, corresponding to different numbers of localised states. These localised states have the freedom to relax during the self-consistency procedure, which ensures that the most optimal

set of orbitals is used to calculate the SIC potential [75]. The various atomic configurations constitute local minima of the energy functional $E^{SIC-LDA}$. If no localised states are assumed the energy minimum attained coincides with the usual LDA minimum. The groundstate of a system is found by comparing the local energy minima of the different configurations and is determined by a competition between SIC energy, which an electron state needs to spatially localise to benefit from, and band formation energy, which an electron loses when it localises as it can no longer hybridise with conduction electron bands [76].

The SIC-LMTO-ASA has proved to be a very successful method, overcoming many of the failures of the conventional LDA. In particular it correctly predicts many of the transition metal oxides to be wide-gap insulators, due to a splitting of the occupied and unoccupied states by the on-site Coulomb interaction, U. In addition, the SIC has provided a useful scheme for determining valency. Associating valency with the number of electrons available for band formation it follows that the number of valence electrons, N_{val}, associated with a particular SIC configuration is given by

$$N_{val} = Z - N_{core} - N_{SIC}, \tag{3.22}$$

where Z is the atomic number, N_{core} is the number of atomic core electrons and N_{SIC} is the number of self-interaction corrected, i.e. localised, electrons [77]. The valency of a system can hence be found by minimising Eq. 3.17 with respect to N_{SIC}. This scheme has been used to has determine the nominal valency of ions in a wide range of systems, e.g. high T_c superconductors [2], rare earths [78] and actinides [79].

Despite the aforementioned success of the SIC-LMTO-ASA method there has been a pressing need to devise an alternative implementation of the SIC. The

reasons for this are twofold. First, the implementation of the SIC-LMTO-ASA is quite cumbersome, due to both a real-space representation being used for Wannier orbitals and a $\mathbf{k}$-space representation being used to solve the eigenvalue problem. A simpler version of the SIC, which is less computationally demanding, is thus desirable. Secondly, there is no easy way of generalising the SIC-LMTO-ASA to deal with disorder, thus limiting the types of systems that can be investigated. In the next chapter a new, simpler, multiple-scattering theory version of the SIC is discussed. This is implemented using the KKR method and is easily generalised to disordered systems using the methods described in section 2.3.

Chapter 4

The Local Self-Interaction Correction Method

In this chapter we describe the so-called *local self-interaction correction* (LSIC), as devised by Lüders *et al* [80]. A key difference between this implementation of the SIC and the LMTO-ASA implementation is the way in which localisation is characterised. In the LMTO-ASA method the spatial extent of Wannier orbitals determine the degree of localisation, whereas the LSIC uses the energy dependence of single-site phase shifts to characterise the localisation of electron states. A resonant phase shift corresponds to a large Wigner delay time, thus meaning an electron will spend a long time on each site. Such slow moving electrons are much more affected by self-interaction than fast-moving, itinerant, electrons and hence it is for these states that the self-interaction is calculated. This involves specifying single-site charge densities associated with these states, from which a SIC potential can be evaluated. The justification for this single-site approach is that in the LMTO-ASA implementation, where the spatial extent of localised Wannier orbitals are allowed to relax during the self-consistency procedure, over

98% of the electron charge is found to remain localised within the central unit cell. In section 4.1 we describe in detail the multiple-scattering implementation of the LSIC and then, in section 4.2, we use the famous $\alpha \rightarrow \gamma$ transition in cerium [10] to demonstrate the method.

4.1 Multiple Scattering Theory Implementation

Within the KKR formalism, described previously in section 2.2, the charge density at a site i is given by

$$n^i_\sigma(\mathbf{r}) = -\frac{1}{\pi}\int_{E_B}^{E_F} dE\, \mathrm{Im}\,[\sum_{LL'} Z^i_L(\mathbf{r}_i,E)\tau^{ii}_{\sigma LL'}(E)Z^i_{L'}(\mathbf{r}_i,E) - \sum_L Z^i_L(\mathbf{r}_i,E)J^i_L(\mathbf{r}_i,E)], \tag{4.1}$$

where Eqs. 2.42 and 2.43 have been used. Here, E_B is the bottom of the valence band energy. To define the charge density associated with a particular SIC state is it necessary to decompose the charge density given by Eq. 4.1 into different angular momentum channels. This is accomplished using a *symmetry-adapted* representation. Here, a unitary transformation, U, is applied to the usual real (or complex) spherical harmonics, $Y_L(\hat{r})$, such that the on-site scattering path operator, $\tau^{ii}_{\sigma LL'}$, becomes diagonal in angular momentum space:

$$\sum_{L_1,L_2} U^\dagger_{LL_1}\tau^{ii}_{\sigma L_1L_2}(E)\; U_{L_2L'} = \delta_{LL'}\tilde{\tau}^{ii}_{\sigma LL}(E). \tag{4.2}$$

The charge density associated with a particular angular momentum L and spin σ is then defined as

$$\tilde{n}^{i,SIC}_{L\sigma}(\mathbf{r}) = -\frac{1}{\pi}\int_{E_B}^{E_F} dE\; \mathrm{Im}[Z^i_L(\mathbf{r}_i,E)\tilde{\tau}^{ii}_{\sigma LL}(E)Z^j_L(\mathbf{r}_i,E) - Z^i_L(\mathbf{r}_i,E)J^i_L(\mathbf{r}_i,E)], \tag{4.3}$$

where henceforth all quantities evaluated in the symmetrised representation are denoted with a tilde. When integrated, this density should capture the charge of

one electron, i.e. $\int d\mathbf{r}\ \tilde{n}^{i,SIC}_{L\sigma}(\mathbf{r}) = 1$. Indeed, numerical tests [80] show that this is satisfied to within an error of a hundredth of an electron.

The effective one-body potential seen by an electron with the charge density $\tilde{n}^{i,SIC}_{L\sigma}$ is given by

$$\tilde{V}^{SIC-LDA}_{eff,iL\sigma}(\mathbf{r}) = v^{LDA}_{eff,\sigma}[n](\mathbf{r}) - V_H[\tilde{n}^{SIC}_{iL\sigma}](\mathbf{r}) - V^{LDA}_{xc}[\tilde{n}^{SIC}_{iL\sigma}, 0](\mathbf{r}), \tag{4.4}$$

where $v^{LDA}_{eff,\sigma}$ is the usual LDA potential, defined in Eq. 2.5. Note that since the LDA potential depends only on the total charge density, n, it is independent of which representation is used. The single-site scattering t-matrix corresponding to the potential $\tilde{V}^{SIC-LDA}_{eff,iL\sigma}$ is denoted $\tilde{t}^{i,SIC-LDA}_{L\sigma}$. The overall t-matrix of a multi electron state system is determined by evaluating first the t-matrix for the LDA potential, $V^{LDA}_{eff,\sigma}$, and then, for each self-interaction corrected channel $L' = (l', m')$ and σ', replacing the L'th element of the LDA t-matrix by the corresponding element of $\tilde{t}^{i,SIC-LDA}_{L'\sigma'}$:

$$\tilde{t}^{i}_{L\sigma} = t^{i,LDA}_{L\sigma}(1 - \delta_{L,L'}\delta_{\sigma\sigma'}) + \tilde{t}^{i,SIC-LDA}_{L'\sigma'}\delta_{L,L'}\delta_{\sigma\sigma'}. \tag{4.5}$$

$\tilde{t}^{i}_{L\sigma}$ can be converted to the standard (unsymmetrised) representation by applying the reverse unitary transformation, $U^{\dagger}$. This t matrix can then be used in Eq. 2.44 to construct a new on-site scattering path matrix, τ^{ii-new}. From this a new total charge density, n, can be evaluated and hence a new effective LDA potential, $V^{LDA-new}_{eff,\sigma}$, can be determined. Finally, a new set of SIC charges can be calculated by transforming τ^{ii-new} to the symmetrised representation and substituting it into Eq. 4.3. This whole procedure can be repeated *ad infinitum* until self-consistency is achieved.

4.2 The $\alpha \rightarrow \gamma$ Transition in Cerium

One of the early successes of the SIC-LMTO-ASA was to model the isostructural (fcc $\rightarrow$ fcc) transition in cerium between the high volume paramagnetic γ phase and low volume nonmagnetic α phase [81, 82, 83]. This transition has been the subject of numerous investigations [84, 85, 86, 87, 88, 89] and provides a good test case for electronic structure theories of strongly correlated systems. The transition will be used in this section to give a first demonstration of the LSIC method.

Cerium occupies a special place in the periodic table, being the first element to accommodate an f electron. The energy of this 4f electron is nearly the same as the valence 6s and 4d electrons, yet the state is spatially localised, giving rise to strong correlation effects. At low temperatures the α phase of Cerium is stable, while at room temperature the γ phase is more stable, but transforms back to the α phase at a pressure of 8kbar. This phase transition is characterised by a volume collapse of about about 15-17% and a quenching of the magnetic moment. The phase boundary of this transition terminates at a critical point. Many theoretical models have been proposed to describe the transition, the 3 most important of which will be discussed here. The first is the promotional model [90], where the transition from the γ to the α phase involves a promotion of the 4f electron into the 5d-6s valence band. Positron annihilation [91] and photoemission [92] data, however, show no substantial change in the occupation of the 4f orbitals across the transition. This suggests that the 4f state is occupied in both phases, which motivates the next two models. The first is the Mott transition model [31], where the 4f states change from being localised and non-bonding in the γ phase to itinerant and bonding in the α phase. The transition is hence governed by the competition between the onsite Coulomb f-f interaction, which favours localisation,

and the f-(spd) hybridisation energies which favours band formation. In the second model, the Kondo Volume Collapse (KVC) [93], the 4f state is localised in both the α and the γ phase, but the conduction electron screening changes during the transition, with the γ phase consisting of unscreened localised moments and the α phase consisting of screened moments. In accord with the KVC model, photoemission data is well described using the Anderson impurity model [94].

The Mott transition model and KVC evidently have a similar underlying picture, with the f state occupied in both phases and the f electrons playing a more active role in cohesion in the α phase. This picture can be translated into a DFT framework by saying that a band-like LDA description is appropriate for the f electrons in the α phase, whilst a localised SIC description is more suited for the γ phase. Such rationale was used in the SIC-LMTO-ASA investigations of Ce, where the itinerant f states of the α phase were described using the LDA and the more atomic f states of the γ phase were described using the SIC. The same approach will be taken here, with the γ phase described using the LSIC. Similar calculations to the ones presented here can be found in the paper by Lüders [80].

Figure 4.1 shows calculated ground state energies for Ce as a function of volume, using both the standard LDA and the LDA-SIC. The cubic symmetry of the fcc lattice splits the f states into a singlet (A_2u) and two triplets (T_1u and T_2u), giving rise to 3 distinct SIC configurations. The global SIC minimum occurs when the A_2u state is localised. The volume at this minimum is given in table 4.1, where the minimising LDA volume and bulk moduli are also listed. It is clear that the LDA minimum occurs in the region of the experimental α-phase volume, whilst the SIC minimum occurs in the region of the γ-phase volume. The volume underestimation of both phases can be attributed to the well-known KKR l-convergence problem [95], which arises because during the evaluation of

the Green's function, Eq. 2.43, the sum over angular momenta is truncated at some finite l value. This volume underestimation causes the large error in the bulk moduli.

Figure 4.1 shows a volume collapse of 24% at the $\gamma \rightarrow \alpha$ transition, which compares well with the experimental value of 15-17% and also that obtained from LMTO-ASA calculations, 23%. The overestimate of the volume collapse can be attributed to the large underestimate of the α phase volume, which is significantly greater than that of the γ phase. Since the l-convergence problem should affect both phases equally this implies that the LDA gives a poorer description of the α phase than the LSIC does of the γ phase. This is not surprising, since the LDA treats the f electron as being totally delocalised, giving α-Ce a valency of 4, whereas experimental data suggests that it actually has a noninteger valence of 3.67 [96]. Tetravalency is exhibited only at high pressures, when α-Ce transforms to α'-Ce, a C-centered orthorhombic phase. The LDA thus overestimates the itineracy of the f electron in the α phase, causing an excessive cohesive contribution from the f states. The non-integer valency of the α phase could potentially be modelled in terms of a pseudoalloy alloy, consisting of tetravalent and trivalent cerium atoms. In terms of the notation of section 2.3, each lattice site would be occupied by either a potential v^A with probability c=0.67 or a potential v^B with probability 1-c=0.33, where v^A and v^B correspond to a Ce^{4+} and Ce^{3+} ion respectively. Computationally, v^A would correspond to a LDA potential and v^B to a LSIC potential. The CPA method could then be used to determine self-consistently the electronic structure of the disordered $A_{\mathrm{c}}B_{1-\mathrm{c}}$ 'alloy' system. Such calculations were performed in reference [80].

We examine now the differences between the electronic structure of the α and γ phases, as described by the LDA and LDA-SIC respectively. Figure 4.2

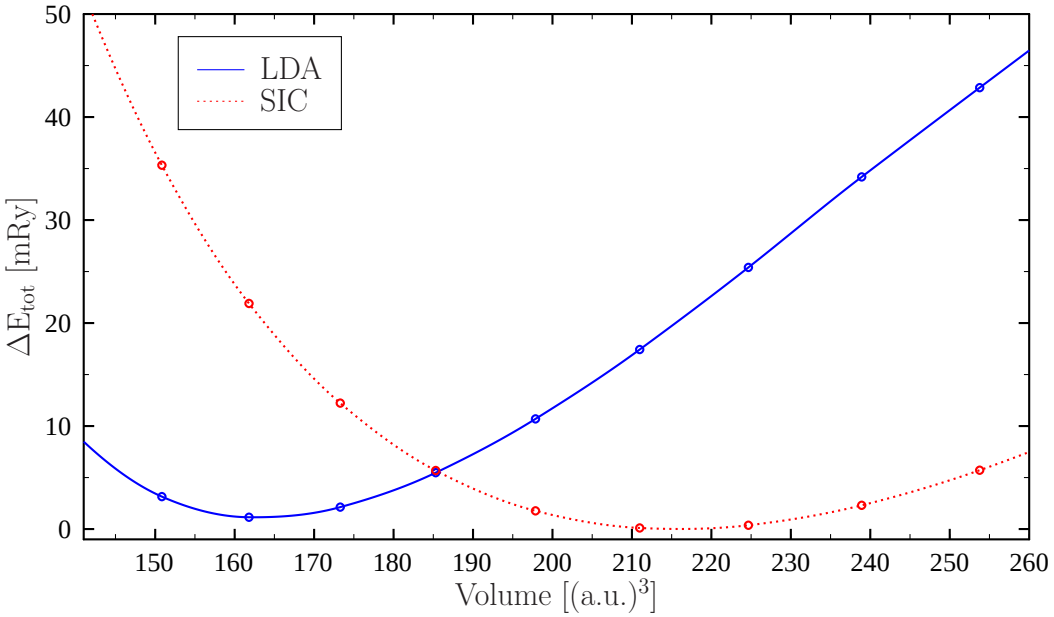

Figure 4.1: Calculated total energies of Ce as a function of volume.

Table 4.1: Equilibrium volumes and bulk moduli of the α and γ phases of cerium. The bulk moduli were evaluated at the theoretical equilibrium volumes.

	α-Ce		γ-Ce	
Method	V [a.u.^{3}]	B [kbar]	V [a.u.^{3}]	B [kbar]
LSIC	163	508	215	307
SIC-LMTO-ASA[a]	175	443	229	340
Experiment[b]	190	270	232	239

[a]Reference [81].

[b]Taken from reference [10].

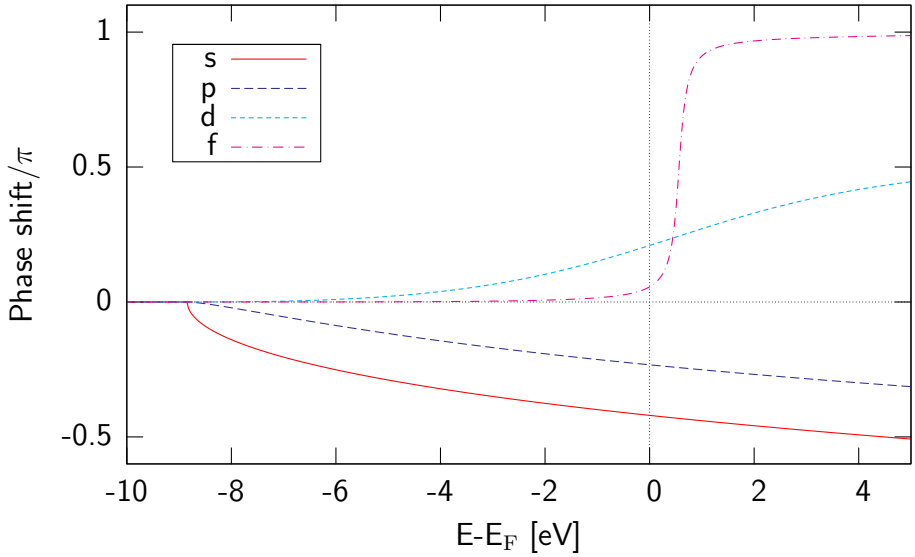

Figure 4.2: Phase shifts of electron states in Ce, obtained from LDA calculation.

shows phase shifts for all the different l channels of Ce, obtained from the LDA calculation. The f states are seen to have a sharp resonance above the Fermi energy, implying that, even in the α phase, these states have a strong degree of localisation. Figure 4.3 shows the f electron phases obtained from the LDA-SIC calculation, with the A_2u state localised. As in the LDA calculation, the non SIC corrected f states have a sharp resonance, corresponding to a large Wigner delay time. The corrected f state is shifted down in energy and becomes a bound state, with the phase shift jumping abruptly by π.

Figure 4.4 compares the DOS of the LDA and LDA-SIC calculations. In the LDA-SIC DOS there is a substantial splitting between the occupied f states, occurring at about -8meV, and the unoccupied states occurring at about 1.5meV. The presence of a magnetic moment in the γ phase, estimated to be 1.24 μ_B, manifests itself through a clear exchange splitting between the minority and majority spin states above the Fermi energy. The hybridisation of the f band states

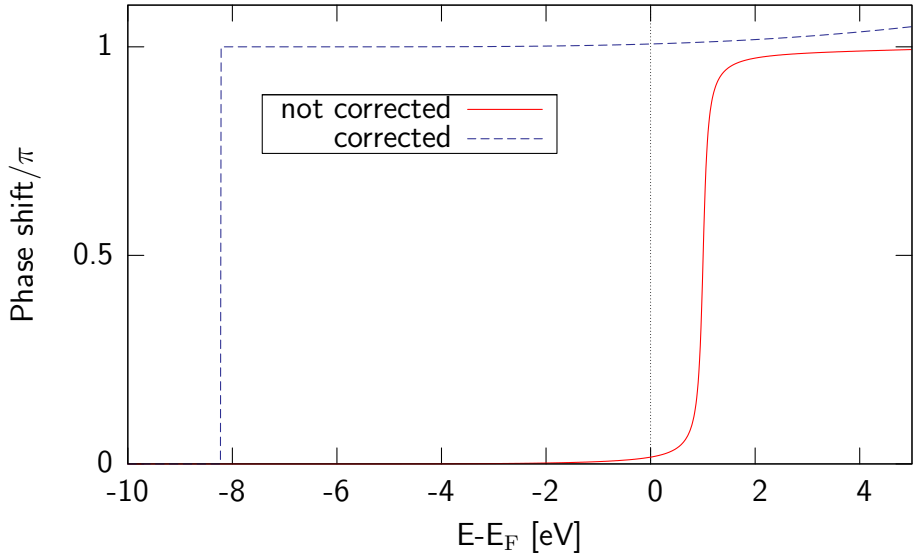

Figure 4.3: Phase shifts of self-interaction-corrected and non-corrected f states in Ce, obtained from LDA-SIC calculation.

with other band states is much smaller in the LDA-SIC calculation then it is in the LDA calculation, as shown by the lower DOS at the Fermi energy.

It should be noted that the calculations presented here assume full lattice periodicity, which means that γ-Ce is implicitly treated as ferromagnetic. To investigate other possible arrangements of moments one can consider two different approaches. The first is to compare the groundstate energies of different magnetic structures through a super-cell method. Here, a lattice of repeating supercells, each containing several atomic unit cells, is used to mimic a particular magnetic structure. For example an antiferromagnetic structure of type 1 (AF1), where there is a simple parallel/antiparallel alternation of moments, can be represented by a supercell consisting of two atoms with antiparallel moments. A disadvantage of this approach is that each of the structures looked at has to be specified *a priori*. A second, perhaps more appealing, approach is to investigate the presence of any underlying ordering tendencies in the high temperature (paramagnetic) phase of a

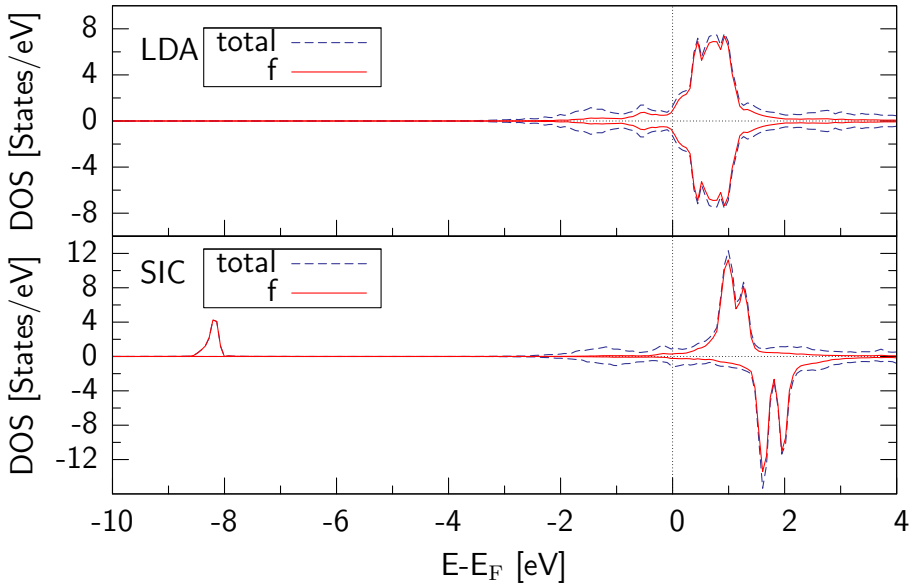

Figure 4.4: Density of states of Ce. Minority states are plotted with negative values of the DOS.

system. This involves examining the response of the paramagnetic state to some applied magnetic field and has the advantage that the possible magnetic orderings are not limited to some pre-defined set of structures. This thesis will focus on the second approach. In order to model the paramagnetic state we will need to consider the effect of finite temperatures on the electronic structure of the system. In particular, the influence of thermally activated spin fluctuations will need to be taken into account. This will be the subject of the next chapter, where a first principles theory of finite magnetism for strongly-correlated systems is developed.

Chapter 5

Finite Temperature Magnetism

We begin this chapter by setting down the foundations of finite temperature density functional theory. A straightforward generalisation of EFT to non-zero temperatures is provided by Merino [97], who, in analogy with the groundstate theories of Hohenberg and Kohn, proved that in the grand canonical ensemble at a given temperature T and chemical potential ν there exists a grand potential functional, $\Omega[n(\mathbf{r}), \mathbf{m}(\mathbf{r})]$, of the charge density $n(\mathbf{r})$ and magnetisation density $\mathbf{m}(\mathbf{r})$ which is minimised at the equilibrium charge and magnetisation densities, $n_0(\mathbf{r})$ and $\mathbf{m}_0(\mathbf{r})$. Moreover, the minimum, $\Omega[n_0(\mathbf{r}), \mathbf{m}_0(\mathbf{r})]$, is equal to the thermodynamic grand potential, $\hat{\Omega}[n_0(\mathbf{r}), \mathbf{m}_0(\mathbf{r})]$. Like the minimisation of the groundstate energy functional in section 2.1, the procedure to minimise $\Omega[n(\mathbf{r}), \mathbf{m}(\mathbf{r})]$ leads to a set of one-electron equations, from which the charge and magnetisation densities can be determined self-consistently. Since $\mathbf{m}_0(\mathbf{r})$ is an equilibrium average it possesses full crystalline symmetry, which means that it has to point in the same direction in each unit cell. A consequence of this is that the bulk magnetisation of a system can only go to zero if $\mathbf{m}_0(\mathbf{r})$ is identically zero. The Mermin generalisation can hence be considered as a DFT version of the Stoner-Wohlfarth model of magneti-

sation [98], where ferromagnetism vanishes only if the exchange splitting between spin up and spin down bands is destroyed. This destruction occurs due to *Stoner excitations*, where electrons are transferred from filled states in the majority spin band to empty states in the minority spin band, creating electron-hole pairs.

Within the Stoner model an estimate of the Curie temperature, T_C, is given by $k_B T_C \sim \Delta_{\mathrm{ex}}$, where Δ_{ex} is the exchange energy splitting between the spin up and down bands. Early electronic structure calculations for ferromagnetic iron [99] gave an exchange splitting of $\sim$2eV between the spin up and down d-electron bands, to which the magnetism of the system was ascribed. From this exchange splitting T_C is estimated to be $\sim$ 20000 K, which is an order of magnitude larger than the observed value of 1040 K. This suggested that there must be some other thermal excitations capable of reducing the magnetisation and that the energy associated with these excitations is an order of magnitude smaller than that of the Stoner excitations. The study of magnetic insulators provides the answer to what these excitations are. In these systems a well defined spin, $\mathbf{S}_n$, can be assigned to each atomic site, n, with the interactions between the spins described using the Heisenberg Hamiltonian, $H = -\sum_{n,m} J_{n,m} \mathbf{S}_n \cdot \mathbf{S}_m$, where $J_{n,m}$ is an exchange integral involving the sites n and m. In this model the magnetisation is reduced as the temperature is increased by the spins, which are initially aligned, having their orientations thermally randomised. This means that the bulk magnetism can vanish without the magnetisation of individual atomic sites going to zero.

In metallic systems, where the electrons are itinerant, it is not possible to assign a well defined spin to each atomic site and hence a simple Heisenberg description can't be used. Nonetheless, Schrieffer *et al* [100, 101] and Cyrot [102, 103] devised a theory based on the notion of localised spins, but with an itinerant description of electrons. In this picture electrons move itinerantly between

atomic sites, but each site is dominated by electrons with a particular spin direction. This influences the motion of the electrons, such that the spin orientation of an electron arriving at a particular site tends to agree with that of the dominant spin direction at that site. The itinerant electrons hence set up self-maintaining 'local moments' at all the lattice site, which are analogous to the localised spins of the Heisenberg model. Hubbard [7, 104, 105] formulated this physical picture into what is referred to now as the 'Disordered Local Moment' (DLM) model of magnetism. A key assumption of this model is that there is a time scale separation between the fast electronic motion associated with itinerant behaviour, i.e. the electron hopping time scale, and the slow motion associated with orientational fluctuations. At an intermediate time scale well defined moments exist at all lattice sites. The statistical mechanics of these local moments are described via their thermodynamic free energy, F, which takes into account both the entropy associated with the orientational fluctuations and also the production of electron-hole pairs associated with Stoner excitations. In the DLM approach F is evaluated using a mean-field approximation.

In this chapter we describe a first principles implementation of the DLM model, using the KKR multiple-scattering approach. Section 5.1 outlines how the electronic structure of the DLM paramagnetic state can be modelled. This uses techniques developed for the study of substitutionally disordered alloy systems, specifically the CPA method which was described in section 2.3. The response of the electronic structure of the paramagnetic state to some applied magnetic field is examined in section 5.2, with the corresponding magnetic response of the system considered in section 5.3, where an expression for the paramagnetic spin susceptibility is derived. We describe how the wavevector dependence of this susceptibility can be used to gain information about the type of magnetic

order that may occur in the groundstate. In section 5.4 we extend the DLM scheme to multi-sublattice systems, enabling cases where there are more than one atom per unit cell to be studied. We illustrate this multi-sublattice formalism by investigating the dilute magnetic semiconductor manganese-stabilised zirconia. Finally, in section 5.5, we open up the way to using the DLM model to study strongly-correlated systems, by describing how it can be implemented with the LSIC. This new implementation is demonstrated by performing calculations for the γ-phase of cerium.

5.1 The Disordered Local Moment State

This section introduces the KKR-CPA implementation of the DLM picture, focusing on the paramagnetic regime where the local moments have the same probability of being orientated in any direction. The formulation begins by specifying a particular arrangement of local moments, whose directions are described using a set of unit vectors, $\{\hat{\mathbf{e}}_i\}$. The local moment phase space specified by $\{\hat{\mathbf{e}}_i\}$ is assumed to be ergodic, hence long time averages can be replaced by ensemble averages. These averages use the Gibbsian measure

$$P(\{\hat{\mathbf{e}}_i\}) = Z^{-1} \exp[-\beta\Omega(\{\hat{\mathbf{e}}_i\})], \tag{5.1}$$

where the partition function, Z, is given by

$$Z = \prod_j \int d\hat{\mathbf{e}}_j \exp[-\beta\Omega(\{\hat{\mathbf{e}}_i\})] \tag{5.2}$$

and $\beta = (k_B T)^{-1}$. $\Omega(\{\hat{\mathbf{e}}_i\})$ is a 'generalised' grand potential, the term 'generalised' referring to the fact that $\Omega(\{\hat{\mathbf{e}}_i\})$ is not associated with a thermal equilibrium state. In the DLM approach a mean-field approximation for $\Omega(\{\hat{\mathbf{e}}_i\})$ is constructed by expanding it about a single-site reference spin Hamiltonian,

$\Omega_0(\{\hat{\mathbf{e}}_i\}) = -\sum_i \mathbf{h}_i \cdot \hat{\mathbf{e}}_i$. The parameters $\mathbf{h}_i$ evidently play the role of a Weiss field and are determined using a variational approach, whereby the free energy of the system, $F = \beta^{-1} \log Z$, is minimised. The details of this procedure will be given in section 5.3.

The probability function, P_0, associated with Ω_0 can be written as a product of single-site measures:

$$P_0(\{\hat{\mathbf{e}}_i\}) = \prod_i P_i(\hat{\mathbf{e}}_i), \tag{5.3}$$

where

$$P_i(\hat{\mathbf{e}}_i) = Z_i^{-1} \exp[\beta \mathbf{h}_i \cdot \hat{\mathbf{e}}_i] \tag{5.4}$$

and

$$Z_i = \int d\hat{\mathbf{e}}_i \exp[\beta \mathbf{h}_i \cdot \hat{\mathbf{e}}_i]. \tag{5.5}$$

Specifying these single-site probabilities, P_i, opens up the possibility of using a CPA type scheme to deal with the disorder arising from the randomly orientated local moments. Here, the CPA effective medium would be such that the motion of an electron in it approximates the ensemble averaged motion of an electron travelling through a lattice of randomly orientated moments. Such a scheme can be formulated mathematically using the so-called *cpa-projectors*:

$$\mathbf{D_i}(\hat{\mathbf{e}}_i) = [1 + [(t(\hat{\mathbf{e}}_i))^{-1} - (t_i^c)^{-1}]\tau^{c,00}]^{-1}, \tag{5.6}$$

where the matrix $t(\hat{\mathbf{e}}_i)$ describes scattering from a site with a local moment orientated in the direction $\hat{\mathbf{e}}_i$ and t_i^c specifies the CPA effective medium. For a site in the CPA effective medium these two scattering matrices are formally the same and hence $\mathbf{D_i} = 1$. By the CPA self-consistency condition the single-site average of $\mathbf{D_i}(\hat{\mathbf{e}}_i)$ must also take this value, i.e.

$$\int d\hat{\mathbf{e}}_i P_i(\hat{\mathbf{e}}_i) \mathbf{D_i}(\hat{\mathbf{e}}_i) = \mathbf{1}. \tag{5.7}$$

In the paramagnetic regime, where the moments have no preferred orientation, P_i and $\mathbf{D_i}$ become site independent. Moreover $P(\hat{\mathbf{e}}_i) = P^0 = \frac{1}{4\pi}$ and Eq. 5.7 simplifies to

$$\frac{1}{4\pi}\int d\hat{\mathbf{e}}_i \mathbf{D}^0(\hat{\mathbf{e}}_i) = \mathbf{1}, \tag{5.8}$$

where the superscript 0 signifies that the CPA projector is evaluated in the paramagnetic state.

To solve Eq. 5.8 we consider a change of coordinates. For each site i there is a local frame of reference in which the matrix $\mathbf{D}^0$ is diagonal in spin space. This spin frame of reference is specified by the z-axis being parallel to $\hat{\mathbf{e}}_i$ and within it $\mathbf{D}^0$ has the form

$$\begin{pmatrix} D^0_+ & 0 \\ 0 & D^0_- \end{pmatrix},$$

where

$$D^0_{+(-)} = [1 + [(t^{-1}_{+(-)} - (t^c_i)^{-1}]\tau^{c,00}]^{-1} \tag{5.9}$$

and $t_{+(-)}$ represents the scattering of an electron with spin parallel (antiparallel) to $\hat{\mathbf{e}}_i$. In the common (global) frame of reference $\mathbf{D}^0$ is given by

$$\mathbf{D}^0 = \frac{1}{2}(D^0_+ + D^0_-)\mathbf{1} + \frac{1}{2}(D^0_+ - D^0_-)\sigma\cdot\hat{\mathbf{e}}_i, \tag{5.10}$$

where σ_x, σ_y and σ_z are the three Pauli spin matrices defined according to the global z-axis. With $\mathbf{D}^0$ written in this form it can be shown that Eq. 5.8 reduces to [106]

$$\frac{1}{2}D^0_+ + \frac{1}{2}D^0_- = 1. \tag{5.11}$$

Equation 5.11 is evidently just the CPA equation for a system with 50% of moments pointing 'up' and 50% pointing 'down' (an Ising system). It can thus be treated using the techniques described in section 2.3 for the binary alloy problem, A_cB_{1-c}, with the 'real' alloy components A and B replaced by two 'pseudo' alloy

components that have anti-parallel local moments. A self-consistent electronic structure scheme, of the type discussed at the end of section 2.3, can hence be used to describe the paramagnetic DLM state, with 50% of sites occupied by 'up' moments and the other 50% occupied by 'down' moments.

The results of early calculations for bcc Iron [107] showed that such a self-consistent scheme is capable of yielding the "local exchange splitting" required for local moment formation. In particular the finite temperature band structure, evaluated at selected points in the Brillouin zone, showed that electrons with spin $+\frac{1}{2}$ had a large spectral weight at 'up' sites at energies below the Fermi energy and a large weight at 'down' sites at energies above the Fermi energy. For an electron with spin -$\frac{1}{2}$ the opposite was found, i.e. a large amplitude at 'down' sites below the Fermi energy and a large amplitude at 'up' sites above the Fermi energy. Consequently electrons with spin $+\frac{1}{2}$ and -$\frac{1}{2}$ were predicted to be spatially separated, with the former residing mainly on 'up' sites and the latter mainly on 'down' sites. Of course, this prediction relies on the band splitting being present throughout a substantial portion of the Brillouin zone and not just at a few selected $\mathbf{k}$ points. Indeed, the local exchange splitting was actually found to be strongly $\mathbf{k}$-dependent and to vanish altogether at some points. Such wavevector dependent splitting was also observed in photoemission [108] and inverse photoemission [109] experiments. Nevertheless, after integrating the relevant quantities over the Brillouin zone a local moment of $\approx 1.85\mu_B$ was found, indicating a prevalence of 'local exchange splitting' in the band structure.

The discussion of bcc iron in the preceding paragraph demonstrates how the DLM approach is capable of yielding local moments in the paramagnetic state, even though there is no overall spin polarisation. Of course, in order to be a complete theory of magnetisation the DLM scheme must also be able to describe

the ordered phase of a system that occurs when it is cooled below some transition temperature. The approach which will be taken here for investigating the onset of magnetic order will be to consider the response of the DLM paramagnetic state to the application of some external, site-dependent magnetic field. This will cause the single-site probabilities to become site dependent and hence the CPA medium will no longer be homogeneous. The next section considers the formulation of such an inhomogeneous CPA scheme, within which the electronic structure response of a system to an applied magnetic field is described. The corresponding magnetic response of the system is considered in Section 5.3, where an expression for the paramagnetic susceptibility is derived.

5.2 Linear Response of the Paramagnetic State

The application of a site-dependent magnetic field will mean that the probabilities P_i will no longer be site independent, i.e.

$$P_i(\hat{\mathbf{e}}_i) = P_0(\{\hat{\mathbf{e}}_i\}) + \delta P_i(\hat{\mathbf{e}}_i). \tag{5.12}$$

Consequently, the CPA effective medium will also no longer be site independent. Such an inhomogeneous CPA medium can be specified formally by adding a site-dependent perturbation to the effective scattering t-matrices:

$$t_i^{c,-1} = t_0^{c,-1} + \delta t_i^{c,-1}. \tag{5.13}$$

Since the scattering path operator $\tau^{c,ij}$ and CPA projector $\mathbf{D}(\hat{\mathbf{e}}_i)$ are defined in terms of t, these quantities will also alter in the inhomogeneous medium. In particular the latter quantity can be written as

$$\mathbf{D}(\hat{\mathbf{e}}_i) = \mathbf{D}^0(\hat{\mathbf{e}}_i) + \delta \mathbf{D}_i(\hat{\mathbf{e}}_i), \tag{5.14}$$

Substituting Eqs. 5.12 and 5.14 into the CPA equation, Eq. 5.7, and requiring that is satisfied to each order separately gives

$$\begin{aligned} \int \mathbf{d}\hat{\mathbf{e}}_i \; P^0(\hat{\mathbf{e}}_i)\mathbf{D}^0(\hat{\mathbf{e}}_i) = \mathbf{1} \quad \text{zeroth order} \\ \int \mathbf{d}\hat{\mathbf{e}}_i \; [\delta P_i(\hat{\mathbf{e}}_i)\mathbf{D}_i^0(\hat{\mathbf{e}}_i)] + P^0(\hat{\mathbf{e}}_i)\delta\mathbf{D}_i(\hat{\mathbf{e}}_i)] = \mathbf{0} \quad \text{first order.} \end{aligned} \tag{5.15}$$

The zeroth order equation is evidently just the CPA condition for the paramagnetic state, which we have already seen how to solve. To solve the first order equation we first need to evaluate $\delta P_i(\hat{\mathbf{e}}_i)$ and $\delta\mathbf{D}_i(\hat{\mathbf{e}}_i)$. Since we are interested in the onset of magnetic order, where the average magnetisation $\mathbf{m}_i \equiv < \hat{\mathbf{e}}_i >$ is small, it makes sense to expand $P_i(\hat{\mathbf{e}}_i)$ and $\mathbf{D}(\hat{\mathbf{e}}_i)$ in terms of powers of $\mathbf{m}_i$. Using this approach and retaining only first order terms in $\mathbf{m}_i$, it can be shown [33] that the first order equation of Eq. 5.15 reduces to an equation for the response function $\Lambda^{ij}_{LL'}(\epsilon) \equiv \frac{1}{2}\frac{\partial}{\partial m_j}(t_+^{c,-1} - t_-^{c,-1})$:

$$\Lambda^{ij}_{LL'}(\epsilon) = \Lambda^{0,i,j}_{LL'}(\epsilon) + \sum_{q,rL''L'''} \Lambda^{0,i,q}_{LL'} X^{qr}_{L''L'''} \Lambda^{rj}_{L'''L'}, \tag{5.16}$$

where

$$\Lambda^{0,i,j}_{LL'}(\epsilon) = (D^0_{+L} - D^0_{-L})\delta_{ij}\delta_{LL'} \tag{5.17}$$

and

$$X^{ij}_{LL'} = \tau^{c,ij}_{LL'}(\epsilon)\tau^{c,ji}_{LL'}(\epsilon) - \delta_{LL'}\delta_{ij}[\tau^{c,ii}_{LL}(\epsilon)]^2 \tag{5.18}$$

Equations 5.16, 5.17, 5.18 constitute the fundamental equations of the inhomogeneous CPA. All the quantities entering Eqs. 5.17 and 5.18, i.e. D^0_+, D^0_- and $\tau^{c,ji}$, are obtained from the solution of the homogeneous CPA problem.

5.3 Paramagnetic Spin Susceptibility

In the previous section we introduced the quantity $\mathbf{m}_i$, the average moment orientation at a site i. This quantity can be evaluated formally using the probability function P_i of Eq. 5.4, from which we obtain

$$\mathbf{m}_i = \int \mathbf{d\hat{e}}_i \; P_i(\hat{\mathbf{e}}_i)\hat{\mathbf{e}}_i = m_i \hat{h}_i, \tag{5.19}$$

where the unit vector $\hat{h}_i$ denotes the direction of $\mathbf{h}_i$ and

$$m_i = L(\beta h_i), \tag{5.20}$$

where $L(x)$ is the *Langevin function*, defined by $L(x) = \coth(x) - 1/x$. As mentioned at the beginning of section 5.1, we employ a variational approach to evaluate the parameters h_i. In particular, we use the Feynman-Peierls inequality [110] to give a variational upper bound for F:

$$F \leq F_0 + < \Omega - \Omega_0 >_0, \tag{5.21}$$

where the average $<>_0$ is with respect to the probability distribution P_0 defined in Eq. 5.3 and

$$F_0 = \beta^{-1} \log Z_0 = \beta^{-1} \sum_i \log Z_i, \tag{5.22}$$

where Z_i is defined in Eq. 5.5.

Substituting Eq. 5.22 into Eq. 5.21 and using $\Omega_0(\{\hat{\mathbf{e}}_i\}) = -\sum_i \mathbf{h}_i \cdot \hat{\mathbf{e}}_i$ we obtain

$$F \leq \beta^{-1} \log Z_0 + \sum_i \mathbf{m}_i \cdot (\mathbf{h}_i - \mathbf{h}_i^{ext}) + < \Omega >, \tag{5.23}$$

where an external field $\mathbf{h}_i^{ext}$ has been added, which we eventually set to zero. Minimising the right hand site of Eq. 5.23 we obtain

$$0 = \sum_\gamma \frac{\partial m_{i\gamma}}{\partial h_{i\alpha}} (h_{i\gamma} - h_{i\gamma}^{ext}) + \frac{\partial < \Omega >}{\partial h_{i\alpha}}. \tag{5.24}$$

Multiplying this by $\partial h_{i\alpha}/\partial m_{i\gamma}$ and summing over α leads to

$$h_{i\lambda} = -\frac{\partial < \Omega >}{\partial m_{i\lambda}} + h_{i\lambda}^{ext}, \tag{5.25}$$

hence

$$\mathbf{h}_i = -\nabla_{\mathbf{m}_i} < \Omega > + \mathbf{h}_i^{ext} \tag{5.26}$$

Substituting this into Eq. 5.20 gives

$$\mathbf{m}_i = L(\beta | -\nabla_{\mathbf{m}_i} < \Omega > + \mathbf{h}_i^{ext}|) \frac{-\nabla_{\mathbf{m}_i} < \Omega > + \mathbf{h}_i^{ext}}{|-\nabla_{\mathbf{m}_i} < \Omega > + \mathbf{h}_i^{ext}|}. \tag{5.27}$$

In the paramagnetic state $\mathbf{m}_i = 0$ for all i. However, at the onset of magnetic order $\mathbf{m}_i$ will become finite. For small x, $L(x) = x/3 + O(x^3)$, and hence near the ordering phase transition

$$\mathbf{m}_i = \frac{1}{3}\beta(-\nabla_{\mathbf{m}_i} < \Omega > + \mathbf{h}_i^{ext}). \tag{5.28}$$

Having formally evaluated $\mathbf{m}_i$, we can write down an expression for the dimensionless spin susceptibility, $\overline{\chi}$:

$$\overline{\chi}_{i\alpha,j\gamma} \equiv \frac{\partial m_{i,\alpha}}{\partial h_{j,\gamma}^{ext}}|_{h_{j,\gamma}^{ext}=0} = \frac{1}{3}\beta \frac{\partial(-\partial < \Omega > /\partial m_{i\alpha})}{\partial h_{j,\gamma}^{ext}} + \frac{1}{3}\beta\delta_{ij}\delta_{\alpha\gamma}. \tag{5.29}$$

Since $\partial < \Omega > /\partial m_{i\alpha}$ depends on $h_{j,\gamma}^{ext}$ only through the variables $\{\mathbf{m}_i\}$

$$\frac{\partial(-\partial < \Omega > /\partial m_{i\alpha})}{\partial h_{j,\gamma}^{ext}} = \sum_{k\eta} \left(\frac{\partial(-\partial < \Omega > /\partial m_{i\alpha})}{\partial m_{k,\eta}}\right)\left(\frac{\partial m_{k,\eta}}{\partial h_{j,\gamma}^{ext}}\right) \tag{5.30}$$

and hence we can rewrite Eq. 5.29 as

$$\overline{\chi}_{i\alpha,j\gamma} = \frac{1}{3}\beta \sum_{k\eta} S_{i\alpha,k\eta}^{(2)} \overline{\chi}_{k\eta,j\gamma} + \frac{1}{3}\beta\delta_{ij}\delta_{\alpha\gamma}, \tag{5.31}$$

where we have defined the so-called direct correlation function $S^{(2)}$ according to

$$S_{i\alpha,k\eta}^{(2)} \equiv -\frac{\partial^2 < \Omega >}{\partial m_{i,\alpha}\partial m_{k,\eta}} \tag{5.32}$$

In the paramagnetic state $S^{(2)}_{i\alpha,j\eta} = \delta_{\alpha\eta} S^{(2)}_{ij}$ and depends only on the vector difference $\mathbf{R}_i - \mathbf{R}_j$ between sites i and j. This enables us to take the lattice Fourier transform of Eq. 5.31, from which we obtain

$$\overline{\chi}\left(\mathbf{q}, T\right) = \frac{1}{3}\beta / \left(1 - \frac{1}{3}\beta S^{(2)}\left(\mathbf{q}, T\right)\right) \tag{5.33}$$

The evaluation of the response function $S^{(2)}$ involves formally taking derivatives of $< \Omega >$ with respect to m_i, for which the inhomogeneous CPA formalism can be employed. It can be shown that [33]:

$$S^{(2)}(\mathbf{q}) = \frac{1}{\pi}\mathrm{Im}\int d\epsilon f(\epsilon - \nu) \sum_{LL'} D^0_{L+}(t^{-1}_{L+} - t^{-1}_{L-}) D_{L-} \sum_{L'L''} X_{LL'}(\mathbf{q}) \Lambda_{LL'}(\mathbf{q}), \tag{5.34}$$

where $X_{LL'}(\mathbf{q})$ and $\Lambda_{LL'}(\mathbf{q})$ are obtained from the lattice Fourier transforms of Eqs. 5.16 and 5.18 respectively.

In order to construct the full paramagnetic spin susceptibility, χ, we need to consider the addition of a Zeeman interaction potential,

$$V_{ext} = -\sum_i \int_{V_i} d^3 r \mu_i(\mathbf{r}; \{\hat{e}_i\}) \hat{e}_i \cdot \mathbf{H}(\mathbf{r}), \tag{5.35}$$

to the grand potential functional Ω, where $\mathbf{H}(\mathbf{r})$ is a static external field and μ_i is the magnitude of the local moment at the ith site. A priori, μ_i depends on the local moment distribution $\{\hat{e}_i\}$ and will respond to the external field both directly and also because of the change in $\mathbf{m}_i$. However, we will use a rigid moment approach, where we assume that μ does not depend on the local moment orientations or the external magnetic field. This means that the applied field affects only the orientations of the moments. The change in magnetisation in the ith unit cell, $\delta\mathbf{M}_i$, can thus be written as

$$\delta\mathbf{M}_i = \mu_i \mathbf{m}_i, \tag{5.36}$$

If $\mathbf{H}(\mathbf{r})$ is constant within each unit cell we can write

$$V_{ext} = -\sum_i \mu_i \hat{e}_i \cdot \mathbf{H}_i(\mathbf{r}), \tag{5.37}$$

where $\mathbf{H}_i$ is the value of $\mathbf{H}(\mathbf{r})$ in the ith unit cell. Clearly, $\mu_i H_i$ will play the role of an external magnetic field in Eq. 5.23, i.e.

$$h_i^{ext} = \mu_i H_i. \tag{5.38}$$

For systems where the size of the moments are site independent, i.e. $\mu_i = \mu$, we can use equations 5.36 and 5.38 to write

$$\chi_{ij} \equiv \frac{\partial M_i}{\partial H_j} = \mu^2 \frac{\partial m_i}{\partial h_j^{ext}} = \mu^2 \overline{\chi}_{ij}. \tag{5.39}$$

Hence, the full wavevector dependent paramagnetic susceptibility differs from that in Eq. 5.33 by a factor of μ^2, i.e.

$$\chi(\mathbf{q}, T) = \frac{1}{3}\beta\mu^2 / \left(1 - \frac{1}{3}\beta S^{(2)}(\mathbf{q}, T)\right). \tag{5.40}$$

This expression can be used to gain information about the type of magnetic order that might occur in a system as the temperature is lowered through a phase transition. In particular the expression yields information about the spin fluctuations that characterise the paramagnetic state. For example in ferromagnetic materials the paramagnetic state is characterised by ferromagnetic spin fluctuations, which have long wavelengths with wave vectors $\mathbf{q} \approx 0$, and becomes unstable to them at the Curie temperature, T_C. For systems that order with an anti-ferromagnetic structure the paramagnetic state is dominated by 'anti-ferromagnetic' spin fluctuations, with a finite, wave vector $\mathbf{q} = \mathbf{Q}$. Below the Néel temperature, T_N, these antiferromagnetic spin fluctuations become a spin density wave (SDW), which is a static magnetisation wave characterised by the wave vector $\mathbf{Q}$. The transition temperature can be found by setting the determinant $1 - \frac{1}{3}\beta S^{(2)}(\mathbf{q}, T)$ to zero.

The DLM scheme, implemented using the LDA, has proved to be extremely successful at describing the magnetic properties of transition metals [33]. Systems that have been studied have simple lattice structures, with 1 atom per unit cell, and electrons that behave in a predominantly band like fashion. In the next two sections we describe how the DLM approach can be generalised to more complicated systems, where the type of crystal structure or the effects of strong electron correlations means that they cannot be treated using the conventional DLM implementation. In particular, section 5.4 considers structures where there is more than one atom per unit cell and section 5.5 considers systems containing states for which an atomic-like, rather than a band-like, description is more-appropriate, for which we employ the LSIC.

5.4 Multi-Sublattice Formalism

So far in this thesis we have assumed that each lattice unit cell contains only one scattering centre. Whilst this is true for the α and γ phases of cerium, there are many important systems for which the unit lattice cell contains more than one atom. One such example is the heavy rare earth metals, where the elements crystallise into hexagonally closed packed (hcp) structures that contain two atoms per unit cell. Metal compounds, i.e. systems containing more than one type of element, necessarily contain more than atom per unit cell. One such example is the transition metal monoxides, which will be discussed in chapter 7. These all crystallise into the rock salt (NaCl) structure. In this section we describe how the DLM formalism can be generalised to deal with such systems. In particular, an expression is derived for the paramagnetic spin susceptibility for the case of an arbitrary number, n, of atoms per unit cell.

Segall [111] provided a generalisation of the electronic structure methods of Korringa, Kohn and Rostoker, for the case of n nonoverlapping muffin tin spheres per unit cell. This formalism was later extended to disordered systems by Pindor *et al* [112], who devised a CPA scheme for the case of multiple atoms per unit cell. The approach taken there was to consider a system with n atoms per unit cell as being built up from n interpenetrating sublattices. The CPA medium then consists of n different lattices of effective scattering centres, each lattice being described by a scattering matrix $t^{c,j}$, where $j = \{1, 2, ..., n\}$. These scattering matrices are determined by setting up separately an impurity problem for each of the sublattices, of the sort described by equation 2.46. During the CPA self-consistency procedure the equations for each of these n impurity problems become coupled through the calculation of the effective site-diagonal scattering path operator, $\tau^{c,00}$. This CPA scheme can be used to model the paramagnetic DLM state of a multi sublattice system via the techniques described in section 5.1. In particular, 50% of sites on each sublattice will be occupied by 'up' moments and 50% by 'down' moments.

In order to proceed formally with an expression for the paramagnetic spin susceptibility a $3n$ component vector, $\mathbf{e}_i$, will be assigned to each unit cell. This vector is specified by $\mathbf{e}_i = (\hat{\mathbf{e}}_i^1, \hat{\mathbf{e}}_i^2, ..., \hat{\mathbf{e}}_i^n)$, where $\hat{\mathbf{e}}_i^\lambda$ is a unit vector specifying the local moment orientation at the λth atomic position in the ith unit cell. A corresponding "local magnetic field" $\mathbf{h}_i = (\mathbf{h}_i^1, \mathbf{h}_i^2, ..., \mathbf{h}_i^n)$, can then be assigned to each unit cell and the grand potential of the system approximated by a reference spin hamiltonian $\Omega_0 = -\sum_i (\mathbf{h}_i \cdot \hat{\mathbf{e}}_i)$. The probability distribution associated with Ω_0 is given by

$$P_0(\{\mathbf{e}_i\}) = \prod_i \prod_{\lambda=1}^{n} P_i^\lambda(\hat{\mathbf{e}}_i^\lambda), \tag{5.41}$$

where

$$P_i^{\lambda}(\hat{\mathbf{e}}_i^{\lambda}) = Z_i^{\lambda,-1} \exp[\beta \mathbf{h}_i^{\lambda} \cdot \hat{\mathbf{e}}_i^{\lambda}] \tag{5.42}$$

and

$$Z_i^{\lambda} = \int d\hat{\mathbf{e}}_i^{\lambda} \exp[\beta \mathbf{h}_i^{\lambda} \cdot \hat{\mathbf{e}}_i^{\lambda}]. \tag{5.43}$$

Using the Feynman variational approach to determine the parameters $\mathbf{h}_i$, we arrive at the following expression for the quantity $\mathbf{m}_i^{\lambda}$, the average moment orientation at the λth site of the ith unit cell:

$$\mathbf{m}_i^{\lambda} = \int d\hat{\mathbf{e}}_i^{\lambda} \; P_i^{\lambda}(\hat{\mathbf{e}}_i^{\lambda}) \hat{\mathbf{e}}_i^{\lambda} = \frac{1}{3}\beta(-\nabla_{\mathbf{m}_i^{\lambda}} < \Omega > + \mathbf{h}_i^{\lambda,ext}), \tag{5.44}$$

where $\mathbf{h}_i^{ext}$ is a $3n$ component external magnetic field which will be set to zero. The dimensionless susceptibility $\overline{\chi}$ is hence given by

$$\overline{\chi}_{i\alpha,j\gamma}^{\lambda,\xi} \equiv \frac{\partial m_{i\alpha}^{\lambda}}{\partial h_{j\gamma,}^{\xi,ext}}|_{h_{j\gamma}^{\xi,ext}=0} = \frac{1}{3}\beta \frac{\partial(-\partial < \Omega > /\partial m_{i\alpha}^{\lambda})}{\partial h_{j,\gamma}^{\xi,ext}} + \frac{1}{3}\beta\delta_{ij}\delta_{\alpha\gamma}\delta_{\lambda\xi}, \tag{5.45}$$

where the superscripts λ and ξ refer to sublattices and the subscripts α and γ, and i and j, respectively refer to spatial components and unit cells.

Using the same arguments as those leading to Eq. 5.31, we can rewrite Eq. 5.45 as

$$\overline{\chi}_{i\alpha,j\gamma}^{\lambda,\xi} = \frac{1}{3}\beta \sum_{\kappa=1}^{n} \sum_{k,\eta} S_{i\alpha,k\eta}^{(2),\lambda,\kappa} \overline{\chi}_{k\eta,j\gamma}^{\kappa,\xi} + \frac{1}{3}\beta\delta_{ij}\delta_{\alpha\gamma}\delta_{\lambda\xi}, \tag{5.46}$$

where

$$S_{i\alpha,k\eta}^{(2),\lambda,\kappa} \equiv -\frac{\partial^2 < \Omega >}{\partial m_{i\alpha}^{\lambda} \partial m_{k\eta}^{\kappa}}. \tag{5.47}$$

In the paramagnetic state $S_{i\alpha,k\eta}^{(2),\lambda,\kappa} = \delta_{\alpha,\eta} S_{i,k}^{(2),\lambda,\kappa}$ and we can take a lattice Fourier transform of Eq. 5.46 to obtain

$$\overline{\chi}^{\lambda\xi}(\mathbf{q}) = \frac{1}{3} \sum_{\kappa=1}^{n} \beta S^{(2),\lambda,\kappa}(\mathbf{q}) \overline{\chi}^{\kappa\xi}(\mathbf{q}) + \frac{1}{3}\beta\delta_{\lambda\xi}. \tag{5.48}$$

Equation 5.48 can be written in matrix form:

$$\overline{\boldsymbol{\chi}}(\mathbf{q}) = 1/3\beta\mathbf{S}^{(\mathbf{2})}(\mathbf{q})\overline{\boldsymbol{\chi}}(\mathbf{q}) + 1/3\beta\mathbf{I}_n, \tag{5.49}$$

where the $\lambda\xi$th entry of $\overline{\boldsymbol{\chi}}(\mathbf{q})$ ($\mathbf{S}^{(\mathbf{2})}(\mathbf{q})$), is $\overline{\chi}(\mathbf{q})^{\lambda,\xi}$ ($S^{(2),\lambda,\xi}(\mathbf{q})$). Solving for $\overline{\boldsymbol{\chi}}(\mathbf{q})$ we obtain

$$\overline{\boldsymbol{\chi}}(\mathbf{q}) = \frac{1}{3}\beta[\mathbf{I}_n - 1/3\beta\mathbf{S}^{(\mathbf{2})}(\mathbf{q})]^{-1} \tag{5.50}$$

The magnetic ordering temperature T_c, i.e. the temperature at which the susceptibility diverges, is thus given by the solution of

$$\det[\mathbf{I}_n - 1/3\beta\mathbf{S}^{(\mathbf{2})}(\mathbf{q})] = 0. \tag{5.51}$$

5.4.1 Results for Manganese Stabilised Cubic Zirconia

In order to demonstrate the multi-sublattice formulation of the DLM method, we consider now the dilute magnetic semiconductor manganese-stabilised zirconia. Zirconia (zirconium dioxide) exists in a cubic phase between 2663K and its melting point, crystallising into a *fluorite* structure. Here, zirconium atoms form a face-centered cubic array, with oxygen atoms residing in the tetrahedral holes. The corresponding primitive unit cell has a zirconium atom at the origin and oxygen atoms located at (0.25,0.25,0.25) and (0.75,0.75,0.75). When doped with MnO the cubic phase of ZrO_2 can be stabilised at room temperature. In such a manganese-stabilised cubic zirconia (Mn-SZ), zirconium atoms are randomly substituted with manganese atoms to give $Zr_{1-x}Mn_xO_2$. The partially filled 3d shell of the manganese ions leads to the formation of local magnetic moments and we investigate here whether Mn-SZ has an ordered magnetic phase. This entails using the CPA to deal both with local moment disorder as well as compositional disorder arising from the random substitution of Zr with Mn.

As for all the systems studied in this thesis, the self-consistent potentials that we generate for Mn-SZ are restricted to a muffin-tin form. However, the fluorite structure has an unoccupied octahedral site, the potential around which will vary considerably due to the surrounding ions. This means that the assumption that the potential between spheres is constant can no longer be considered a good approximation. This situation can be rectified using the *empty spheres* technique [113]. Here, 'hollow' spheres, containing no nuclei charge, are introduced and the potential within them determined self-consistently. For Mn-SZ we introduce an empty sphere at the octahedral position, (0.5,0.5,0.5). We thus consider Mn-SZ as being composed of four interpenetrating sublattices, one of which is randomly occupied by zirconium and manganese atoms, two of which are occupied by oxygen atoms and the final one occupied by empty spheres.

We consider Mn-SZ for concentrations of manganese ranging from 5% to 40%, with experimental lattice parameters used. Our self-consistent calculations for the DLM state yield a magnetic moment of $\approx 3.23\mu_{\mathrm{B}}$ on the Mn sites, for all concentrations. We calculate the paramagnetic spin susceptibility using Eq. 5.50. Since the Mn sites are the only ones to possess a non-negligible magnetic moment, the only component of the susceptibility of importance is that corresponding to Mn. This is plotted in Fig. 5.1, for a Mn-SZ system with 25% manganese concentration. The susceptibility is seen to peak strongly at $\mathbf{q} = \mathbf{0}$, implying that the system has a tendency to order ferromagnetically. Such behaviour was also observed for all the other concentrations investigated here. The temperature at which the ordering is expected to occur, T_{C}, can be evaluated using Eq. 5.51 and was found to be 585K for 25% manganese. Since the average magnetic moment per unit cell will increase with Mn concentration, the magnetic ordering temperature might be expected to increase as the Mn concentration increases. Indeed, this is what

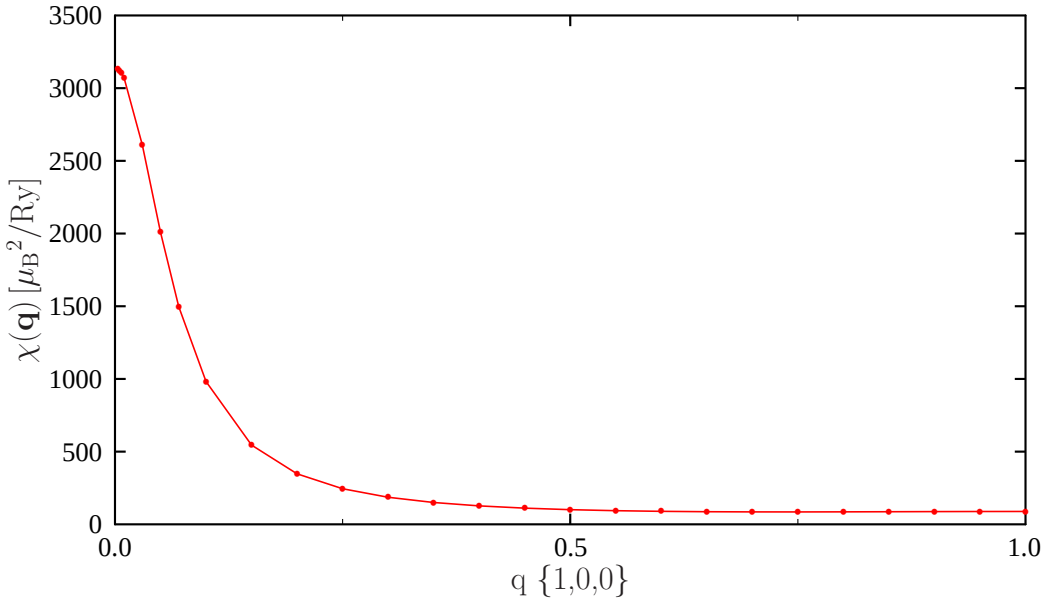

Figure 5.1: Paramagnetic spin susceptibilities for $Zr_{0.75}Mn_{0.25}O_2$ for wavevectors along the [1,0,0] direction.

is observed, as shown in Fig. 5.2 where the ordering temperature is plotted as a function of manganese concentration. Further details of this investigation of Mn-SZ, as well as much more analysis, can be found in reference [11].

5.5 LSIC Implementation

The DLM approach, outlined in the introduction of this chapter, was based on an amalgam of the localised and itinerant pictures of magnetism. In some respects the SIC electronic structure scheme provides a natural framework in which to study this approach. In particular it is clear how, within the SIC method, a local moment type picture can emerge; SIC corrected, i.e. localised, states will establish atomic-like moments, which will influence the motion of itinerant electrons, described by a non-corrected potential, such that the spin of electrons arriving at a site tend to

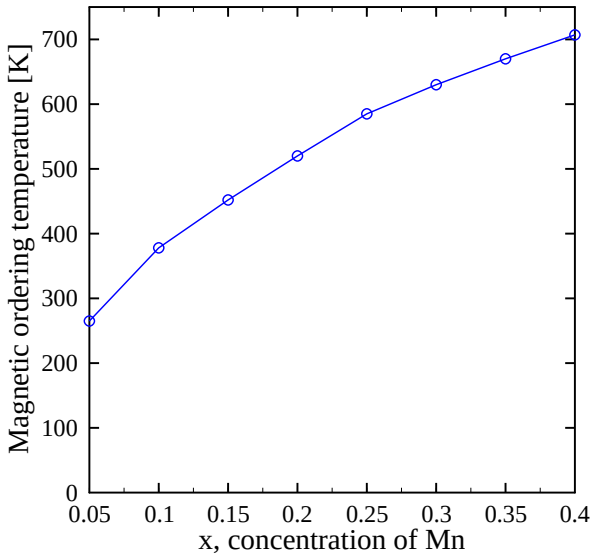

Figure 5.2: Magnetic ordering temperature, T_{C}, of Mn-SZ as a function of manganese concentration, x.

reinforce the moment at that site.

The DLM formalism given in this chapter can easily be incorporated with the multiple-scattering version of the SIC electronic scheme, i.e. the LSIC. In particular, the KKR-CPA procedure can be used to treat local moment disorder. Working in a reference frame local to some site i, we compute the matrices t_+/t_-, representing the scattering of an electron with spin parallel/antiparallel to the local moment direction $\hat{\mathbf{e}}_i$. The SIC corrected channels of these two matrices will differ. Indeed, according to the picture outlined in the previous paragraph, states with spin parallel to $\hat{\mathbf{e}}_i$ are expected to be, on the average, more localised than those with spin antiparallel to $\hat{\mathbf{e}}_i$. Thus the states described by t_+ will be more likely to have a resonance, for which self-interaction should be calculated, than those described by t_-. Once t_+ and t_- have been computed, we can write down the

scattering matrix for the site i in the common (global) frame of reference:

$$\mathbf{t}_i = \frac{1}{2}(t_+ + t_-)\mathbf{1} + \frac{1}{2}(t_+ - t_-)\sigma\cdot\hat{\mathbf{e}}_i, \tag{5.52}$$

where σ_x, σ_y and σ_z are the three Pauli spin matrices defined according to the global z-axis. Using the same arguments as those given in section 5.1, the electronic structure problem presented by the random orientatational configurations $\{\hat{\mathbf{e}}_i\}$ reduces to that of a binary pseudo alloy, with 50% of sites occupied by 'up' moments and 50% by 'down' moments, which we describe using the CPA. When used in conjunction with the charge self-consistency procedure outlined in section 4.1, this constitutes a fully self-consistent LSIC-KKR-CPA electronic structure scheme.

Once the LSIC-KKR-CPA electronic structure problem has been solved, the linear response approach of section 5.2 can be used to determine the effect of applying a magnetic field to the paramagnetic state. From this, the magnetic response of the system, and consequently the paramagnetic spin susceptibility, can be evaluated. The form of the susceptibility expression derived in section 5.3, Eq. 5.40, does not change in the LSIC case. Indeed, all details of the electronic structure are contained within the direct correlation function $S^{(2)}$. This function can be evaluated using Eq. 5.34, where the quantities entering this expression are obtained now from the LSIC-KKR-CPA.

The DLM-SIC scheme outlined here constitutes a fully *ab initio* theory of finite temperature magnetism in strongly-correlated systems. As a first demonstration of the method we investigate in the following section the onset of magnetic order in γ-Ce, the electronic structure of which we have already discussed in chapter 4.

5.5.1 Results for Cerium

Before proceeding with a DLM-SIC calculation for γ-Ce, we begin by reviewing what is known experimentally about the magnetic properties of cerium. During the 1950s and 1960s many experiments were undertaken to measure the magnetic susceptibility of cerium [114, 115, 116, 117], prompted by advances in the previous decades that had enabled the isolation of pure rare earth metals [118]. Unfortunately, whilst the samples used in the susceptibility measurements were of a high chemical purity, they invariably contained mixtures of different allotropic phases of cerium. At room temperature and pressure the γ phase of cerium is stable, however when cooled to a temperature of ≈ 263K it starts to partially transform to β-Ce, a dhcp structured phase. Continued cooling to ≈ 100K causes any untransformed γ-Ce to transform to α-Ce and, with further cooling, β-Ce starts to partially transform to α-Ce [96].

Since the original susceptibility measurements on cerium, experimental advances have enabled allotropically pure samples of β-Ce and α-Ce to be studied down to low temperatures. These studies showed β-Ce to be antiferromagnetic, with a Néel temperature of 12.5K [119], and α-Ce to be essentially a Pauli paramagnet [120]. There has not yet, however, been any such success in stabilising γ-Ce at low temperatures, with only high temperature susceptibility data available for this system. Nevertheless, these high temperature data can potentially imply information about the low temperature behaviour of the system. The results of early studies of γ-Ce by Colvin [116] and Burr [117], showed that at high temperatures the magnetic susceptibility obeys the Curie-Weiss law. Extrapolating this data gave a negative Weiss temperature θ, one interpretation of which is that the system is antiferromagnetic, with the corresponding Néel temperature given

by $T_N \approx -\theta$. The values for the Weiss temperature in the two studies were, however, quite different, with Colvin giving $\theta = -50$K and Burr $\theta = -9$K. Much uncertainty hence remains about the low temperature magnetic behaviour of γ-Ce, providing motivation for the present theoretical investigation of this system.

Figure 5.3 shows paramagnetic spin susceptibilities for γ-Ce, obtained using the formalism described in section 5.5. Following the analysis given in section 4.2, we SIC correct the f state of A_{2u} symmetry. The susceptibility is seen to attain its maximum value at $\mathbf{q} = \mathbf{0}$, indicating a ferromagnetic, rather than antiferromagnetic, ordering tendency. Solving the equation $1 - \frac{1}{3}\beta S^{(2)}(\mathbf{q} = \mathbf{0}) = 0$, gives a Curie temperature $T_C = 42$K.

Figure 5.4 shows the temperature dependence of the susceptibility, where a Curie-Weiss type behaviour is observed. Upon examining the formula for χ, Eq. 5.40, it is clear that such behaviour corresponds to when the 'exchange-integral' $S^{(2)}(\mathbf{q}, T)$ depends only weakly on temperature. Near the temperature axis the inverse susceptibility data deviates slightly from the linear trend, which explains why the intercept temperature, 46K, is slightly higher than the critical temperature $T_C = 42$K obtained by solving the equation $1 - \frac{1}{3}\beta S^{(2)}(\mathbf{q} = \mathbf{0}) = 0$, where high temperature $S^{(2)}$ data was used. This temperature dependence of $S^{(2)}(\mathbf{q}, T)$ is a manifestation of the Fermi factor in Eq. 5.34.

In summary, we have presented here a first demonstration of our new LSIC implementation of the DLM method. Our calculations for γ-Ce, a system whose magnetic groundstate has not been determined experimentally, indicate a ferromagnetic ordering tendency. In the next chapter we use our DLM-SIC scheme to investigate magnetic ordering in some other 4f systems, namely the heavy rare earth metals. Unlike γ-Ce, a wealth of experimental data exists for these systems, which show a complex array of different magnetic ordering types.

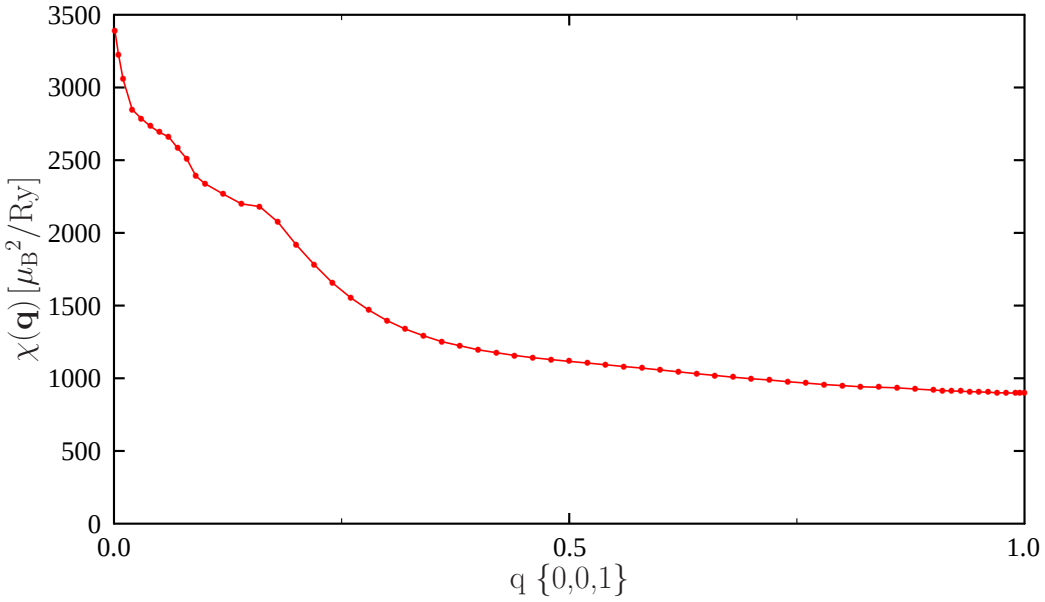

Figure 5.3: Paramagnetic spin susceptibilities for γ-Ce, calculated at a temperature of 60K.

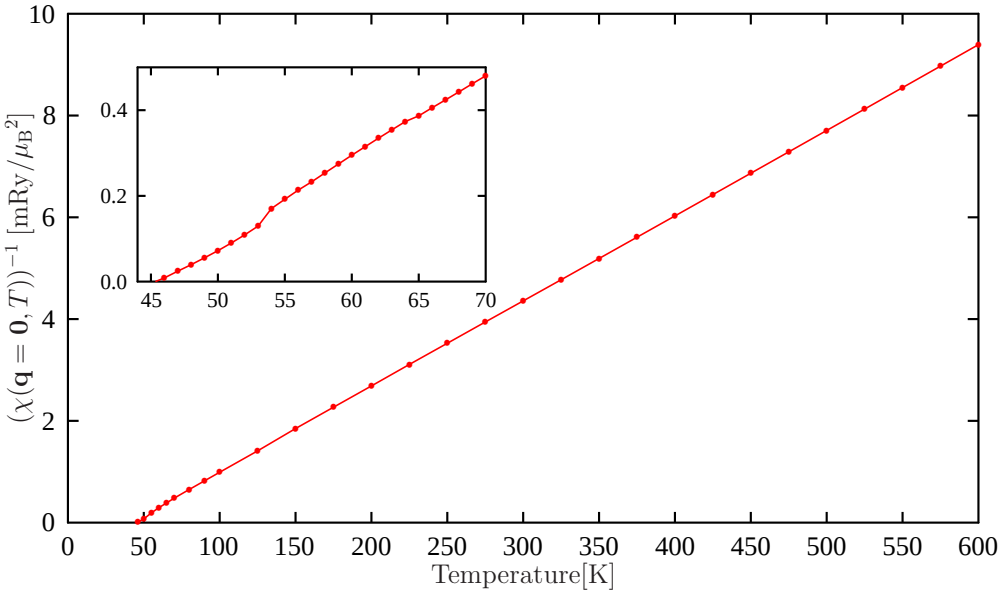

Figure 5.4: Inverse spin susceptibilities for γ-Ce as a function of temperature. The inset shows an enlargement of the critical temperature region.

Chapter 6

Results for Heavy Rare Earth Metals

The heavy rare earth (RE) elements, gadolinium (Gd) to thulium (Tm), exhibit a rich variety of magnetic structures. Gadolinium exhibits a paramagnetic to ferromagnetic transition, while the high temperature ordered phases of the later elements (terbium $\rightarrow$ thulium) are all antiferromagnetically modulated along the c axis, where layers of atoms normal to the c axis are uniformly magnetised in a direction which changes from layer to layer. In terbium, dysprosium and holmium the direction in which the layers are magnetised is perpendicular to the c axis, resulting in a helix structure, whereas in Er and Tm the direction of magnetisation is parallel to the c-axis, resulting in a longitudinally polarised structure [96]. This array of magnetic structures will be the subject of this chapter, where we use the DLM approach to analyse the ordering mechanisms at work in the heavy REs.

Being members of the lanthanide series the heavy RE elements are, like cerium, characterised by an incompletely filled 4f shell. The 4f states are highly localised and establish substantial local spin moments. Since the direct overlap

between 4f orbitals on neighbouring atoms is negligible the 4f electrons contribute little to chemical bonding and are usually considered chemically inert. Consequently the heavy REs, which differ only in the number of these 4f electrons and have a common outer $(5d)^1(6s)^2$ electronic configuration, are chemically very similar.

As well as being chemically similar the heavy REs are also structurally similar, with hcp structures being adopted by all members of the series. The crystal field associated with the hcp lattice acts on the 4f electron clouds, giving rise to magnetocrystalline anisotropies. Consequently there are certain directions, relative to the crystal structure, in which magnetic moments prefer to align themselves along. It is these magnetic *easy axes* that determine whether a helix or longitudinally polarised structure is adopted in the late heavy rare earth elements [121]. To be able to describe this anisotropy in the DLM theory the effects of spin-orbit coupling need to be incorporated. Such a *relativistic* DLM implementation is described in reference [122]. This implementation is founded around relativistic density functional theory [123], where, in analogy with the Kohn-Sham approach of standard density functional theory, self-consistent solutions are sought of a single-particle Dirac equation. In order to avoid the complications of this relativistic formalism, this chapter will focus mainly on the first member of the heavy REs, gadolinium, for which, on account of its zero orbital moment in the ground state, the effects of spin orbit coupling can be neglected. However, as will be argued in section 6.2, the results obtained from the study of gadolinium can be used to explain trends in magnetism across the whole heavy RE series. Moreover, it will be shown how simple scaling relations can be used to take into account the different orbital angular momentum values of the heavy REs, such that estimates of their ordering temperatures can be given.

The crystal field effect outlined in the previous paragraph is an example of a *single-ion interaction*. Such interactions act independently at each lattice site and do not depend on the orientations of magnetic moments at other sites. Magnetic correlations, on the other hand, depend on cooperative effects between moments on different sites. In the rare earths such cooperative effects are due mainly to *two-ion interactions* between pairs of 4f moments. Of these the most important is an *indirect exchange* interaction by which pairs of 4f moments are coupled through the polarisation of the conduction electrons. This is termed the Ruderman-Kittel-Kasuya-Yosida (RKKY) interaction [13], the theory of which will be outlined now.

The starting point for discussing RKKY coupling is the so-called *s-f* interaction between a 4f ionic spin $\mathbf{S}_i$ and some conduction-electron charge density $\mathbf{s}(\mathbf{r})$:

$$\mathcal{H}_{sf}(i) = -\int d\mathbf{r}\ A(\mathbf{r}-\mathbf{R}_i)\mathbf{S}_i \cdot \mathbf{s}(\mathbf{r}), \tag{6.1}$$

where $\mathbf{R}_i$ is the position of the ionic spin and the exchange integral , $A(\mathbf{r}-\mathbf{R}_i)$, is determined by the overlap of the 4f and conduction electron clouds. Equation 6.1 can be rewritten as

$$\mathcal{H}_{sf}(i) = -\int d\mathbf{r}\ \mathbf{H}_i(\mathbf{r}) \cdot \mu(\mathbf{r}), \tag{6.2}$$

where $\mu(\mathbf{r}) = \mu_{\mathrm{B}}\mathbf{s}(\mathbf{r})$ is the conduction-electron moment density and $\mathbf{H}_i(\mathbf{r})$ is an effective magnetic field, given by

$$\mathbf{H}_i(\mathbf{r}) = \frac{1}{\mu_{\mathrm{B}}} A(\mathbf{r}-\mathbf{R}_i)\mathbf{S}_i. \tag{6.3}$$

The magnetic field $\mathbf{H}_i(\mathbf{r})$, generated by the ionic spin at $\mathbf{R}_i$, will act on the conduction electron cloud and induce a moment at $\mathbf{r}$, given by

$$\mu(\mathbf{r}) = \int d\mathbf{r}'\ \chi^{\mathrm{conduction}}(\mathbf{r}-\mathbf{r}')\mathbf{H}_i(\mathbf{r}'), \tag{6.4}$$

where $\chi^{\text{conduction}}$ is the susceptibility of the conduction electrons. This moment will interact with the effective magnetic field $\mathbf{H}_j(\mathbf{r})$, generated by an ionic spin at $\mathbf{R}_j$, to give the following coupling between sites i and j:

$$\mathcal{H}(ij) = -\int\int d\mathbf{r}d\mathbf{r}'\ \mathbf{H}_j(\mathbf{r})\chi^{\text{conduction}}(\mathbf{r}-\mathbf{r}')\mathbf{H}_i(\mathbf{r}'). \tag{6.5}$$

Summing Eq. 6.5 over all sites, substituting in $\mathbf{H}_i$ from Eq. 6.3 and taking the lattice Fourier transforms of A and $\chi^{\text{conduction}}$ leads to the following Heisenberg like Hamiltonian for the ff interaction:

$$\mathcal{H}_{ff} = -\sum_{ij}\mathcal{J}_{ij}\mathbf{S}_i\cdot\mathbf{S}_j, \tag{6.6}$$

where the exchange integral $\mathcal{J}_{ij}$ is given by

$$\mathcal{J}_{ij} = \frac{1}{\mu_{\text{B}}^2}\sum_{\mathbf{q}} A^2(\mathbf{q})\chi^{\text{conduction}}(\mathbf{q})e^{i\mathbf{q}\cdot(\mathbf{R}_i-\mathbf{R}_j)}. \tag{6.7}$$

In the RKKY approach $A^2(\mathbf{q})$ is taken to be a constant, A_0, with the real space *s-f* exchange integral thus given by $A(\mathbf{r}-\mathbf{R}_i) = A_0\delta(\mathbf{r}-\mathbf{R}_i)$. Substituting $A^2(\mathbf{q}) = A_0$ into Eq. 6.7 gives

$$\mathcal{J}_{ij} = \frac{A_0^2}{\mu_{\text{B}}^2}\sum_{\mathbf{q}}\chi^{\text{conduction}}(\mathbf{q})e^{i\mathbf{q}\cdot(\mathbf{R}_i-\mathbf{R}_j)}. \tag{6.8}$$

If the conduction electrons are treated as free then $\chi^{\text{conduction}}$ corresponds to the non-interacting susceptibility of an electron gas, given by

$$\chi_0^{\text{conduction}}(\mathbf{q}) = 2\mu_{\text{B}}^2\sum_{nn'\mathbf{k}}\frac{f_n(\mathbf{k})-f_{n'}(\mathbf{k}+\mathbf{q})}{E_{n'}(\mathbf{k})-E_n(\mathbf{k}+\mathbf{q})}, \tag{6.9}$$

where f is the Fermi-Dirac function and $E_n(\mathbf{k})$ is the energy of an electron in the nth band with wavevector $\mathbf{k}$. For pairs of electronic states that are separated by $\mathbf{q}$ and which have similar energies, E_n and $E_{n'}$, the denominator of Eq. 6.9 ≈ 0. If, furthermore, one of the states is occupied and the other unoccupied,

the numerator of Eq. 6.9 is non-negligible and so the pair will provide a large contribution to the sum. Parallel regions of Fermi surface, separated by a *nesting vector* $\mathbf{Q}_0$, can provide large numbers of such pairs. This can produce a peak in the susceptibility, known as a *Kohn anomaly*, at the nesting vector $\mathbf{Q}_0$. Such Fermi surface effects will be important when analysing the results of susceptibility calculations later on in this chapter.

If the sum over k in Eq. 6.9 is replaced by an integral it can be shown [124] that

$$\chi_0^{\text{conduction}}(\mathbf{q}) = 2\mu_{\text{B}}^2 g(E_F) f(\frac{q}{2k_F}), \tag{6.10}$$

where $g(E_F)$ is the density of states at the Fermi energy E_F, $k_F = \sqrt{E_F}$ and

$$f(x) = \frac{1}{2}(1 + \frac{1-x^2}{2x}\ln|\frac{1+x}{1-x}|). \tag{6.11}$$

Using this expression for $\chi_0^{\text{conduction}}$ leads to

$$\sum_{\mathbf{q}} \chi_0^{\text{conduction}}(\mathbf{q}) e^{i\mathbf{q}\cdot\mathbf{r}} = 2\mu_{\text{B}}^2 \frac{2k_F^3}{\pi} g(E_F) F(2k_F r), \tag{6.12}$$

where

$$F(x) = \frac{-x\cos x + \sin x}{x^4}. \tag{6.13}$$

It follows from Eq. 6.8 that

$$\mathcal{J}_{ij} = 4A_0^2 g(E_F) \frac{k_F^3}{\pi} F(2k_F|\mathbf{R}_i - \mathbf{R}_j|) \tag{6.14}$$

Looking at the form of F it is evident that the exchange interaction $\mathcal{J}_{ij}$ oscillates as a function of $|\mathbf{R}_i - \mathbf{R}_j|$. Thus depending on the distance between two f moments they may be ferromagnetically or antiferromagnetically coupled.

To specify the state of a 4f ion the total angular momentum J, rather than the spin angular momentum S, should be used. By projecting J onto S we can

replace the spin by $S = (g_J - 1)J$, where g_J is the Lande' g-factor. Substituting this into Eq. 6.6 we obtain

$$\mathcal{H}_{ff} = -\sum_{ij} 4A_0^2(g_J - 1)^2 g(E_F)\frac{k_F^3}{\pi}F(2k_F|\mathbf{R}_i - \mathbf{R}_j|)\mathbf{J}_i \cdot \mathbf{J}_j. \tag{6.15}$$

The interaction $\mathcal{H}_{ff}$ evidently has the form of a classical Heisenberg Hamiltonian, -$\sum_{ij} \mathcal{J}_{ij}\mathbf{J}_i \cdot \mathbf{J}_j$. For systems described by such Hamitonians, the Weiss molecular field theory gives the following mean field estimate for the magnetic ordering temperature T_C:

$$k_{\mathrm{B}}T_{\mathrm{C}}^{\mathrm{MFA}} = \frac{2}{3}J(J+1)\sum_{j\neq 0}\mathcal{J}_{0j}. \tag{6.16}$$

Thus a mean-field estimate of the ordering temperature of the 4f moments is given by

$$T_{\mathrm{C}}^{\mathrm{MFA}} = \frac{2}{3}J(J+1)(g_J - 1)^2 4A_0^2 g(E_F)\frac{k_F^3}{k_{\mathrm{B}}\pi}\sum_{\mathbf{R}_j\neq\mathbf{R}_i} F(2k_F|\mathbf{R}_i - \mathbf{R}_j|). \tag{6.17}$$

From Eq. 6.17 we expect the ordering temperatures of the heavy REs to be proportional to the so-called *de Gennes factor* $(g_J - 1)^2 J(J+1)$.

6.1 Gadolinium

In this section we investigate in detail the onset of magnetic order in the first member of the heavy REs, gadolinium. Initially, in subsection 6.1.1, we consider the system only at its equilibrium lattice parameters, both those measured experimentally and also those determined theoretically by minimising the energy of the system with respect to these parameters. For the experimental lattice parameters the paramagnetic spin susceptibility of Gd is evaluated using both the LSIC implementation of the DLM theory and also the standard LDA implementation. It is shown that in order to give a proper description of the localised f electrons

and to obtain the correct ordering mechanism it is essential to use the LSIC implementation. Subsection 6.1.2 then goes on to consider gadolinium away from its equilibrium lattice parameters. The magnetic structure of the system is found to depend critically on the c/a ratio of the hcp lattice parameters and this dependency is explained in terms of underlying changes to the Fermi surface of the paramagnetic state.

6.1.1 Equilibrium Lattice Parameters

Since gadolinium crystallises into a hcp structure its lattice constants can be parametrised by two variables, the c/a ratio of the lattice parameters and the atomic unit cell volume, expressed in terms of the Wigner-Seitz (WS) radius. Experimentally these two parameters are 1.597 for the c/a ratio and 3.762 a.u. for the WS radius [125]. The densities of states of gadolinium at these lattice parameters is shown in Fig. 6.1. In the pure LDA calculation the minority 4f states make a significant contribution to the densities of states at the Fermi energy. As will shortly be described, this has important implications for the magnetic ordering exhibited by the system. In the SIC calculation, where all 7 majority 4f states were corrected, a Hubbard gap opens up between the occupied and unoccupied f states. This pushes the majority f states down to approximately 16eV below the Fermi energy and moves the minority f states away from the conduction bands, reducing the f contribution at the Fermi energy. The LSIC DOS thus coincides more closely with the experimental picture, where the f states play little role in conduction.

Figure 6.2 shows paramagnetic spin susceptibilities for gadolinium, corresponding to the electronic structures shown in Fig. 6.1. For the LDA calculation (a) the susceptibility attains its maximum at $\mathbf{q}$=(0,0,1), indicating that the system will order with a commensurate type 1 antiferromagnetic (AF1) structure, where

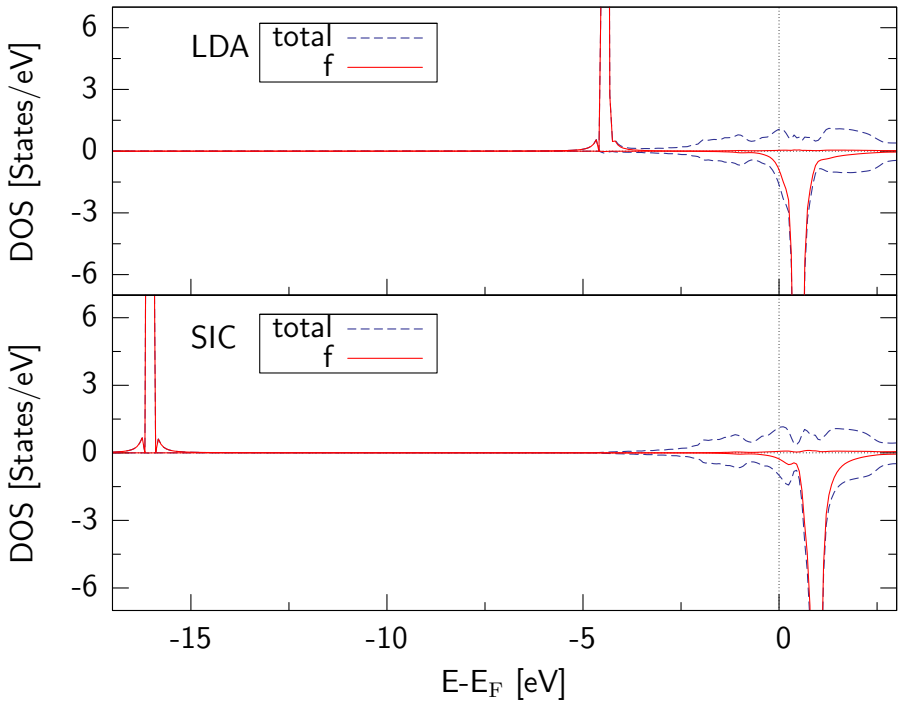

Figure 6.1: Density of states of Gd, in the paramagnetic (DLM) state. Minority states are plotted with negative values of the DOS.

magnetic moments are oppositely aligned in alternate planes along the c-axis. This is consistent with the results of other LDA studies of gadolinium [126], where an antiferromagnetic structure was found to be energetically favourable over the experimentally observed ferromagnetic structure. The origin of this AF1 coupling has been attributed to the close proximity of 4f minority states to the Fermi energy [127], which concurs with the LDA DOS we obtain in Fig. 6.1. Previous investigations have shown that by pushing the 4f states away from the Fermi energy, either by treating them as part of the core [128] or including a Coulomb parameter U for the f states (LDA+U) [129], a ferromagnetic groundstate can be obtained. Since the LSIC has this same effect of pushing the f states away from the Fermi energy, as evidenced by the density of states shown in Fig. 6.1, we expect ferromagnetism to be predicted by the LSIC calculation. Indeed, the paramagnetic spin susceptibility for the LSIC calculation, Fig. 6.2(b), attains its maximum value at $\mathbf{q} = \mathbf{0}$, implying a ferromagnetic ordering tendency. It is worth noting at this stage the presence of a shoulder in the susceptibility along the [001] direction, around $q = 0.2$. This feature will be elaborated on further in section 6.1.2.

Having demonstrated that the LSIC gives an appropriate treatment of the 4f states, leading to a ferromagnetic groundstate, we proceed further with the investigation of gadolinium. To determine the theoretical lattice parameters of the system we consider first some fixed c/a ratio and calculate the total energy as a function of WS radius. By repeating this procedure for different c/a ratios the global energy minimum of the system can be found. Fig. 6.3 shows the results of these calculations for selected c/a ratios. It is evident that the positions of the various energy minima are almost invariant to the c/a ratio. The overall minimum occurs at a c/a ratio of 1.63 and a WS radius of 3.654 a.u. The paramagnetic spin susceptibility for these lattice parameters, shown in Fig. 6.4, attains its maximum

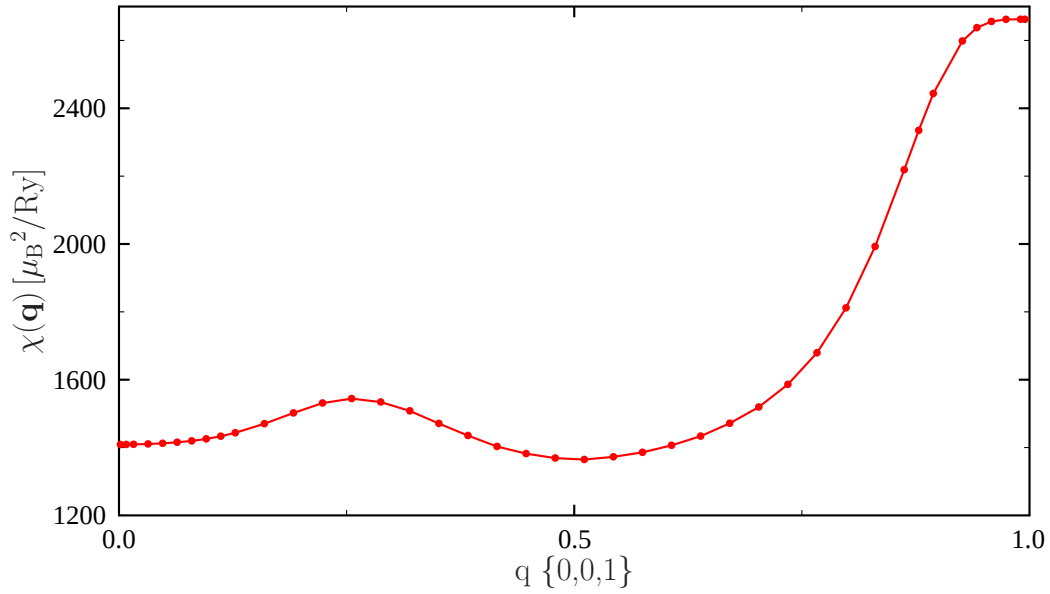

(a)

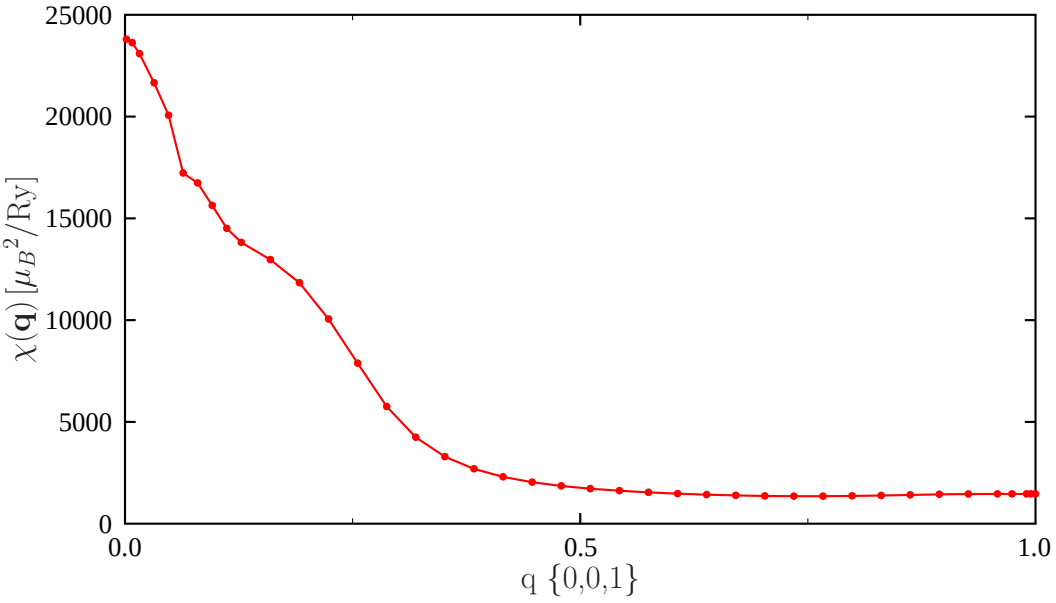

(b)

Figure 6.2: Paramagnetic spin susceptibilities for gadolinium for wavevectors along the [0,0,1] direction, obtained from (a) LDA calculation, (b) LSIC calculation.

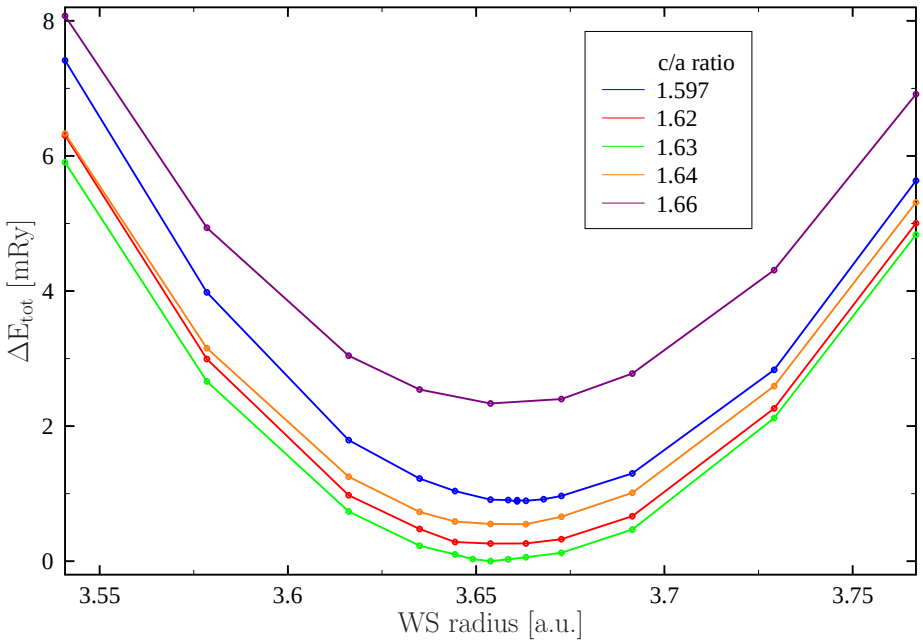

Figure 6.3: Calculated total energies as a function of c/a ratio and WS radius.

at $\mathbf{q} = \mathbf{0}$ and hence ferromagnetic ordering is predicted.

Figure 6.5 shows the temperature dependence of the $\mathbf{q} = \mathbf{0}$ (ferromagnetic) susceptibility of gadolinium. A Curie-Weiss type behaviour is observed, with T_C=280K/324K for the theoretical/experimental lattice parameters. The overestimate of the Curie temperature at the experimental lattice parameters (experimental T_C=293K [121]) can be attributed to the mean-field approximation used in the DLM theory [130]. The effective magnetic moment was 7.34μ_B/7.36μ_B for the theoretical/experimental lattice parameters. These values are in reasonable agreement with the experimental value of 7.63μ_B and also the results from calculations where the 4f states were treated as part of the core (7.44μ_B [131]) or the LDA+U was used (7.41μ_B [127]). Examining the l-decomposed spin densities obtained from the LSIC DOS shows that the magnetic moment originates mainly from the f

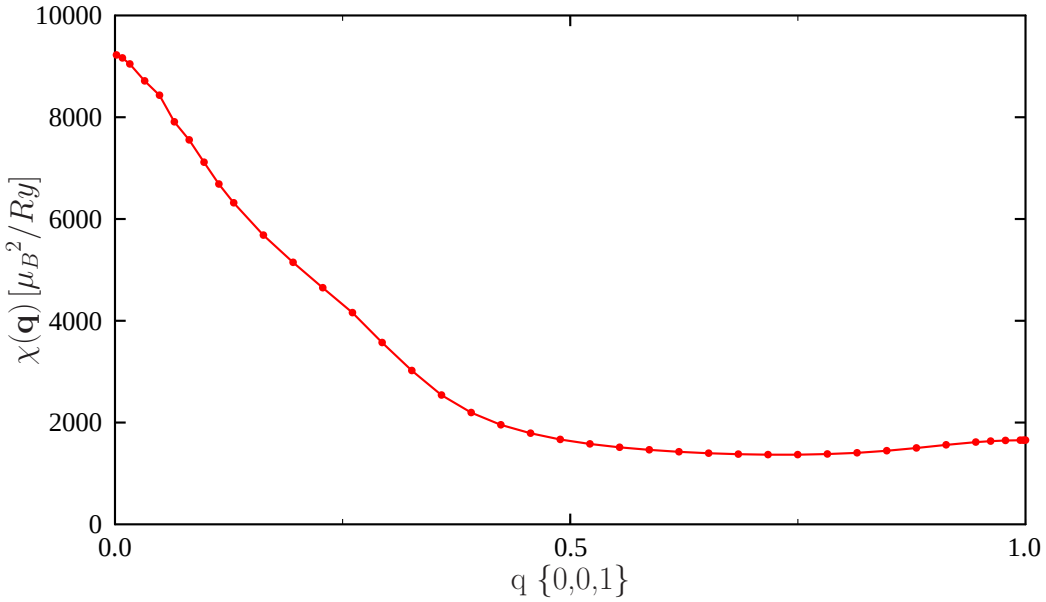

Figure 6.4: Paramagnetic spin susceptibilities for Gd, obtained using theoretical lattice parameters.

states ($\approx 6.95\mu_B$), with the remainder coming from a polarisation of the d states ($\approx 0.34\mu_B$) plus a small contribution from the s and p states ($\approx 0.07\mu_B$). This composition of the spin moment is in qualitative agreement with that obtained from LMTO-LDA calculations [132].

6.1.2 Non-equilibrium Lattice Parameters

In this section we examine how the magnetic ordering tendencies of gadolinium change as the lattice parameters are moved away from their equilibrium values. We consider first the effect of changing the c/a ratio, with the WS-radius fixed at the theoretical value (3.654 a.u.). Figure 6.6 shows paramagnetic spin susceptibilities for gadolinium, with the c/a ratio ranging from 1.54 to 1.66. It is evident that as the c/a ratio decreases the susceptibility starts to develop a shoulder near $\mathbf{q} = (0, 0, 0.2)$, similar to that observed in Fig. 6.2(b). Moreover, at the lowest

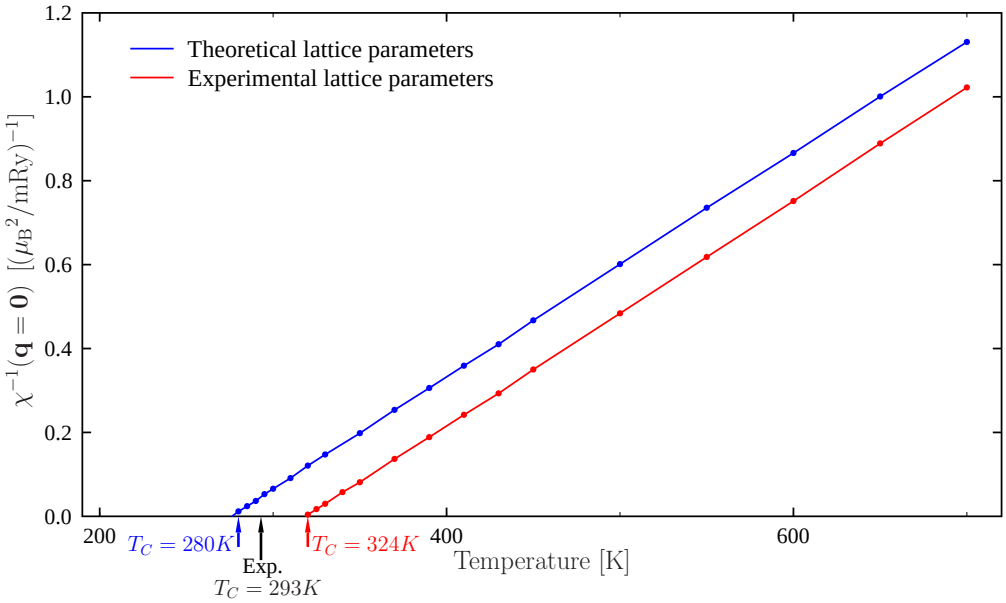

Figure 6.5: Inverse Spin susceptibilities for Gd as a function of temperature.

c/a ratios this shoulder grows into a peak and the susceptibility no longer attains its maximum value at $\mathbf{q} = \mathbf{0}$. The maximum occurs instead at some incommensurate wavevector, q_{inc}, meaning that the system has a tendency to order into some incommensurate magnetic structure. This could be helical, where the helix turn angle, i.e. the angle between magnetic moments in adjacent layers, would be given by πq_{inc}.

Such incommensurate ordering is exhibited by the late heavy rare earth elements, terbium to thulium, and is associated with a feature of the Fermi surface of these systems known as "webbing". This webbing structure contains large parallel sheets of Fermi surface, which can nest together when translated by some vector in $\mathbf{k}$-space. As outlined earlier in this chapter, such nesting can cause an enhancement of the magnetic susceptibility at the nesting vector, and indeed it has been shown, both theoretically [133] and experimentally [134], that the size of

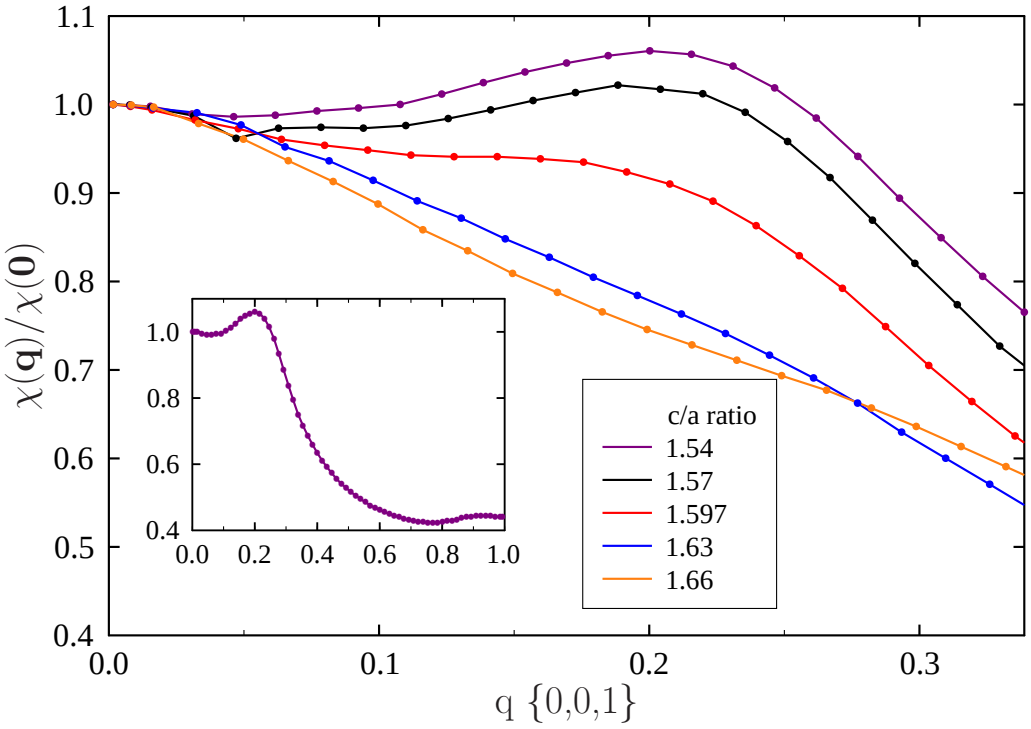

Figure 6.6: Normalised paramagnetic spin susceptibilities for Gd, obtained using the theoretical unit cell volume. The inset shows the susceptibility up to the zone boundary for c/a ratio 1.54.

the nesting vector in the late heavy REs is correlated with their magnetic ordering vectors. The shape of the Fermi surface in heavy RE metals depends critically on the c/a ratio of the lattice parameters [135], which hence implies that the magnetic structures of these elements are sensitive to the c/a ratio. This is corroborated by experimental studies, which have shown that is possible to alter the magnetic state of RE metals and alloys by changing the lattice parameters through application of external pressure or tension [136, 137].

Andrianov [138] investigated experimentally the helical magnetic ordering in several heavy RE elements and RE yttrium alloys and found that when the helix turn angle was plotted as a function of c/a ratio all the points were positioned on a smooth, square-root shaped, curve. He also noted that the helix turn angle varied by several orders of magnitude while the c/a ratio changed by less than 1%. Such behaviour could possibly be interpreted in terms of an electronic topological transition (ETT) [139, 140] at some critical c/a ratio, where the webbing structure of the Fermi surface ruptures.

To analyse the susceptibility results we obtained in Fig. 6.6, we investigate the Fermi surface of paramagnetic gadolinium at various c/a ratios. For a given configuration of local moments this Fermi surface can be defined in the usual way. However, when considering the whole ensemble of moment orientations, the 'Fermi surface' will be a smeared out average of itself over all moment configurations. A useful tool for defining this surface is the *Bloch Spectral Function* (BSF) [28], given by

$$\bar{A}_B(\mathbf{k}, E) = -\frac{1}{\pi}\mathrm{Im}\sum_{nm}\exp[i\mathbf{k}\cdot(\mathbf{R}_n - \mathbf{R}_m)]\int d\mathbf{r} < G(\mathbf{r}+\mathbf{R}_n, \mathbf{r}+\mathbf{R}_m, E) >, \tag{6.18}$$

where the integral over $\mathbf{r}$ is within the unit cell at the origin. G is the real

space Green's function, defined in Eq. 2.18, and the average $<>$ is an ensemble average. $\bar{A}_B(\mathbf{k}, E)$ is periodic in reciprocal space and provides a band structure type description of disordered systems. For ordered systems it consists of a set of δ-function peaks:

$$\bar{A}_B(\mathbf{k}, E) = \sum_n \delta(E - E_n(\mathbf{k})), \tag{6.19}$$

where $E_n(\mathbf{k})$ is the Bloch energy eigenvalue for the wavevector $\mathbf{k}$ and band index n. In disordered systems these peaks broaden but their positions can be regarded as an effective band structure, with their width in energy interpreted as an inverse lifetime [141]. The Fermi surface of a disordered system is defined as the locus of these peaks at the constant energy $E = E_F$.

Figure 6.7 shows the BSF of paramagnetic Gd at the Fermi energy, calculated for the sets of lattice parameters used in Fig. 6.6. For c/a ratios of 1.597 or smaller a webbing feature is displayed, with sections of roughly parallel Fermi surface. The corresponding nesting vector is indicated by an arrow in panel (a). At a c/a ratio of 1.63 (Fig. 6.6(d)) the webbing feature has started to rupture and at a c/a ratio of 1.66 (Fig. 6.6(e)) a complete rupturing has occurred, with the Fermi surface no longer having any significant regions of nesting. This concurs with the results shown in Fig. 6.6, where the susceptibility is enhanced at some incommensurate **q** vector for low c/a ratios, but not for high c/a ratios.

Figure 6.8(a) shows a cross section through the webbing structure for c/a ratio 1.54. The nesting structure is created by two bands which just cross the Fermi energy along the L-M direction. The broadening of the spectral function peaks, caused by the local moment disorder, means that the bands are smeared, which results in them merging together at the L point. The magnitude of the nesting vector, $\mathbf{Q}_0$, is ≈ 0.2 (henceforth the length of all **k**-space vectors will be

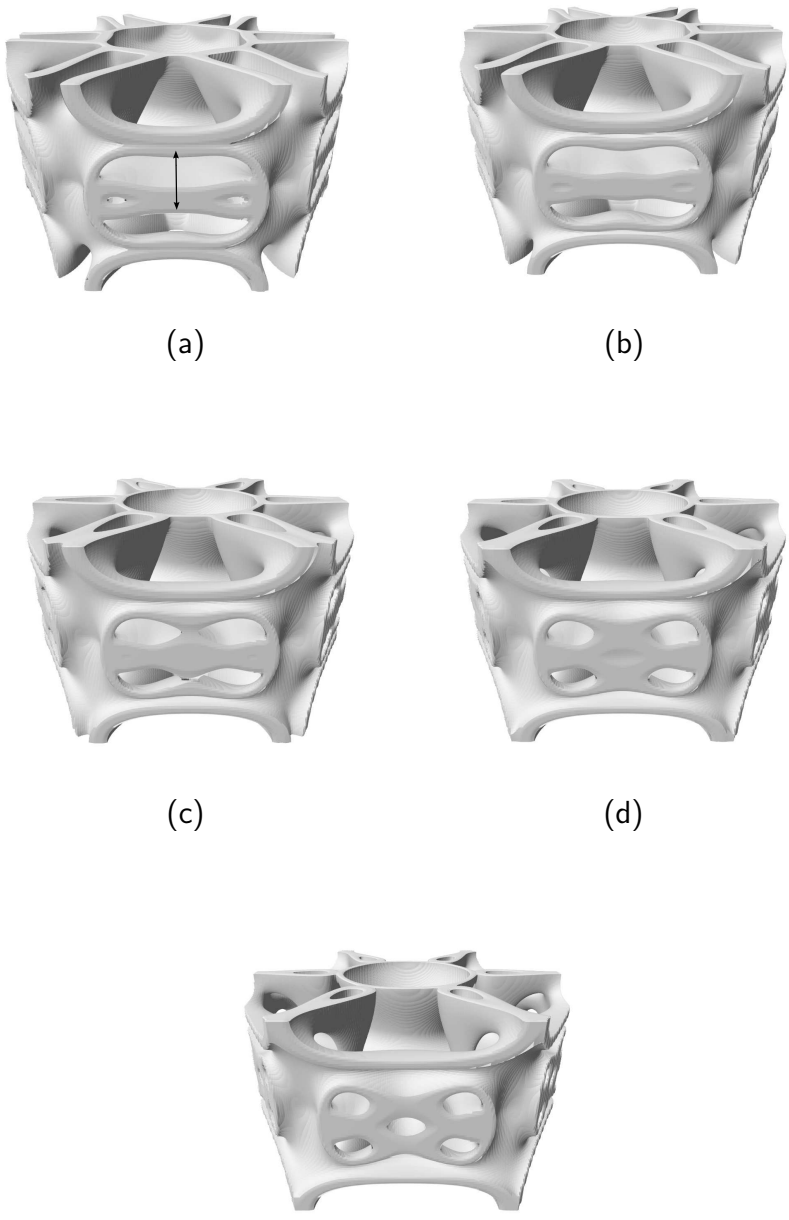

Figure 6.7: Bloch Spectral Function of Gd in the hexagonal Brillouin zone, calculated at the Fermi energy. Panels (a),(b),(c),(d) and (e) are for c/a ratios 1.54, 1.57, 1.597, 1.63 and 1.66 respectively, with theoretical unit cell volumes used.

given in units of $2\pi/c$), which coincides with the size of the magnetic ordering wave vector, q_{inc}, observed in Fig. 6.6(a). Figs. 6.8(b) and (c) show the same cross section of the Brillouin zone, with the BSF evaluated using c/a ratios 1.57 and 1.66 respectively. In (b) the Fermi surface has a distinctive "dog-bone" shape, with two extremal vectors, one centred and the other non-centred, connecting the sheets of Fermi surface. Comparing Figs. 6.8 (a) and (b) it is evident that the length of the centred nesting vector decreases as the c/a ratio increases. This is in keeping with the experimental results of Andrianov, where the length of the magnetic ordering vector decreases continuously as the c/a ratio is increased. However, this is contrary to the susceptibility results shown in Fig. 6.6, where the position of the incommensurate ordering peak is almost invariant to the c/a ratio used. If, instead, we look at the length of the non-centred vector we see that it stays fairly constant as the c/a ratio is altered. It thus appears that it is the non-centred nesting vector which is responsible for the incommensurate ordering observed in our calculations. This is in agreement with recent theoretical work by Nordström and Mavromaras [142] who found that the non-centred vector was the appropriate nesting vector.

We now turn to the magnetic ordering behaviour as a function of unit cell volume. Here, we find two distinct cases, dependent on the c/a ratio of the lattice parameters. For high c/a ratios, corresponding to systems with no webbing feature, ferromagnetic ordering is predicted for all volumes. For low c/a ratios, corresponding to systems with webbing, a more complicated picture emerges as shown in Fig. 6.9. The webbing leads to an enhancement of the susceptibility at the nesting vector for all volumes. However, as the volume increases the height of the incommensurate peak relative to the $\mathbf{q} = \mathbf{0}$ (ferromagnetic) peak decreases and at a WS radius of 3.710 a.u. there is a near degeneracy between the two

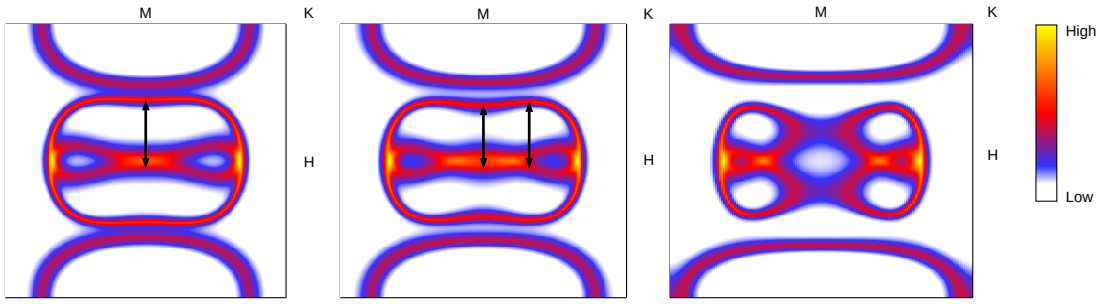

Figure 6.8: Bloch Spectral Function of Gd on the HLMK plane of the hexagonal Brillouin zone. Panels (a), (b) and (c) are for c/a ratios 1.54, 1.57 and 1.66 respectively, with theoretical unit cell volumes used. The centre of the plane is the L point. Nesting vectors are indicated by arrows.

ordering types. For the highest WS-radii the susceptibility obtains its maximum value at $\mathbf{q} = \mathbf{0}$ and so we predict the system to be ferromagnetic. Thus, in order for the nesting enhancement to be strong enough so that incommensurate ordering wins out over ferromagnetic ordering, the unit cell volume needs to be below a certain critical value.

Having analysed the behaviour of the paramagnetic spin susceptibility, χ, we turn our attention now to the direct correlation function, $S^{(2)}$. This function can be fit in terms of real-space parameters:

$$S^{(2)}(\mathbf{q}) = \sum_{n} \sum_{i \in n} S_n^{(2)} \exp(i\mathbf{q} \cdot \mathbf{R}_i), \tag{6.20}$$

where $S_n^{(2)}$ is the direct pair interaction between an atom at the origin and an atom in the nth neighbour shell, with position vector $\mathbf{R}_i$. For the magnetic structures considered in this chapter $\mathbf{q} = (0, 0, q)$ and hence $\exp(i\mathbf{q} \cdot \mathbf{R}_i) = \exp(iqR_z)$, where R_z is the z-component of $\mathbf{R}_i$. Since the heavy rare earths adopt hcp structures, with two atoms per unit cell, they can be thought of as being composed of two interpenetrating sublattices. Consequently two distinct sets of pair corre-

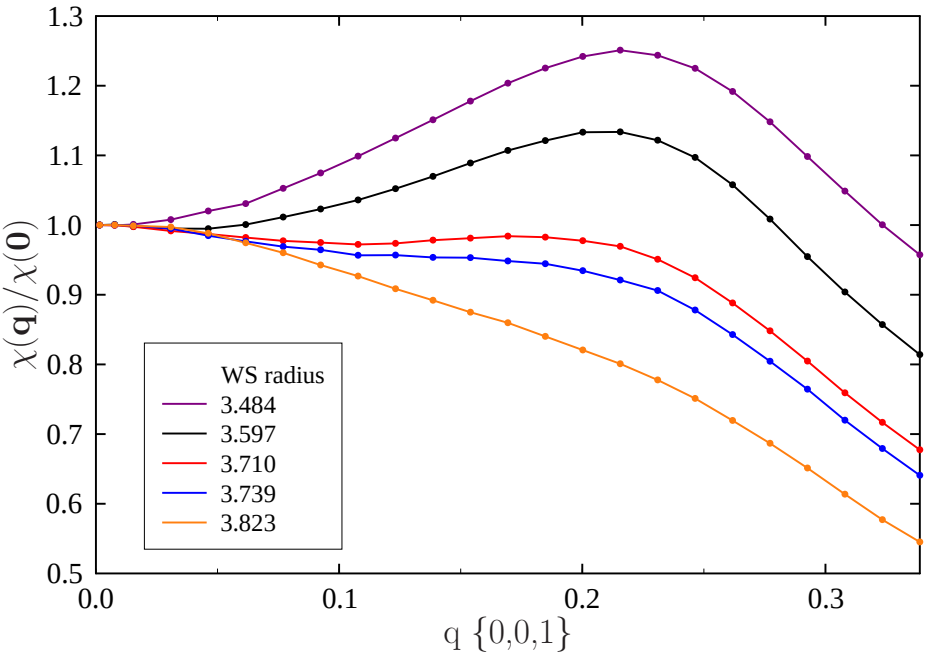

Figure 6.9: Normalised paramagnetic spin susceptibilities for Gd for various WS radii, obtained using a c/a ratio of 1.54.

lations can be considered, one where both sites are on the same sublattice ('intra sublattice') and one where the sites are on different sublattices ('inter sublattice'). For intra (inter) sublattice pairs, $R_z = l * c$ ($R_z = (l - 1/2) * c$) where $l \in \mathbb{Z}$ and c is the 'c' lattice parameter. The 'layer' indices, l, can be used to reparametrise the real space fit of Eq. 6.20:

$$\begin{aligned} S^{(2)-intra}(\mathbf{q}) &= S_0^{(2)-intra} + \sum_{l \in \mathbb{Z} \setminus 0} S_l^{(2)-intra} \exp(iqlc) \\ S^{(2)-inter}(\mathbf{q}) &= \sum_{l \in \mathbb{Z}} S_l^{(2)-inter} \exp(iq(l-1/2)c), \end{aligned} \tag{6.21}$$

where $S_l^{(2)}$ is the sum of all pairwise interactions between sites in the lth layer and the site at the origin. The $S_0^{(2)}$ component corresponds to the sum of pair interactions between the atom at the origin and atoms in the layer containing the origin. Clearly the 'inter' sublattice function, $S^{(2)-inter}$, will not contain a

$S_0^{(2)}$ term, since all atoms in the layer containing the origin belong to the same sublattice as the origin. Equation 6.21 can be cast in a purely real form through use of the identity $\exp(ix) + \exp(-ix) = 2\cos x$:

$$\begin{aligned} S^{(2)-intra}(\mathbf{q}) &= S_0^{(2)-intra} + \sum_{l\in\mathbb{N}} S_l^{(2)-intra}\cos(iqlc) \\ S^{(2)-inter}(\mathbf{q}) &= \sum_{l\in\mathbb{N}} S_l^{(2)-inter}\cos(iq(l-1/2)c) \end{aligned} \tag{6.22}$$

where the $S_l^{(2)}$ differ from those of Eq. 6.21 by a factor of 2.

For the fitting of the direct correlation function to be computationally tractable, the sum over layers, l, in Eq. 6.22 has to be truncated at some finite value, $l_{\max}$. Note that this should not to be confused with the angular momentum truncation which is used during the evaluation of the Green's function, Eq. 2.43. Figure 6.10 shows the fit obtained for $S^{(2)-intra}$ for Gd, at a c/a ratio of 1.54 and the theoretical unit cell volume, with $l_{\max} = 8$ and $l_{\max} = 12$. It is clear that the $l_{\max} = 8$ fit of $S^{(2)-intra}$ is reasonably accurate. However, in order to reproduce the highest harmonics, terms up to $l_{\max} = 12$ need to be considered. This shows the long ranged nature of the 'exchange interaction' $S^{(2)}$, in accord with the RKKY model. Of course, an even better fit of the data can be obtained by increasing $l_{\max}$ further, due to the enlargement of the function space. However, these improvements can be attributed mainly to the fitting of computational noise in the $S^{(2)-intra}$ data, rather than the fitting of anything of physical origin. Indeed, one of the reasons for employing a fitting procedure is to try and eliminate some of the inherent noise of the computed $S^{(2)}$ data. In Fig. 6.11 we show the inter sublattice data, $S^{(2)-inter}$, an accurate fit of which is obtained using $l_{\max} = 8$.

The real-space parameters $S_l^{(2)}$, used to obtain the fits in Figs. 6.10 and 6.11, are given in Fig. 6.12, where integer (half-integer) values of R_z/c correspond

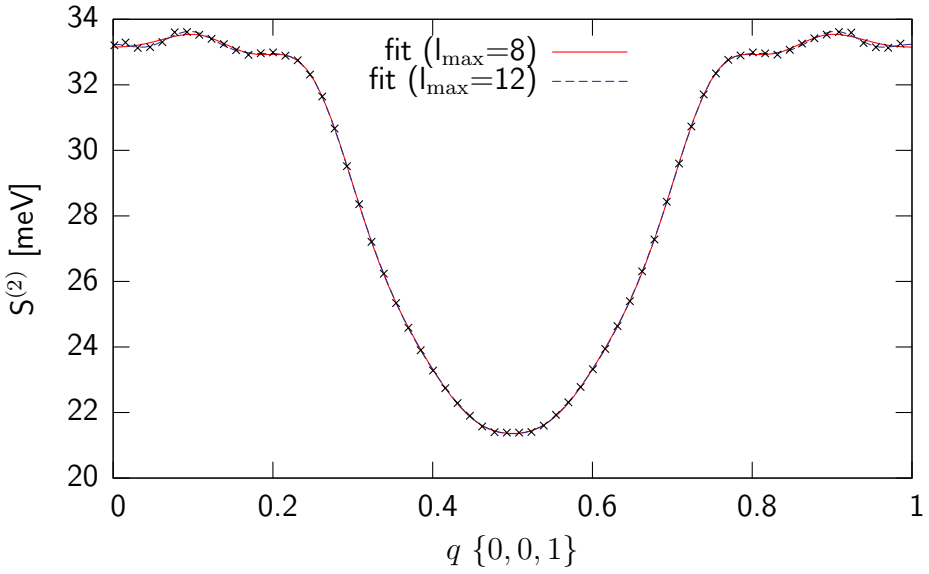

Figure 6.10: Effective intra sublattice exchange interaction, $S^{(2)-intra}$, for gadolinium. The crosses show the data obtained from our *ab initio* calculations. The solid (dashed) line is a fit from Eq. 6.22, with l_{max}=8 (l_{max}=12).

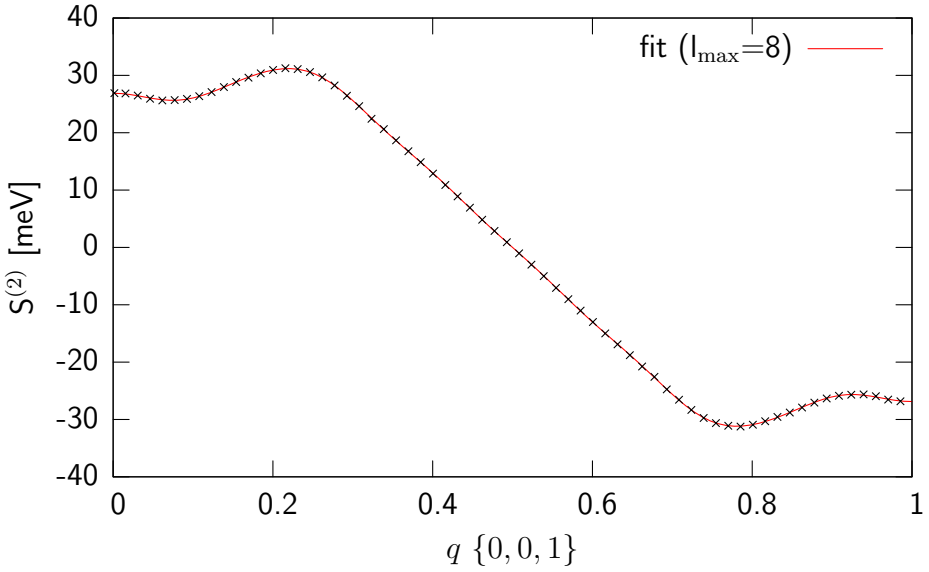

Figure 6.11: Effective inter sublattice exchange interaction, $S^{(2)-inter}$, for gadolinium. The crosses show the data obtained from our *ab initio* calculations. The solid line is a fit from Eq. 6.22, with l_{max}=8.

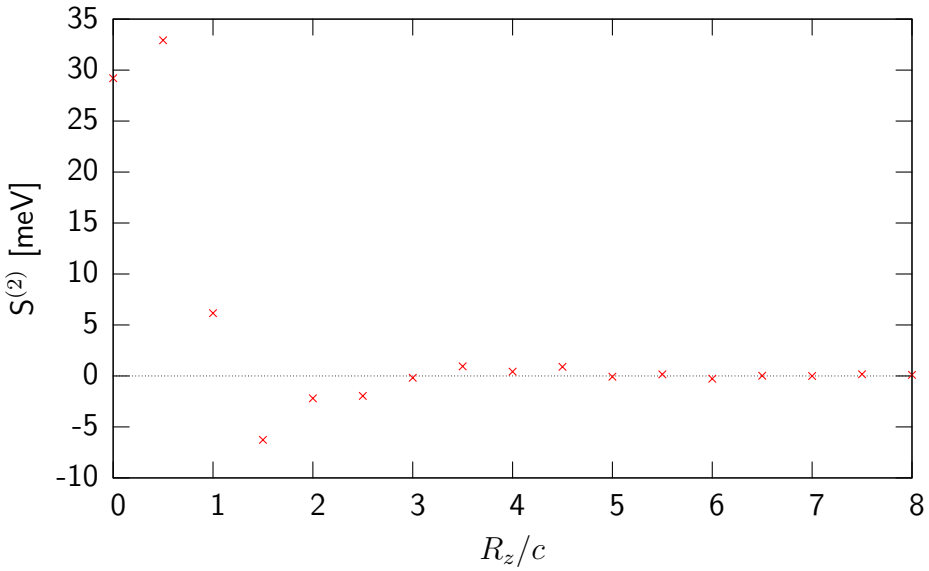

Figure 6.12: Layer resolved components of the effective exchange interaction, $S^{(2)}$.

to intra (inter) sublattice components. The biggest contribution to $S_l^{(2)}$ comes from the layers at $R_z = \pm c/2$. This is to be expected since, in hcp structures that have a c/a ratio less than the ideal value $\sqrt{8/3} \approx 1.63$, the nearest neighbours to any given atom are contained within the layers adjacent to the atom, not the layer in which the atom actually lays. The components of $S^{(2)}$ are seen to oscillate as a function of R_z, in agreement with the oscillatory nature of the RKKY exchange integral, Eq. 6.14. Note, however that we do not expect the components of $S^{(2)}$ to drop off as $1/R_z^3$. This is because the distance R_z refers to a layer, containing atoms at many different positions, rather than the actual distance between two individual atoms as in Eq. 6.14

6.2 Phase Diagram of Heavy Rare Earth Magnetism

The two types of magnetic ordering that we encountered during our investigation of gadolinium (ferromagnetic ordering and incommensurate ordering, modulated along the c-axis) correspond to the two types of ordering that are observed experimentally across the heavy RE series. To investigate the competition between these two ordering types we define a 'magnetic ordering parameter', α, which gives a measure of the relative strengths of the 'incommensurate spin fluctuations' and ferromagnetic spin fluctuations that characterise the paramagnetic state. To do this we examine the wavevector dependent critical temperature, $T_c(\mathbf{q})$, obtained from the solution of Eq. 5.51, $\det[\mathbf{I}_n - 1/3\beta\mathbf{S^{(2)}}(\mathbf{q})] = 0$. We build up the 2x2 $\mathbf{S}^{(2)}$ matrix according to

$$\begin{pmatrix} S^{(2)-intra}(\mathbf{q}) & S^{(2)-inter}(\mathbf{q}) \\ S^{(2)-inter}(\mathbf{q}) & S^{(2)-intra(}\mathbf{q}) \end{pmatrix},$$

where $S^{(2)-intra}(\mathbf{q})$ and $S^{(2)-inter}(\mathbf{q})$ correspond to the fit functions in Eq. 6.22. By using these fit functions we help eliminate computational noise, which may be important when analysing the delicate competition between the two ordering types.

If the critical temperature function $T_c(\mathbf{q})$ has only one peak, at $\mathbf{q} = \mathbf{0}$, we set $\alpha = 0$. If $T_c(\mathbf{q})$ has only one peak, but at some incommensurate q-vector, q_{inc}, we set $\alpha = 1$. Clearly, $\alpha = 0$ corresponds to when the paramagnetic state is dominated by ferromagnetic spin fluctuations and $\alpha = 1$ corresponds to when it is dominated by spin fluctuations with some finite, incommensurate wavevector. Examples of the temperature function in these two cases are respectively shown in Figs. 6.13(a) and (b). When $T_c(\mathbf{q})$ has a two peak structure, as examplified in Fig. 6.13(c), corresponding to a competition between the two ordering types, we

examine the values of $T_c(\mathbf{q})$ at its turning points. We define $T_0 = T_c(\mathbf{q} = \mathbf{0})$, $T_{inc} = T_c(\mathbf{q} = (0, 0, q_{inc}))$ and $T_{min} = T_c(\mathbf{q} = \mathbf{q_{min}})$, where $\mathbf{q_{min}}$ is the position of the minimum that occurs between the $\mathbf{q} = \mathbf{0}$ and $\mathbf{q} = (0, 0, q_{inc})$ maxima. If $T_0 > T_{inc}$ we set

$$\alpha = \frac{T_{inc} - T_{min}}{2(T_0 - T_{min})} \tag{6.23}$$

and if $T_0 < T_{inc}$ we set

$$\alpha = 1 - \frac{T_0 - T_{min}}{2(T_{inc} - T_{min})}. \tag{6.24}$$

Clearly, α is defined such that $\alpha > 0.5$ indicates a stronger tendency towards incommensurate ordering and $\alpha < 0.5$ indicates a stronger tendency towards ferromagnetic ordering.

In Fig. 6.14 we show α for gadolinium, as a function of c/a ratio and unit cell volume. To account for the difference between the theoretical and experimental volumes, the WS-radii in the figure are scaled, such that data shown at the experimental WS radius of gadolinium corresponds to data calculated at the theoretical WS-radius. On this phase diagram we also indicate where the experimental lattice parameters of all the heavy RE elements lie, as well as those of a Gd-Ho alloy. Since the heavy RE elements differ only in how many 4f electrons they have, and it is the sd conduction electrons which are responsible for mediating the interaction between magnetic moments, gadolinium can be considered a magnetic 'prototype' for the later heavy RE elements. Thus, we might expect the behaviour of gadolinium as a function of lattice parameters to mimic that of all the other heavy RE elements. By considering the phase diagram, Fig. 6.14, as being universal to all heavy RE systems, we predict that when going left to right in the heavy RE series there will be a trend away from ferromagnetism and towards incommensurate ordering. This is exactly what is observed experimentally, with

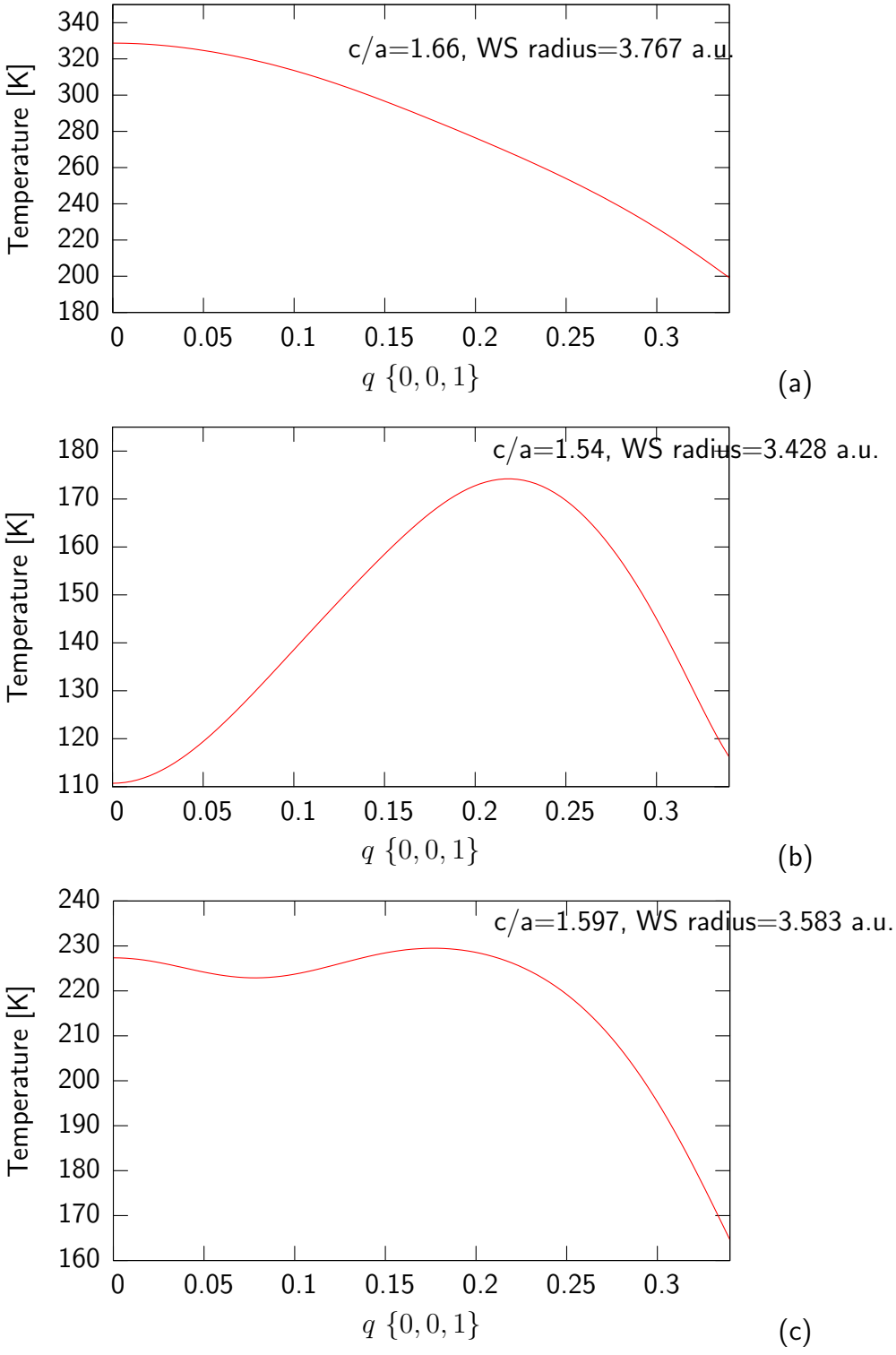

Figure 6.13: Critical temperatures for gadolinium for wavevectors along the [0,0,1] direction, obtained from the solution of Eq. 6.51. The lattice parameters used are given in each of the panels, (a), (b) and (c).

the magnetic modulation vector starting out at zero for gadolinium (ferromagnetic ordering) and then progressively increasing through the series to give rise to various incommensurate antiferromagnetic structures. From the phase diagram we predict that the transition between ferromagnetism and incommensurate ordering occurs very rapidly as a function of c/a ratio, particularly for the higher unit cell volumes. This is consistent with recent experimental work on terbium under uniaxial tension. Terbium exhibits helical ordering and has a WS-radius of 3.724 a.u., with a c/a ratio of 1.580. It was shown [137] that by increasing the c/a ratio by as little as 0.002 the helical ordering could be completely suppressed. In the phase diagram the elements dysprosium and terbium are positioned close to, or within, the transition region between ferromagnetic and incommensurate ordering. This concurs with the experimental behaviour of these two systems, which exhibit incommensurate ordering at high temperatures and ferromagnetic ordering at low temperatures.

Due to their structural similarities, Gd alloys easily with all the other heavy rare earth elements, R. These alloys transform from ferromagnets to incommensurate magnetically structured materials once the concentration of R exceeds a certain critical concentration x_c. We can use the phase diagram to predict these critical alloy concentrations, at which an incommensurate magnetic phase first appears. These are listed in Table 6.1 and are in good agreement with experimental values where known.

We can also compute estimates of the magnetic ordering vectors of all the heavy REs from our susceptibility calculations for gadolinium at the appropriate lattice parameters. The results are shown in Fig. 6.15. For example, when we performed a calculation at the experimental lattice parameters of terbium (Tb), specified by a c/a ratio of 1.580 and a WS-radius of 3.724 a.u., the susceptibility

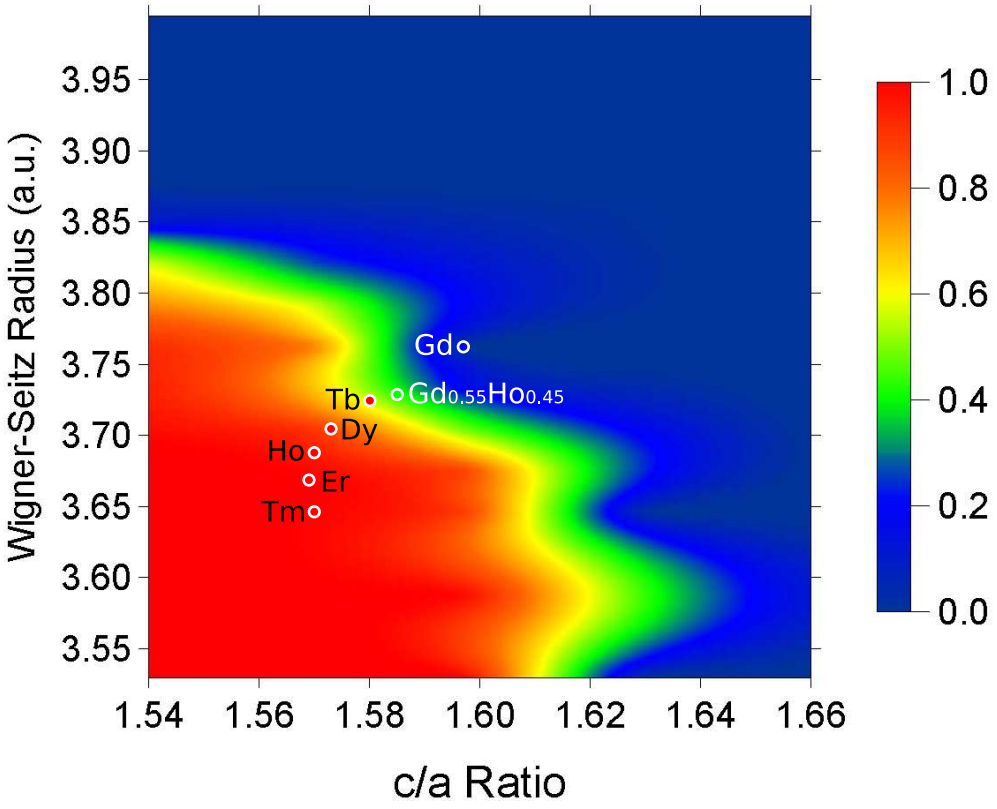

Figure 6.14: Ordering parameter, α, for gadolinium as a function of c/a ratio and WS radius. The experimental lattice parameters of all the heavy RE elements are indicated by circles; A blue (red) filling indicates that experimentally the high temperature ordered state of the element is ferromagnetic (incommensurate antiferromagnetic). The green circle indicates the experimental lattice parameters of a Gd-Ho alloy at the critical concentration of Ho at which an incommensurate antiferromagnetic phase first appears.

peaked at a wave vector **q**=(0,0,0.13), which is in good agreement with the experimental ordering vector of Tb, (0,0,0.11). Overall, we predict a gradual increase in the ordering vector across the heavy RE series, in agreement with experiment. We also find that the magnetic ordering vectors of the last 3 members of the series (Ho, Er and Tm) all lie very close together, again in agreement with experiment.

As outlined in the introduction of this chapter, the reason for concentrating on gadolinium is that the ion has orbital angular momentum $L = 0$ and so we don't need to incorporate spin orbit effects into our calculations. However, when deriving the mean-field expression for transition temperatures in the RKKY model, Eq. 6.17, LS coupling was important. More particularly, this expression was seen to be proportional to the de Gennes factor $(g_J - 1)^2 J(J + 1)$. Thus in order to obtain estimates for the magnetic ordering temperatures of the other REs we scale the ordering temperatures obtained from the gadolinium calculations by this factor. As shown in the inset of Fig. 6.15, the transition temperatures obtained from this approach reproduce the experimental trend, although the magnitudes of the temperatures are systematically underestimated. It is worth noting that when we computed the estimates of the magnetic ordering vectors, spin-orbit coupling was not important. This is because, as argued earlier, the type of magnetic order exhibited by the heavy REs is determined by the *sd* conduction electrons, which are little affected by spin-orbit coupling and which all the heavy REs have in common.

Overall, the physical picture that emerges from the magnetic ordering phase diagram, Fig. 6.14, links unequivocally the lattice parameters of the heavy REs with their magnetic properties. Our results have verified the critical role that the c/a ratio plays in determining the magnetic ordering types of the heavy REs and how this is linked to the Fermi surface of the paramagnetic phase. However, our discovery that the atomic unit cell volume, associated with the lattice parame-

Table 6.1: Critical alloy concentrations of $Gd_{1-x}R_x$ systems.

	Critical concentration, x_c	
System	Theo.	Exp.
$Gd_{1-x}Tb_x$	0.78	
$Gd_{1-x}Dy_x$	0.56	0.50[a]
$Gd_{1-x}Ho_x$	0.49	0.45[b]
$Gd_{1-x}Er_x$	0.45	
$Gd_{1-x}Tm_x$	0.42	

[a]Reference [143].
[b]Taken ref. [136].

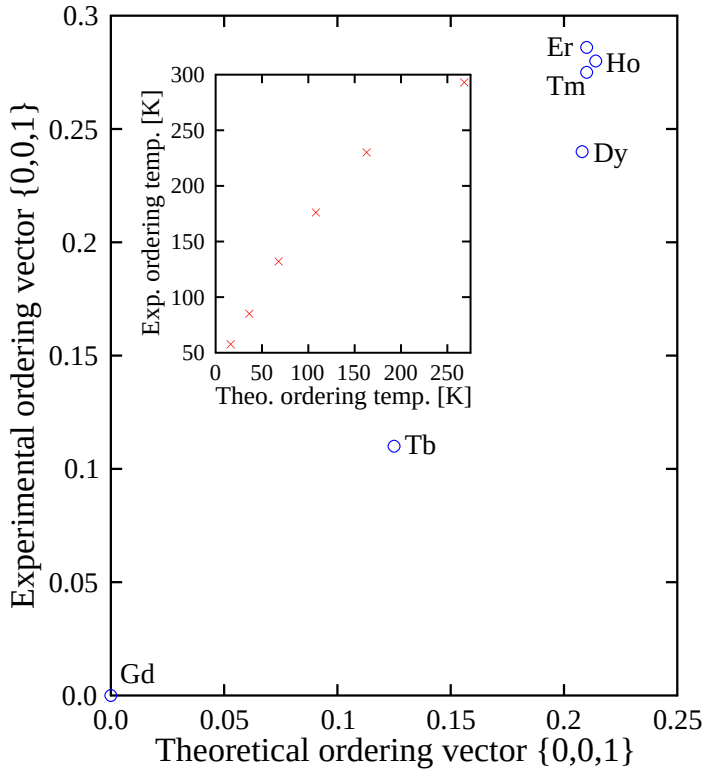

Figure 6.15: Experimental magnetic ordering vectors of the heavy REs versus those predicted from *ab initio* calculations for gadolinium. The inset shows the corresponding ordering temperatures. Experimentally Gd has the highest ordering temperature, which decreases monotonically through the heavy RE series.

ters, is just as important in determining the magnetic properties has enabled us to develop a much more complete understanding of heavy rare earth magnetism. In particular, we have shown that even when the c/a ratio of a heavy RE system is below the critical value needed for a webbing structure, incommensurate antiferromagnetic ordering is not necessarily favoured over ferromagnetic ordering; for incommensurate ordering to win out over ferromagnetic ordering the unit cell volume needs to be below a certain value. Experimentally the unit cell volumes of the heavy REs decrease with increasing atomic number, in accord with the well-known "lanthanide contraction" [124]. This contraction occurs because as the number of electrons in the poorly shielding 4f orbitals is increased, there is an increase in the effective nuclear charge and, correspondingly, a decrease in ionic radii. Our findings evidently suggest that this contraction helps promote the incommensurate ordering in the late heavy REs. The roles that the different types of valence electrons play in determining the magnetic structures of the heavy REs are thus clear; the itinerant sd electrons, common to all the heavy REs, mediate the interaction between magnetic moments and it is the nesting of their Fermi surfaces which can lead to instabilities in the paramagnetic phase with respect to the formation of incommensurate spin density waves. The f electrons, on the other hand, are responsible for setting up the magnetic moments and, as their number increases across the heavy RE series, they play an indirect role in promoting the incommensurate ordering by means of the lanthanide contraction.

Chapter 7

Further Applications

7.1 Atomic Short Range Order

In chapter 5 we showed how, by examining correlations between local moments in the disordered (paramagnetic phase), the low temperature magnetic behaviour of a system can be predicted. For random alloy systems, e.g. the binary Gd-R alloys considered in chapter 6, one can also consider *compositional correlations* , giving rise to *atomic short range order* (ASRO). Such ASRO can lead either to a phase separation of alloy components or the formation of some ordered structure, occurring at some critical *spinodal temperature*.

In order to discuss a formalism for dealing with compositional correlations we consider a binary alloy system A_cB_{1-c}, although the arguments presented here can all be generalised to alloys with more than two components. We define an occupation variable ξ_i, where ξ_i=1 if the ith site of the alloy lattice is occupied by an A atom and 0 if it is occupied by a B atom. At high temperatures, when the alloy is homogeneously disordered, the thermal average of ξ_i, c_i, is independent of i and is equal to the global concentration of A atoms, c. Below the spinodal temperature

the local concentration of A atoms, c_i, will differ from c. This deviation can expressed in terms of *static concentration waves* [144]

$$c_i = c + \frac{1}{2}\sum_j [Q_j \exp(i\mathbf{k}_j \cdot \mathbf{r}) + Q_j^* \exp(-i\mathbf{k}_j \cdot \mathbf{r})], \tag{7.1}$$

where $\mathbf{k}_j$ is a wave vector in the first Brillouin zone and Q_j is the corresponding wave amplitude. Usually only a few wavevectors are needed to describe a long range ordered structure and, for a homogeneously ordered state, only one wavevector, $\mathbf{k}_0$, is required.

In the disordered high temperature phase concentration waves are not stable, but nevertheless provide a description of short-range order. A measure of this short-range order is provided by the short range order parameter $\alpha(\mathbf{k})$, which is defined as the lattice Fourier transform of the atomic pair correlation function $\alpha_{ij} = \beta(< \xi_i\xi_j > - < \xi_i >< \xi_j >)$. If $\alpha(\mathbf{k})$ peaks at $\mathbf{k} = \mathbf{0}$ this indicates that a system has a tendency to phase separate at low temperatures, whereas if it attains its maximum values at finite $\mathbf{k}$ the system will tend to order. The $\mathbf{k}$ values at which these maxima occur specify the wavevectors of the concentration waves, with the values of $\alpha(\mathbf{k})$ at the maxima being proportional to the corresponding wave amplitudes. In x-ray, neutron and electron scattering experiments, the diffuse scattering intensity $I(\mathbf{k})$ is proportional to $\alpha(\mathbf{k})$, thus providing a direct measure of this quantity. In this chapter we outline how $\alpha(\mathbf{k})$ can be obtained from first principles theory. The approach taken mirrors that which was used in chapter 5 for deriving the paramagnetic spin susceptibility. Using this formalism, we investigate atomic short range order in gadolinium yttrium alloys.

7.1.1 First Principles Formalism

When investigating paramagnetic spin fluctuations in chapter 5, the approach taken was to probe the response of the homogeneously disordered paramagnetic state to the application of some external magnetic field. In this section we consider the compositional response of a homogeneously disordered alloy to the application of some 'external' *chemical potential field*, or, more precisely, to a change in the chemical potential difference $\nu = \nu_A - \nu_B$, where ν_A and ν_A are the chemical potentials for A and B atoms respectively. The fluctuation-dissipation theorem connects this compositional response to the atomic pair correlation function, i.e.

$$\frac{\delta c_i}{\delta \nu_j} = \alpha_{ij}. \tag{7.2}$$

As with the DLM approach, we start by separating out slow degrees of freedom from those associated with faster electronic motions. Here, the slow degrees of freedom are that of chemical diffusion, described by the occupation variables ξ_i. The probability of finding a particular arrangement $\{\xi_i\}$ is written as

$$P(\{\xi_i\}) = Z^{-1} \exp[-\beta(\Omega(\{\xi_i\}) - \nu \sum_i \xi_i)], \tag{7.3}$$

where the partition function Z is given by

$$Z = \prod_k \sum_{\xi_k=0,1} \exp[-\beta(\Omega(\{\xi_i\}) - \nu \sum_i \xi_i)]. \tag{7.4}$$

The grand potential $\Omega(\{\xi_i\})$ describes the motion of electrons moving in fields set by the arrangement of nuclei $\{\xi_i\}$. A mean field approximation for $\Omega(\{\xi_i\})$ is constructed by expanding it about a single site compositional-fluctuation Hamiltonian $\Omega_0 = \sum_i V_i^{eff} \xi_i$. The effective chemical potentials V_i^{eff} can be obtained using the Feynman-variational approach outlined in section 5.3 and are given by $V_i^{eff} = \delta\langle\Omega\rangle/\delta c_i$.

Substituting $\Omega(\{\xi_i\}) = \sum_i V_i^{eff}\xi_i$ into Eq. 7.3 and evaluating $c_i = \langle\xi_i\rangle$, where $\langle\rangle$ is the average with respect to P, gives

$$c_i = \exp[-\beta(V_i^{eff} + \nu)]/(\exp[-\beta(V_i^{eff} + \nu)] + 1). \tag{7.5}$$

In the high temperature disordered state $c_i = c\ \forall i$. However, upon applying an 'external' chemical potential field, ν_j^{ext}, local concentration fluctuations δc_i will develop such that $c_i = c + \delta c_i$. In the limit $\nu_j^{ext} = 0$ we obtain

$$\frac{\partial c_i}{\partial \nu_j^{\rm ext}}|_{\nu_j^{\rm ext}=0} = \beta c(1-c)[\frac{\partial V_i^{eff}}{\partial \nu_j^{\rm ext}} + \delta_{ij}]. \tag{7.6}$$

Assuming that the grand potential Ω depends on $\nu^{\rm ext}$ only through the concentration variables, c_i, we can write

$$\frac{\partial V_i^{eff}}{\partial \nu_j^{\rm ext}} = \frac{\partial(\partial\langle\Omega\rangle/\partial c_i)}{\partial \nu_j^{\rm ext}} = \sum_k \frac{\partial^2\Omega}{\partial c_i \partial c_k}\ \frac{\partial c_k}{\partial \nu_j^{\rm ext}}. \tag{7.7}$$

This assumption is equivalent to saying that the only changes to the electronic structure are those associated with *band filling*. This means that we neglect any *charge rearrangements effects*, arising from the response of the electronic density to the presence of concentration waves. The inclusion of such effects are discussed in reference [145].

Substituting Eq. 7.7 into Eq. 7.6 gives

$$\frac{\partial c_i}{\partial \nu_j^{\rm ext}}|_{\nu_j^{\rm ext}=0} = \beta c(1-c)[\sum_k S_{ik}^{(2)}\frac{\partial c_k}{\partial \nu_j^{\rm ext}} + \delta_{ij}], \tag{7.8}$$

where we have defined $S_{ik}^{(2)} = \frac{\partial^2\Omega}{\partial c_i \partial c_k}$. $S^{(2)}$ is a direct correlation function for the compositionally disordered lattice. Taking the lattice Fourier transform of Eq. 7.8 we obtain finally

$$\alpha(\mathbf{k}) = \beta c(1-c)[1 + \alpha(\mathbf{k})S^{(2)}(\mathbf{k})], \tag{7.9}$$

where Eq. 7.2 has been used to substitute in the atomic pair correlation function α. The direct correlation function $S^{(2)}(\mathbf{k})$ can be evaluated by expanding about the

high temperature disordered state, using the inhomogeneous CPA method outlined in section 5.2. An expression for $S^{(2)}$ can be found in reference [145]. Rearranging Eq. 7.9 to

$$\alpha(\mathbf{k}) = \frac{\beta c(1-c)}{1-\beta c(1-c)S^{(2)}(\mathbf{k})}, \tag{7.10}$$

it is clear that the spinodal temperature is given by the solution of

$$1-\beta c(1-c)S^{(2)} = 0. \tag{7.11}$$

7.1.2 Results for Gadolinium-Yttrium Alloys

Yttrium, a trivalent 4d transition metal, exhibits similar chemical behaviour to that of the rare earth metals and, indeed, is sometimes classed as a rare earth [96]. Unlike the lanthanides it contains no f electrons and is unable to establish local moments. However, upon alloying with small quantities of heavy rare earth metals, e.g. terbium [146] or erbium [147], long-range magnetic structures are formed. Positron annihilation data [134] has shown that the Fermi surface of Yttrium possesses a webbing feature, with the magnitude of the nesting vector in close agreement with the magnetic ordering vectors of the dilute yttrium heavy rare earth alloys. The magnetic ordering in these systems is thus thought to arise from a RKKY mechanism, whereby the local moments of the heavy rare earth ions are coupled via the polarisation of the nested yttrium conduction bands.

Gadolinium-yttrium alloy systems exhibit particularly interesting magnetic behaviour, having two high temperature ordered phases, planar ferromagnet and helical, as well as a low temperature canted ferromagnetic phase at certain compositions. The crossover between the two high temperature phases, ferromagnetic to helical, occurs when the concentration of yttrium exceeds 32.5% [148]. It is at this alloy concentration that we investigate compositional ordering.

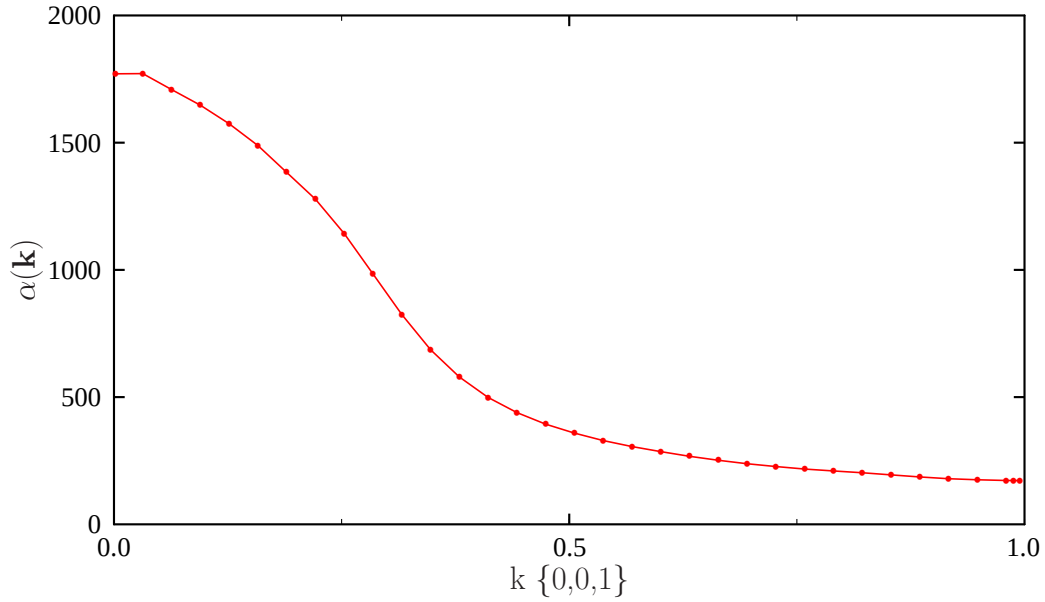

Figure 7.1: Compositional correlation function of $Gd_{67.5}Y_{32.5}$, calculated at 125K.

Figure 7.1 shows the compositional correlation function for $Gd_{67.5}Y_{32.5}$, calculated using the formalism described in section 7.1.1. The lattice parameters used were determined by a Vegard's law interpolation of the experimental lattice parameters of pure gadolinium and pure yttrium. $\alpha(\mathbf{k})$ is seen to peak at $\mathbf{k} = \mathbf{0}$, indicating that the alloy has a tendency to phase separate. The spinodal temperature, obtained from Eq. 7.11, was found to be 105K.

A phase separation of the alloy would mean that gadolinium ions are surrounded by other gadolinium ions. Thus the gadolinium magnetic moments might be expected to behave as if they were in a system of pure gadolinium, the only difference being that the lattice parameters would be different to that of pure a gadolinium crystal. Therefore we might hope to use the picture developed in chapter 6, linking the magnetic order of gadolinium to its lattice parameters, to be able to explain the crossover between ferromagnetic and incommensurate (he-

lical) ordering in gadolinium yttrium alloys. However, it should be noted that the temperature that $Gd_{67.5}Y_{32.5}$ orders magnetically is 210K, significantly higher than the compositional ordering temperature of 105K that we obtain. Thus at the onset of magnetic order we predict that the system will not have phase separated, suggesting that a simple gadolinium-only picture is not valid. Indeed, using the magnetic ordering phase diagram of chapter 6, Fig. 6.14, we predict the critical concentration of yttrium to be 62%, almost double the experimental value of 32.5%.

7.2 Transition Metal Oxides

All the systems that we have treated with the LSIC have so far been characterised by f electrons. In this section we turn our attention to some systems whose physics is dominated by d electrons, namely the transition metal monoxides MnO and NiO. These systems have a type 2 antiferromagnetic (AF2) groundstate, where the moments within a $\langle 111 \rangle$ layer are aligned, but are antiparallel in successive layers. Such AFM order was originally thought to be the origin of the band gap in these systems [149]. However, as was outlined in chapter 3, these band gaps are now attributed to correlation effects between the 3d electrons and are not connected to magnetic order. Indeed, photoemission experiments on NiO [150] have shown that there is no significant change in the valence band structure as the temperature is increased through the Néel temperature.

MnO and NiO both crystallise into the fcc (rocksalt) structure. When calculating the electronic structures of these systems we introduce two empty spheres per unit cell, positioned in the interstitial volume between the transition metal and oxygen muffin tin spheres. For MnO, which has a half-filled 3d band,

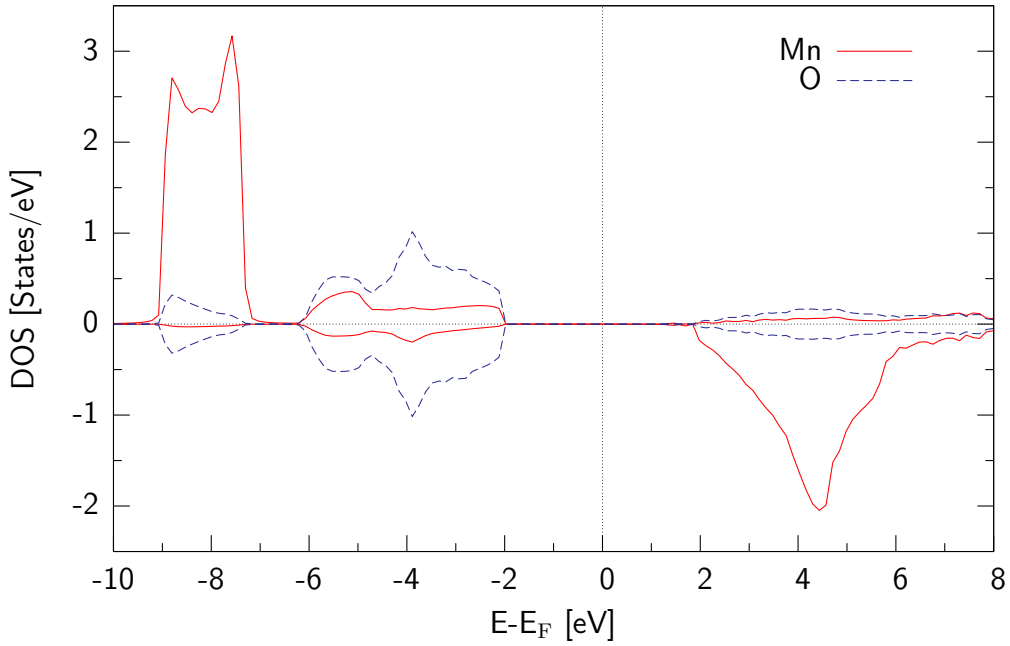

Figure 7.2: Density of states of MnO. Minority states are plotted with negative values of the DOS.

we SIC correct all majority d states. For NiO, which has an additional 3 electrons, we SIC correct all majority d states plus all the minority t_{2g} triplet states. Figures 7.2 and 7.3 show densities of states for the paramagnetic (DLM) state, obtained using experimental lattice parameters. Both systems are found to exhibit a band gap. For NiO the size of the gap is smaller than that measured in experiment, but compares well to the values obtained from other correlated band theories, as detailed in table 7.1. For MnO the size of the gap is in good agreement with experiment. Table 7.1 also shows the values we obtain for the magnetic moments, which are found to be in excellent agreement with experiment for both systems.

Paramagnetic spin susceptibilities, calculated using the DLM-SIC, are shown in figures 7.4 and 7.5. For both MnO and NiO the susceptibility attains it maximum value at the wavevector $\mathbf{q} = (0.5, 0.5, 0.5)$, indicating that the system will order into the AF2 structure. For MnO we find a Néel temperature of 123K, in

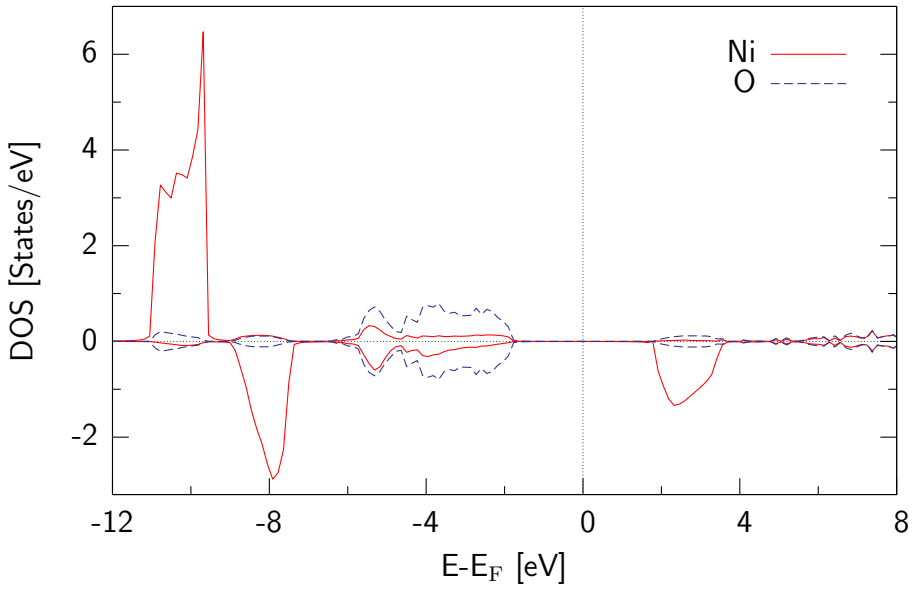

Figure 7.3: Density of states of NiO. Minority states are plotted with negative values of the DOS.

Table 7.1: Band gaps and spin moments of MnO and NiO.

	MnO		NiO	
Method	Band gap [eV]	Spin moment [μ_B]	Band gap [eV]	Spin moment [μ_B]
LSIC	3.54	4.67	3.41	1.74
SIC-LMTO-ASA[a]	3.57	4.64	2.66	1.49
LDA+U[b]	3.5	4.61	3.1	1.59
GW[c]	4.2	4.52	3.7	1.56
Experiment[d]	3.6-3.8	4.79, 4.58	4.0, 4.3	1.64, 1.77, 1.90

[a]Reference [75].
[b]Reference [61].
[c]Reference [151].
[d]From Ref. [75].

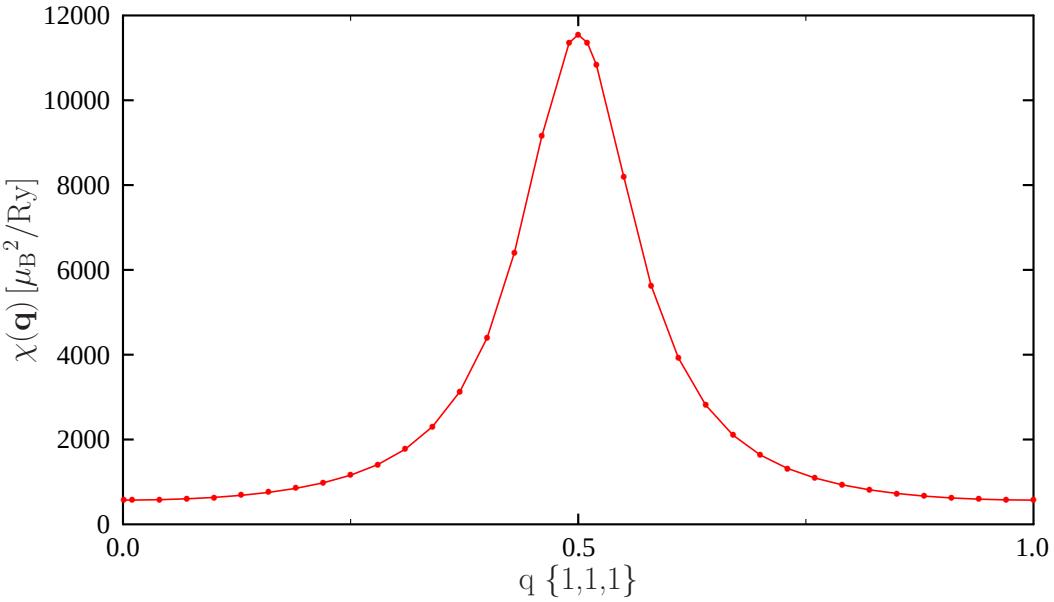

Figure 7.4: Paramagnetic spin susceptibilities for MnO.

good agreement with the experimental value of 118K. For NiO we obtain a Néel temperature of 383K, substantially smaller than the experimental value of 523K. According to Hund's rules, Nickel ions have non-zero orbital angular momentum in the groundstate. Thus we might hope to improve the value of the Néel temperature by using a de-Gennes scaling argument. However, the orbital moment of 3d ions is usually quenched in solids by crystal field splittings [152] and, indeed, the measured cation moment in NiO agrees to within 5% with the spin-only moment of an isolated Ni^{2+} ion [153]. This suggests that the error we find in the Néel temperature has a less simplistic explanation. In particular, the static mean-field approach that we use may not give an adequate account of the physics of this system, a point which we expand on in the next chapter.

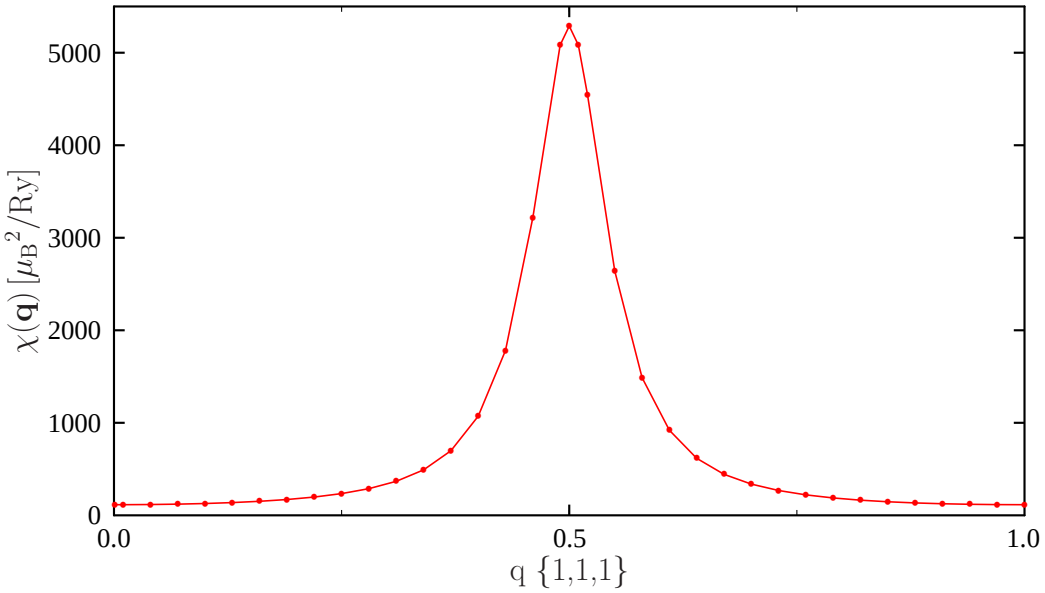

Figure 7.5: Paramagnetic spin susceptibilities for NiO.

7.3 Thin Film Magnetism

Up till this point in the thesis, we have limited our discussion to that of bulk solids, i.e. systems with three-dimensional geometry. Often, however, the surface or interface of systems, where there is a two-dimensional geometry, are of interest. For example, interfaces of transition metal oxides with ferromagnets [154] are of technological importance due to their application in magnetoresistance devices. Developments in experimental techniques, such as x-ray magnetic linear dichroism [155] and x-ray absorption spectroscopy [156], mean that is now possible to resolve the surface magnetic structure of systems. There is, hence, a clear motivation to be able to model the magnetism of two dimensional systems. In this section we outline how the disordered local moment formalism of chapter 5 can be adapted to layered systems with two dimensional symmetry and suggest how such a scheme could be implemented.

We consider a film consisting of n layers, within which local moments $\mathbf{e}_i$ are set up by the collective motion of electrons. The intralayer two-dimensional translational symmetry of the system means that the magnitudes of the local moments $\{\mu_i\}$ are the same in each layer, but may vary between layers. Following the approach of section 5.3, we investigate the response of the paramagnetic state to the application of some external, site dependent magnetic field. In particular, we consider the net magnetisation at a site i, $\mathbf{m}_i = \mu_i\langle\mathbf{e}_i\rangle$, arising from the application of an external magnetic field at a site j, $\mathbf{h}_j$. If the layers containing sites i and j are respectively denoted P and Q then the dimensionless paramagnetic susceptibility, Equation 5.31 in chapter 5, can be written as

$$\overline{\chi}_{iP,Qj} \equiv \frac{\partial m_{iP}}{\partial h^{ext}_{Qj}}|_{h^{ext}_{Qj}=0} = \frac{1}{3}\beta\sum_{Rk} S^{(2)}_{PiRk}\overline{\chi}_{Rk,Qj} + \frac{1}{3}\beta\delta_{PQ}\delta_{ij}, \tag{7.12}$$

where the sum extends over all layers R and all sites k within each layer.

For a given pair of layers, P and Q, the quantity $S^{(2)}_{PiRk}$ will depend only on the distance in two dimensional separation space between sites i and j. Thus a 2D dimensional lattice Fourier transform can be taken of Eq. 7.12 to give

$$\chi_{PQ}(\mathbf{q}\|) = \frac{1}{3}\beta\sum_{R} S^{(2)}_{PR}(\mathbf{q}\|)\chi_{RQ}(\mathbf{q}\|) + \frac{1}{3}\beta\delta_{PQ}, \tag{7.13}$$

where $\mathbf{q}\|$ is a wave vector in the 2D Brillouin zone. The full paramagnetic spin susceptibility, incorporating the magnitudes of the local moments, can be deduced using the same arguments as those given at the end of section 5.31 and is given by

$$\chi_{PQ}(\mathbf{q}\|) = \frac{1}{3}\beta\sum_{R} S^{(2)}_{PR}(\mathbf{q}\|)\chi_{RQ}(\mathbf{q}\|) + \frac{1}{3}\beta\mu_P^2\delta_{PQ}, \tag{7.14}$$

where μ_P is the local moment magnitude of sites in the Pth layer.

Equation 7.14 can be considered as a matrix equation in layer space, the

solution of which is given by

$$\chi(\mathbf{q}\|) = \frac{1}{3}\beta\mu^2[\mathbf{I}_n - \frac{1}{3}\beta S^{(2)}(\mathbf{q}\|)]^{-1}, \tag{7.15}$$

where the PQth entry of $\chi(\mathbf{q}\|)$ ($S^{(2)}(\mathbf{q}\|)$ is $\chi_{PQ}(\mathbf{q}\|)$ ($S^{(2)}_{PQ}(\mathbf{q}\|)$ and μ is a diagonal matrix with elements μ_P. From Eq. 7.15 it is clear that the condition for the susceptibility to diverge is $\det[\mathbf{I}_n - \frac{1}{3}\beta S^{(2)}(\mathbf{q}\|)] = 0$. For a given temperature T this will occur for values of $\mathbf{q}$ for which the eigenvalues of $S^{(2)}(\mathbf{q}\|)$ are equal to $3k_bT$. Thus the magnetic ordering temperature of the system, i.e. the highest temperature at which an instability occurs, will be given by the condition $\|I - \frac{1}{3}\beta S^{(2)}(\mathbf{q}^{\max}\|)\| = 0$, where $\mathbf{q}^{\max}\|$ is the wavevector for which the matrix $S^{(2)}(\mathbf{q}\|)$ has the largest positive eigenvalue.

The approach taken for evaluating $S^{(2)}(\mathbf{q}\|)$ can proceed along similar lines to that used in section 5.31. In particular, the self-consistent electronic structure of the paramagnetic DLM state can be determined by performing a CPA calculation with 50% of moments pointing 'up' on each layer and 50% pointing 'down'. Such a calculation can be implemented using the KKR method for layered system [157]. $S^{(2)}(\mathbf{q}\|)$ can be then be determined by expanding about the disordered state, using the inhomogeneous CPA. An analytic expression for $S^{(2)}(\mathbf{q}\|)$, involving convolution integrals of the type given by the lattice Fourier transform of Eq. 5.18, is given in [158]. Some of the quantities entering this expression are the solution of layerwise coupled equations, making its evaluation computationally intensive. A more approximate, less demanding, way of obtaining $S^{(2)}$ is to evaluate it numerically from $S^{(1)}$, where $S^{(1)}_i \equiv -\frac{\partial <\Omega>}{\partial m_i}$. We outline such a procedure here, restricted to the case $\mathbf{q}\| = \mathbf{0}$. This means that we can only consider systems where $S^{(2)}(\mathbf{q}\|)$ attains its maximum positive eigenvalue for $\mathbf{q}\| = \mathbf{0}$, i.e. those where the moments within each layer are ferromagnetically coupled. The coupling

between layers may, however, be ferromagnetic or antiferromagnetic. We begin by considering the change in $S^{(1)}$ for a particular layer P arising from the application of a small external magnetic field to every site j in layer Q. This can be written as

$$\Delta S_P^{(1)} = \sum_{i \in P} \Delta S_{Pi}^{(1)} = \sum_{i \in P} \sum_{Qj} S_{PiQj}^{(2)} \Delta m_Q, \tag{7.16}$$

where Δm_j is the induced magnetisation at each site in layer Q and we have used the definition $S_{PiQj}^{(2)} = -\frac{\partial^2 <\Omega>}{\partial m_{Pi} \partial m_{Qj}}$. The identity

$$S_{PQ}^{(2)}(\mathbf{q}\| = \mathbf{0}) = \sum_{i \in P} \sum_{j \in Q} S_{PiQj}^{(2)} \tag{7.17}$$

can be used to rewrite Eq. 7.16 as

$$\Delta S_P^{(1)} = \sum_{Q} S_{PQ}^{(2)}(\mathbf{q}\| = \mathbf{0}) \Delta m_Q. \tag{7.18}$$

Equation 7.18 evidently provides a direct relation between $S^{(2)}(\mathbf{q}\| = \mathbf{0})$ and $S^{(1)}$. The quantity $S_P^{(1)}$ can be determined using the inhomogeneous CPA and is given by [33]

$$S_P^{(1)} = \frac{\mathrm{I}m}{\pi} \int dE \; f(E, \nu) [\ln \|D_+^P\| - \ln \|D_-^P\|], \tag{7.19}$$

where the D^P are CPA projectors for the Pth layer:

$$D_{+(-)}^P = [1 + [(t_{+(-)}^P) - 1 - (t^{c,P})^{-1}] \tau^{c,P0P0}]^{-1}, \tag{7.20}$$

where $t^{c,P}$ and $\tau^{c,P0P0}$ are respectively the cpa t matrix and site-diagonal scattering path operator for the Pth layer.

To actually compute $S_{PQ}^{(2)}(\mathbf{q}\| = \mathbf{0})$ from Eq. 7.18, we consider a CPA calculation in which one of the layers Q has a slight imbalance between 'up' and 'down' moments. If the probability of a site in layer Q being occupied by an 'up'

moment is $0.5+\delta$ and the probability of it being occupied by a 'down' moment is $0.5-\delta$, equation 7.18 gives

$$S^{(2)}_{PQ}(\mathbf{q}\| = \mathbf{0}) = \frac{\Delta S^{(1)}_P}{2\delta}, \tag{7.21}$$

where for each layer, P, $\Delta S^{(1)}_P$ can be evaluated according to Eq. 7.19. By repeating this procedure for all Q, the full matrix $S^{(2)}$ can be obtained.

Chapter 8

Conclusions and Outlook

In this thesis we have presented a new formalism for investigating the onset of magnetic order in Strongly-Correlated electron systems. Based on a first-principles, density functional theory description of the electronic structure, our scheme contains no adjustable parameters and at no stage was the many-electron problem fit onto an effective model Hamiltonian. Central to including strong electron correlation effects in our mean-field DLM approach to magnetism, was our new LSIC implementation, which we outlined in section 5.5. This greatly extends the range of systems which can be treated using the DLM, in particular to those in which electron states have much more of an atomic, rather than a Bloch like, nature. We also outlined, in section 5.4, how the DLM scheme can be generalised to more than one atom per unit cell, again expanding the range of systems that can be treated.

Using our new LSIC implementation of the DLM, we carried out a major investigation of heavy rare earth magnetism in chapter 6. The results we obtained were analysed with reference to the RKKY model of magnetism. We illustrated how Fermi surface nesting in the paramagnetic state promotes the formation of

incommensurate magnetic structures. By arguing that the type of magnetic order is determined by the sd conduction electrons, common to all the heavy rare earths, we suggested that gadolinium could be used as a magnetic prototype for the whole heavy rare earth series. On the basis of this we proposed a 'unified phase diagram' of heavy rare earth magnetism, linking the magnetic ordering tendencies of the elements to their lattice parameters. Importantly, this phase diagram has predictive power. Indeed, we showed that it could be used to predict critical alloy concentrations, at which new magnetic phases appear. The phase diagram could also potentially be used to make experimental predictions about the pressure or tension needed to convert the magnetic ordering of a heavy rare earth systems from one type to another. Such predictive capability underlines the strength of our first principles approach.

To further our study of the heavy rare earths, as well as to provide additional validation for our use of gadolinium as a magnetic prototype, we would need to actually generate self-consistently the electronic structures of the other heavy rare elements. As outlined in chapter 6, this would require spin-orbit effects to be taken into account because, unlike gadolinium, the other heavy rare earth metals have non zero orbital moment in the groundstate. A relativistic generalisation of the LSIC would hence be required. Such a generalisation already exists for the conventional (LMTO-ASA) implementation of the SIC [159]. The results of LMTO-ASA-SIC calculations for thulium [160], the last member of the heavy rare earths, show that the most energetically favourable SIC configuration changes when spin orbit coupling is included, thus showing the importance of this effects.

Another noteworthy feature of the LMTO-ASA calculations [160], was that the different SIC configurations for thulium were found to be very close in energy. This suggests that interactions between different orbital configurations of

the system, corresponding to the different SIC configurations, might need to be considered. In particular, rather than treating the system as having one specific orbital configuration, it should be treated as being in some intermediate state between two or more different configurations. This is closely linked to ideas we discussed in chapter 4 concerning the non-integer valence of γ-cerium, where it was suggested that the f electron should be viewed as being in some intermediate state between being fully localised or fully delocalised. We proposed that this could be modelled in terms of a pseudoalloy, where the f electron was localised on one 'alloy' component and delocalised on the other, with the former being described using an LDA potential and the latter by an SIC potential. We could consider doing a similar thing but with two SIC potentials, corresponding to different localisation configurations. This would describe a system with statically disordered orbital configurations. To be able to describe the dynamical interactions of different orbital configurations, we could consider the two different SIC potentials as being two states of an atom and allow the atom to tunnel between the states, so as to form a so-called two level system [161]. Applying a similar reasoning to potentials describing different moment orientations, opens up a way to take into account dynamic moment fluctuations. This could be used as the basis of a dynamical generalisation of the DLM method, of the sort proposed in chapter 3. In such an DMFT-DLM-SIC scheme, the energy scales associated with dynamic spin and orbital fluctuations might be in the thermal range. One example where this physics is relevant is the determination of the Néel temperature of NiO and this new theory could potentially improve the value from that obtained using our static, fixed orbital approach.

Bibliography

[1] T. Arai, Phys. Rev. **134**, A824 (1964).

[2] W. M. Temmerman, H. Winter, Z. Szotek, and A. Svane, Phys. Rev. Lett. **86**, 2435 (2001).

[3] H. Ohno, Science **281**, 951 (1998).

[4] Y. Tokura, Reports on Progress in Physics **69**, 797 (2006).

[5] M. Imada, A. Fujimori, and Y. Tokura, Rev. Mod. Phys. **70**, 1039 (1998).

[6] R. O. Jones and O. Gunnarsson, Rev. Mod. Phys. **61**, 689 (1989).

[7] J. Hubbard, Phys. Rev. B **19**, 2626 (1979).

[8] J. S. Faulkner, Phys. Rev. B **19**, 6186 (1979).

[9] J. P. Perdew and A. Zunger, Phys. Rev. B **23**, 5048 (1981).

[10] B. Johansson *et al.*, Phys. Rev. Lett. **74**, 2335 (1995).

[11] S. Ostanin *et al.*, Phys. Rev. Lett. **98**, 016101 (2007).

[12] I. D. Hughes *et al.*, nature **446**, 650 (2007).

[13] *Magnetism, Vol. IIB*, edited by G. T. Rado and H. Suhl (Academic Press Inc., New York, 1966), p. 215.

[14] P. Hohenberg and W. Kohn, Phys. Rev. **136**, B864 (1964).

[15] W. Kohn and L. J. Sham, Phys. Rev. **140**, A1133 (1965).

[16] J. P. Perdew and Y. Wang, Phys. Rev. B **45**, 13244 (1992).

[17] O. Gunnarson and B. I. Lundqvist, Phys. Rev. B **13**, 4274 (1976).

[18] R. G. Parr and W. Yang, *Density-Functional Theory of Atoms and Molecules* (Clarendon, Oxford, 1989).

[19] J. Korringa, Physica **13**, 392 (1947).

[20] L. Rayleigh, Philos. Mag. **34**, 481 (1892).

[21] W. Kohn and N. Rostoker, Phys. Rev. **94**, 1111 (1954).

[22] R. Zeller, J. Phys. C: Solid State Phys. **20**, 2347 (1987).

[23] P. W. Atkins and R. S. Friedman, *Molecular Quantum Mechanics* (Oxford University Press, Oxford, 1997).

[24] A. Gonis, *Greens Functions for Ordered and Disordered Systems* (North-Holland, Amsterdam, 1992).

[25] B. L. Gyorffy and G. M. Stocks, *Electrons in Disordered Metals and at Metallic Surfaces* (Plenum Press, New York, 1979), edited by P. Phariseau, B.L. Gyorffy and L. Scheire.

[26] P. Lloyd and P. V. Smith, Adv. Phys. **21**, 69 (1972).

[27] B. Gyorffy and M. Stott, *Band Structure Spectroscopy of Metals and Alloys* (Academic Press, London, 1973), edited by D. J. Fabian and L. M. Watson.

[28] J. S. Faulkner, Prog. Mater. Sci **27**, 1 (1982).

[29] R. M. Martin, *Electronic Structure: Basic Theory and Practical Methods* (Cambridge University Press, Cambridge, 2004).

[30] J. S. Faulkner and G. M. Stocks, Phys. Rev. B **21**, 3222 (1980).

[31] N. F. Mott, Phil. Mag. **22**, 287 (1936).

[32] Hüfner, S. and Wertheim, G. K. and Cohen, R. L. and Wernick, J. H., Phys. Rev. Lett. **28**, 488 (1972).

[33] B. L. Gyorffy *et al.*, J. Phys. F:Met. Phys. **15**, 1337 (1985).

[34] J. Korringa, J. Phys. Chem. Solids **7**, 252 (1958).

[35] R. Mills and P. Ratanavaraksa, Phys. Rev. B **18**, 5291 (1978).

[36] A. Mookerjee, P. K. Thakur, and M. Yussouff, J. Phys. C: Solid State Phys. **18**, 4677 (1985).

[37] P. Soven, Phys. Rev. **156**, 809 (1967).

[38] Soven, P, Phys. Rev. B **2**, 4715 (1970).

[39] H. Shiba, Progr. Theoret. Phys. (Kyoto) **46**, 77 (1971).

[40] B. L. Gyorffy, Phys. Rev. B **5**, 2382 (1972).

[41] H. Winter and G. M. Stocks, Phys. Rev. B **27**, 882 (1983).

[42] P. J. Durham, B. L. Gyorffy, and A. J. Pindor, J. Phys. F:Met. Phys. **10**, 661 (1980).

[43] K. Terakura, T. Oguchi, A. R. Williams, and J. Kübler, Phys. Rev. B **30**, 4734 (1984).

[44] A. Delin *et al.*, Phys. Rev. B **58**, 4345 (1998).

[45] W. E. Pickett, Rev. Mod. Phys. **61**, 433 (1989).

[46] N. F. Mott and R. Peierls, Proceedings of the Physical Society **49**, 72 (1937).

[47] J. Hubbard, Royal Society of London Proceedings Series A **276**, 238 (1963).

[48] N. F. Mott, Proceedings of the Physical Society. Section A **62**, 416 (1949).

[49] J. Zaanen, G. A. Sawatzky, and J. W. Allen, Phys. Rev. Lett. **55**, 418 (1985).

[50] G. Kotliar and D. Vollhardt, Physics Today **57**, 53 (2004).

[51] P. Hohenberg and W. Kohn, Phys. Rev. **136**, B864 (1964).

[52] D. C. Langreth and J. P. Perdew, Phys. Rev. B **15**, 2884 (1977).

[53] D. C. Langreth and M. J. Mehl, Phys. Rev. Lett. **47**, 446 (1981).

[54] J. P. Perdew and W. Yue, Phys. Rev. B **33**, 8800 (1986).

[55] P. Bagno, O. Jepsen, and O. Gunnarsson, Phys. Rev. B **40**, 1997 (1989).

[56] P. Dufek, P. Blaha, and K. Schwarz, Phys. Rev. B **50**, 7279 (1994).

[57] L. Hedin, Phys. Rev. **139**, A796 (1965).

[58] F. Aryasetiawan and O. Gunnarsson, Reports on Progress in Physics **61**, 237 (1998).

[59] R. W. Godby, M. Schlüter, and L. J. Sham, Phys. Rev. B **37**, 10159 (1988).

[60] S. Massidda, A. Continenza, M. Posternak, and A. Baldereschi, Phys. Rev. Lett. **74**, 2323 (1995).

[61] V. I. Anisimov, J. Zaanen, and O. K. Andersen, Phys. Rev. B **44**, 943 (1991).

[62] V. I. Anisimov *et al.*, Phys. Rev. B **48**, 16929 (1993).

[63] A. Georges and G. Kotliar, Phys. Rev. B **45**, 6479 (1992).

[64] A. Georges, G. Kotliar, W. Krauth, and M. J. Rozenberg, Rev. Mod. Phys. **68**, 13 (1996).

[65] V. I. Anisimov *et al.*, Journal of Physics: Condensed Matter **9**, 7359 (1997).

[66] S. Biermann, F. Aryasetiawan, and A. Georges, Phys. Rev. Lett. **90**, 086402 (2003).

[67] Y. Kakehashi, Phys. Rev. B **66**, 104428 (2002).

[68] O. Gunnarsson and R. O. Jones, *Local Density Approximations in Quantum Chemistry and Solid State Physics* (Plenum, New York, 1984), p. 229, Edited by J. P. Dahl and J. Avery.

[69] A. Svane, Phys. Rev. B **51**, 7924 (1995).

[70] K. Ruedenberg, *Computational Methods for Large Molecules and Localised States in Solids* (Plenum, New York, 1973), Edited by F. Herman, A. D. McLean and R. K. Nesbet.

[71] G. H. Wannier, Phys. Rev. **52**, 191 (1937).

[72] A. Svane and O. Gunnarsson, Phys. Rev. B **37**, 9919 (1988).

[73] R. A. Heaton, J. G. Harrison, and C. C. Lin, Phys. Rev. B **28**, 5992 (1983).

[74] O. K. Andersen, Phys. Rev. B **12**, 3060 (1975).

[75] Z. Szotek, W. M. Temmerman, and H. Winter, Phys. Rev. B **47**, 4029 (1993).

[76] L. Petit, A. Svane, Z. Szotek, and W. M. Temmerman, Molecular Physics Reports **38**, 20 (2003).

[77] Z. Szotek *et al*, Phys. Rev. B **68**, 054415 (2003).

[78] P. Strange *et al.*, Nature (London) **399**, 756 (1999).

[79] L. Petit, A. Svane, Z. Szotek, and W. M. Temmerman, Science **301**, 498 (2003).

[80] Lüders, M. *et al*, Phys. Rev. B **71**, 205109 (2005).

[81] Z. Szotek, W. M. Temmerman, and H. Winter, Phys. Rev. Lett. **72**, 1244 (1994).

[82] A. Svane, Phys. Rev. Lett. **72**, 1248 (1994).

[83] A. Svane, Phys. Rev. B **53**, 4275 (1996).

[84] R. Podloucky and D. Glötzel, Phys. Rev. B **27**, 3390 (1983).

[85] W. E. Pickett, A. J. Freeman, and D. D. Koelling, Phys. Rev. B **23**, 1266 (1981).

[86] B. I. Min, H. J. F. Jansen, T. Oguchi, and A. J. Freeman, Phys. Rev. B **34**, 369 (1986).

[87] M. Lavagna, C. Lacroix, and M. Cyrot, J. Phys. F:Met. Phys. **13**, 1007 (1983).

[88] O. Gunnarsson and K. Schönhammer, Phys. Rev. B **28**, 4315 (1983).

[89] O. Eriksson, M. S. S. Brooks, and B. Johansson, Phys. Rev. B **41**, 7311 (1990).

[90] R. Ramirez and L. M. Falicov, Phys. Rev. B **3**, 2425 (1971).

[91] D. R. Gustafsson, J. D. McNutt, and L. O. Roellig, Phys. Rev. **183**, 435 (1969).

[92] E. Willoud, H. R. Moser, W. D. Schneider, and Y. Baer, Phys. Rev. B **28**, 7354 (1983).

[93] J. W. Allen and R. M. Martin, Phys. Rev. Lett. **49**, 1106 (1982).

[94] I. Z. Liu *et al.*, Phys. Rev. B **45**, 8934 (1992).

[95] N. Y. Moghadam *et al*, J. Phys. Chem. Solids **13**, 3073 (2001).

[96] *Handbook on the Physics and Chemistry of Rare Earths Vol. 1*, edited by K. A. Gschneidner and L. Eyring (North Holland, Amsterdam, 1978).

[97] N. D. Mermin, Phys. Rev. **137**, A1441 (1965).

[98] E. P. Wohlfarth, Rev. Mod. Phys. **25**, 211 (1953).

[99] R. A. Tawil and J. Callaway, Phys. Rev. B **7**, 4242 (1973).

[100] S. Q. Wang, W. E. Evenson, and J. R. Schrieffer, Phys. Rev. Lett. **23**, 92 (1969).

[101] W. E. Evanson, J. R. Schrieffer, and S. Q. Wang, J. Appl. Phys. **41**, 1199 (1970).

[102] M. Cyrot, Phys. Rev. Lett. **25**, 871 (1970).

[103] P. Lacour-Gayet and M. Cyrot, J. Phys. C: Solid State Phys. **7**, 400 (1974).

[104] J. Hubbard, Phys. Rev. B **20**, 4584 (1979).

[105] J. Hubbard, Phys. Rev. B **23**, 5974 (1981).

[106] A. J. Pindor, J. Staunton, G. M. Stocks, and H. Winter, J. Phys. F:Met. Phys. **13**, 979 (1983).

[107] J. Staunton *et al.*, J. Phys. F:Met. Phys. **15**, 1387 (1387).

[108] E. Kisker, K. Schröder, M. Campagna, and W. Gudat, Phys. Rev. Lett. **52**, 2285 (1984).

[109] J. Kirschner, M. Glöbl, V. Dose, and H. Scheidt, Phys. Rev. Lett. **53**, 612 (1984).

[110] R. P. Feynman, Phys. Rev. **97**, 660 (1955).

[111] B. Segall, Phys. Rev. **105**, 108 (1957).

[112] A. J. Pindor, W. M. Temmerman, and B. L. Gyorffy, J. Phys. F:Met. Phys. **13**, 1627 (1983).

[113] J. Keller, Journal of Physics C: Solid State Physics **4**, L85 (1971).

[114] L. F. Bates, S. J. Leach, and R. G. Loasby, Proc. Phys. Soc. B **68**, 859 (1955).

[115] J. M. Lock, Proc. Phys. Soc. B **70**, 566 (1957).

[116] R. V. Colvin, S. Arajs, and J. M. Peck, Phys. Rev. **122**, 14 (1961).

[117] C. R. Burr and S. Ehara, Phys. Rev. **149**, 551 (1966).

[118] F. H. Spedding, A. F. Voigt, E. M. Gladrow, and N. R. Sleight, J. Am. Chem. Soc. **69**, 2777 (1947).

[119] P. Burgardt *et al.*, Phys. Rev. B **14**, 2995 (1976).

[120] D. C. Koskimaki and K. A. Gschneidner, Phys. Rev. B **11**, 4463 (1975).

[121] J. Jensen and A. K. Mackintosh, *Rare Earth Magnetism* (Clarendon, Oxford, 1991), pp. 50–67.

[122] J. B. Staunton *et al.*, Phys. Rev. Lett. **93**, 257204 (2004).

[123] A. H. MacDonald and S. H. Vosko, J. Phys. C: Solid State Phys. **12**, 2977 (1979).

[124] K. N. R. Taylor and M. I. Darby, *Physics of Rare Earth Solids* (Chapman and Hall, London, 1972).

[125] J. R. Banister, S. Legvold, and F. H. Spedding, Phys. Rev. **94**, 1140 (1954).

[126] M. Heinemann and W. M. Temmerman, Phys. Rev. B **49**, 4348 (1994).

[127] P. Kurz, G. Bihlmayer, and S. Blügel, J. Phys. Condens. Matter **14**, 6353 (2002).

[128] Eriksson, O. *et al*, Phys. Rev. B **52**, 4420 (1995).

[129] B. N. Harmon *et al.*, J. Phys. Chem. Solids **56**, 1521 (1994).

[130] J. B. Staunton and B. L. Gyorffy, Phys. Rev. Lett. **69**, 371 (1992).

[131] I. Turek, J. Kudrnovský, G. Bihlmayer, and S. Blügel, J. Phys. Condens. Matter **15**, 2771 (2003).

[132] J. A. Duffy *et al.*, Phys. Rev. B **61**, 14331 (2000).

[133] S. C. Keeton and T. L. Loucks, Phys. Rev. **168**, 672 (1968).

[134] Dugdale, S.B. *et al*, Phys. Rev. Lett. **79**, 941 (1997).

[135] A. P. Cracknell and K. C. Wong, *The Fermi Surface* (Clarendon, Oxford, 1973).

[136] A. V. Andrianov and O. D. Chistiakov, Phys. Rev. B **55**, 14107 (1997).

[137] A. V. Andrianov, D. I. Kosarev, and A. I. Beskrovnyi, Phys. Rev. B **62**, 13844 (2000).

[138] A. V. Andrianov, J. Magn. & Magn. Mater. **140-144**, 749 (1995).

[139] I. M. Lifshitz, Sov. Phys. JETP **11**, 1130 (1960).

[140] Y. M. Blanter, M. I. Kaganov, A. V. Pantsulaya, and A. A. Varlamov, Phys. Rep. **245**, 159 (1994).

[141] Z. Szotek, B. Gyorffy, G. Stocks, and W. M. Temmerman, J. Phys. F:Met. Phys. **14**, 2571 (1984).

[142] L. Nordström and A. Mavromaras, Europhys. Lett. **49**, 775 (2000).

[143] F. Milstein and L. B. Robinson, Phys. Rev. **159**, 466 (1967).

[144] A. Khachaturyan, *Theory of Stuctural Transformations in Solids* (Wiley, New York, 1983).

[145] J. B. Staunton, D. D. Johnson, and F. J. Pinski, Phys. Rev. B **50**, 1450 (1994).

[146] N. Wakabayashi and R. M. Nicklow, Phys. Rev. B **10**, 2049 (1974).

[147] R. Caudron *et al.*, Phys. Rev. B **42**, 2325 (1990).

[148] S. Bates *et al.*, Phys. Rev. Lett. **55**, 2968 (1985).

[149] J. C. Slater, Phys. Rev. **82**, 538 (1951).

[150] O. Tjernberg *et al.*, Phys. Rev. B **54**, 10245 (1996).

[151] S. Massidda, A. Continenza, M. Posternak, and A. Baldereschi, Phys. Rev. B **55**, 13494 (1997).

[152] P. A. Cox, *Transition Metal Oxides: An Introdution to their Electronic Structure and Properties* (Clarendon, Oxford, 1992).

[153] A. K. Cheetham and D. A. O. Hope, Phys. Rev. B **27**, 6964 (1983).

[154] H. Ohldag *et al.*, Phys. Rev. Lett. **86**, 2878 (2001).

[155] J. Stöhr *et al.*, Phys. Rev. Lett. **83**, 1862 (1999).

[156] D. Alders *et al.*, Phys. Rev. B **57**, 11623 (1998).

[157] L. Szunyogh, B. Újfalussy, P. Weinberger, and J. Kollár, Phys. Rev. B **49**, 2721 (1994).

[158] S. S. A. Razee, J. B. Staunton, L. Szunyogh, and B. L. Györffy, Phys. Rev. B **66**, 094415 (2002).

[159] S. V. Beiden, W. M. Temmerman, Z. Szotek, and G. A. Gehring, Phys. Rev. Lett. **79**, 3970 (1997).

[160] Z. Szotek, private communication.

[161] K. Vladár, G. T. Zimányi, and A. Zawadowski, Phys. Rev. Lett. **56**, 286 (1986).